

Systems thinking: Biological systems

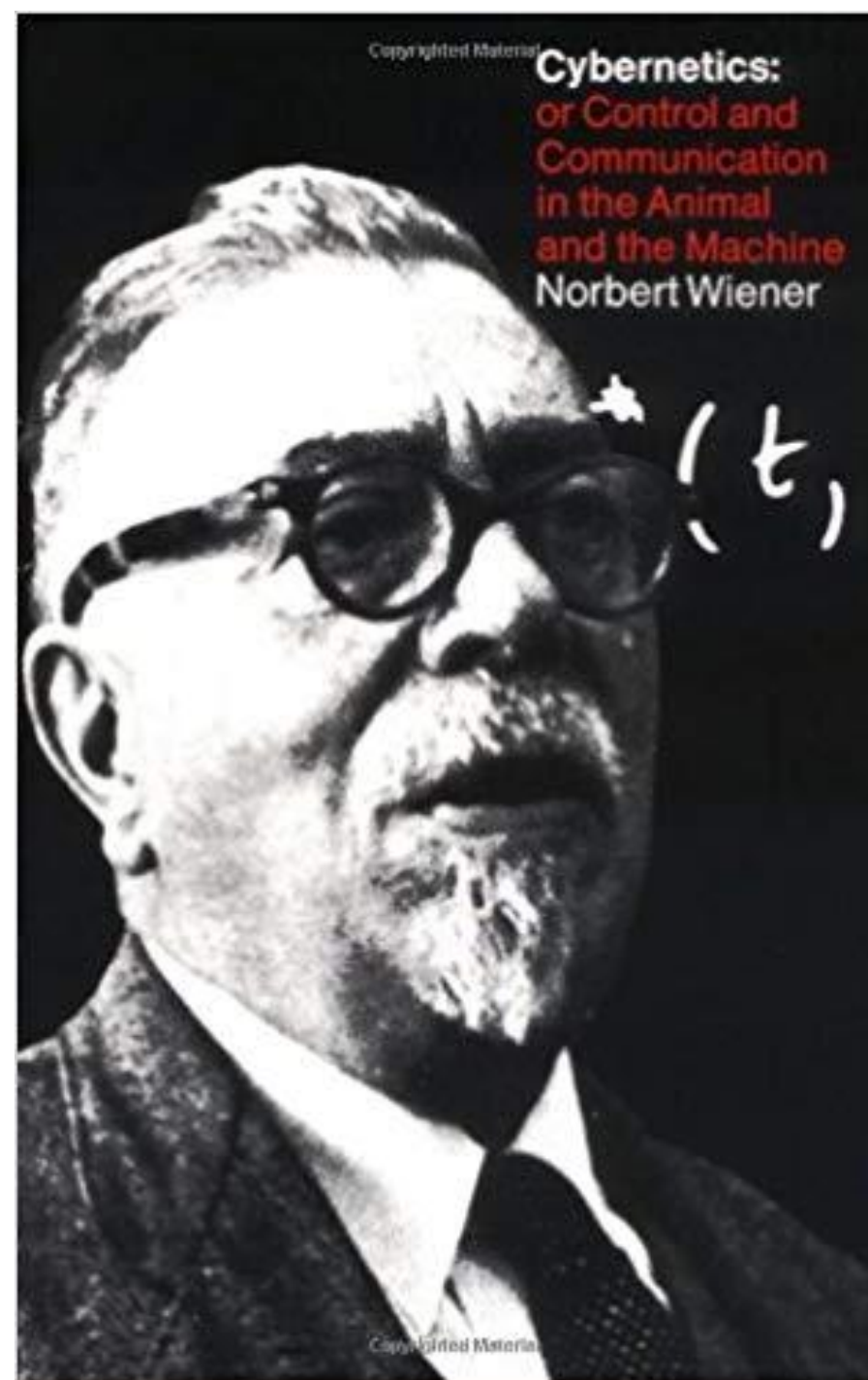
Application of control theory to biological systems

A historical perspective

“Engineers have produced many machines that are able to receive and react to information and to exert control by using feedback Evidently these machines work very much like living things and we can recognise a great number of feedback systems in the body It should be possible to use the precise language developed by the engineers to improve our understanding of those feedback systems that produce the stability of our lives. It cannot be said that physiologists have been able to go very far with this method. The living organism is so complicated that we seldom have enough data to be able to work out exactly what is happening by means of the mathematics the engineer uses. Up to the present, the general ideas and terminology used by these engineers have been of more use to biologists than have the detailed application of their techniques.”

J.Z. Young, Doubt and Certainty in Science : A biologist's reflections on the brain, The B.B.C. Reith lectures, Oxford University Press, 1950.

Wiener N. Cybernetics, or Control and Communication in the Animal and the Machine. New York: Wiley, 1948.



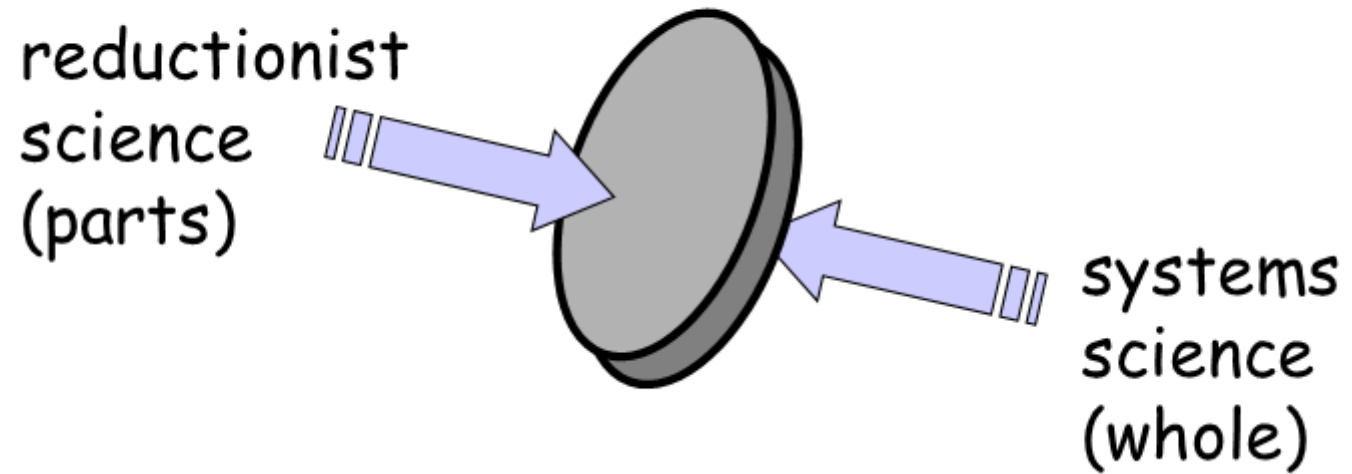
Systems Science...

...is the use of mathematics to study how the parts of a complex system fit together to function in ways that transcend the properties of the individual parts.

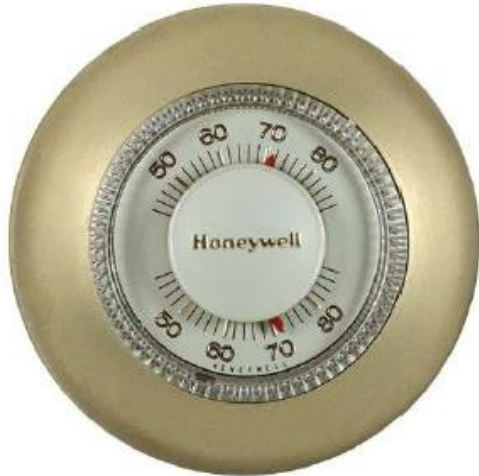


Karl Ludwig von Bertalanffy was an Austrian biologist known as one of the founders of general systems theory

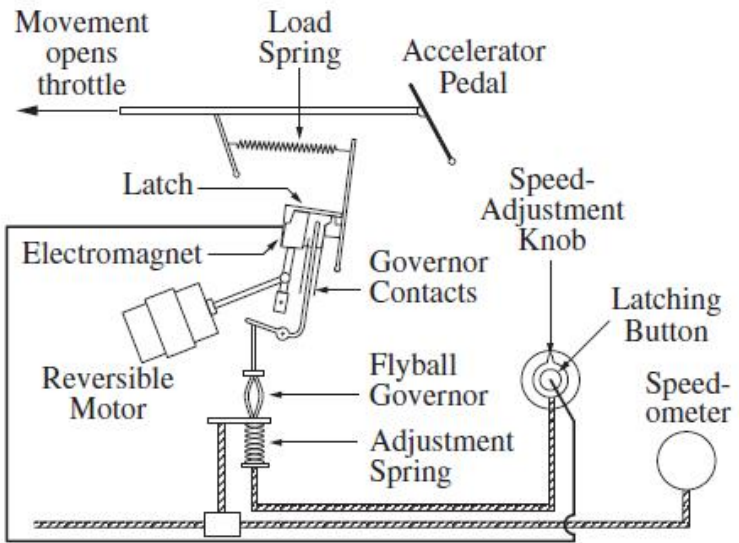
Systems Science is the flip-side of Reductionist Science.



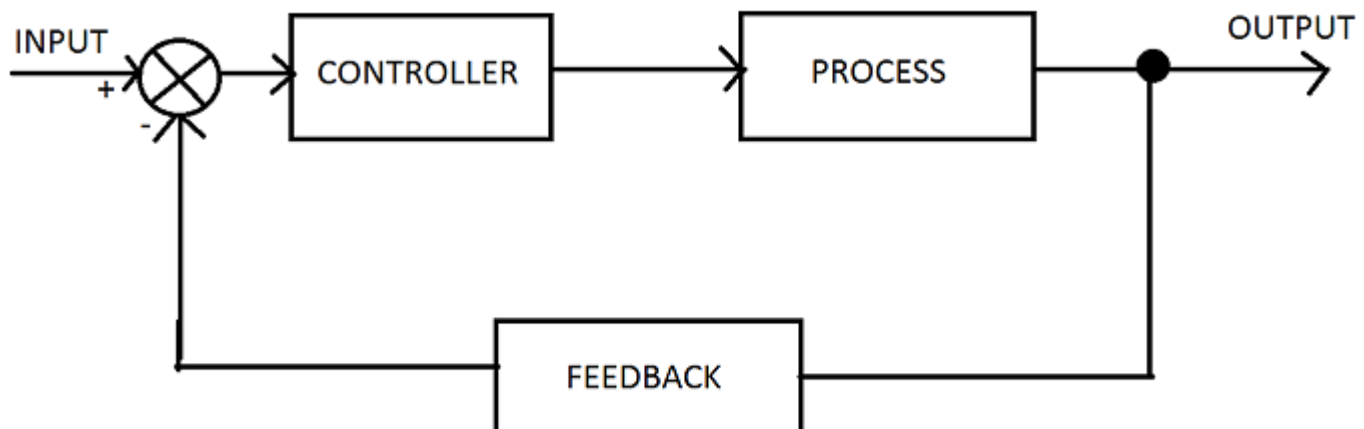
Early control devices



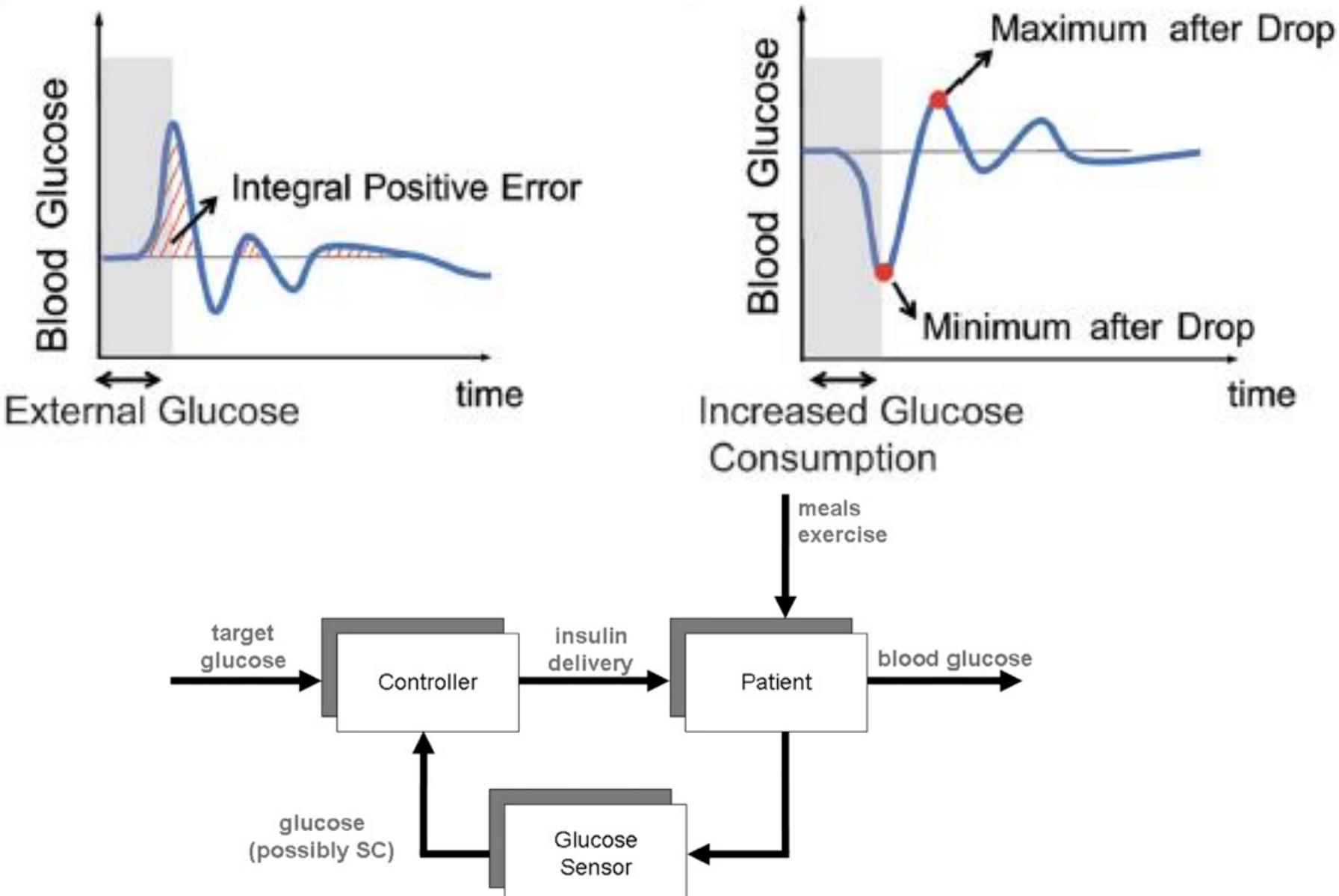
Honeywell thermostat, 1953

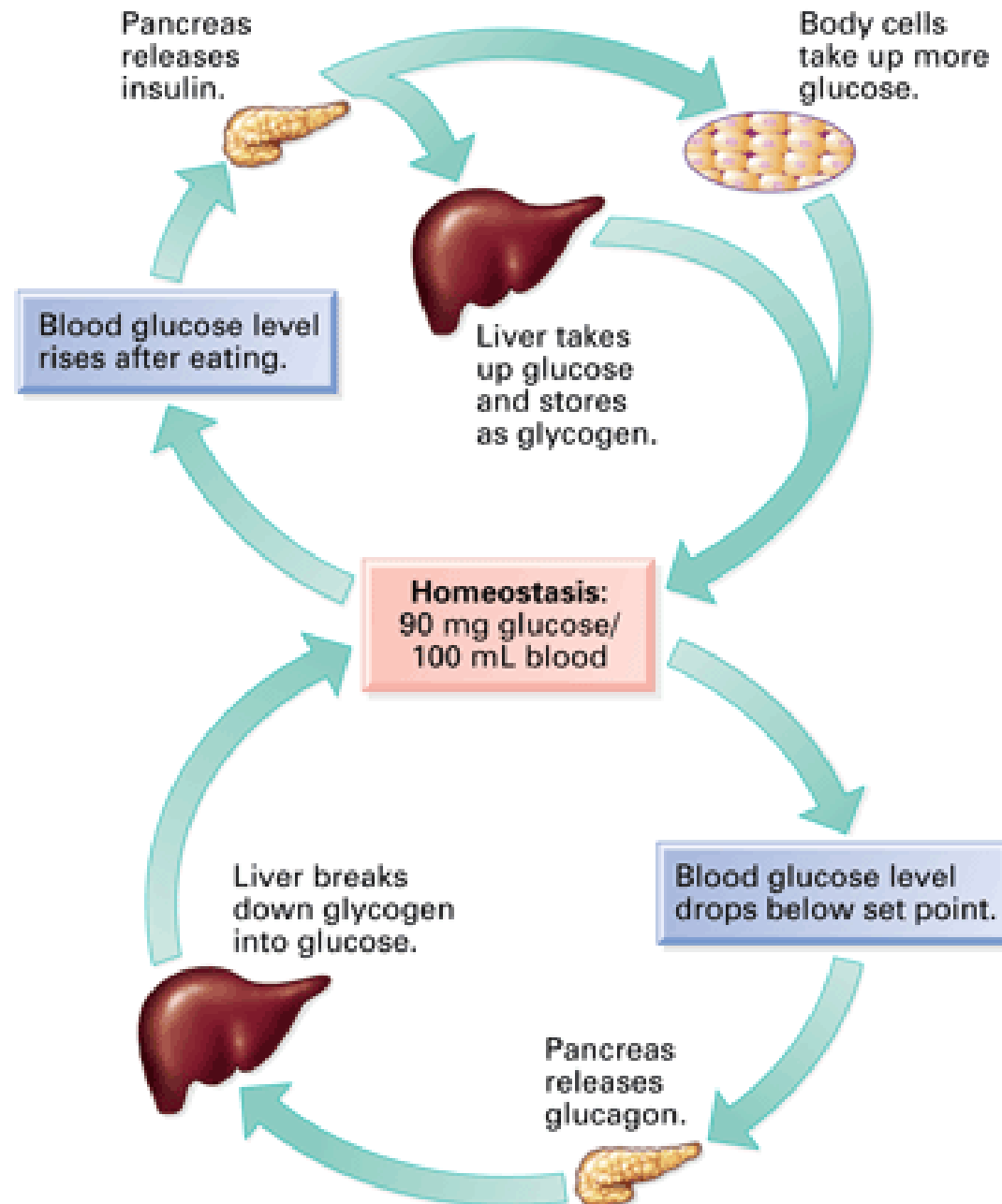


Chrysler cruise control, 1958

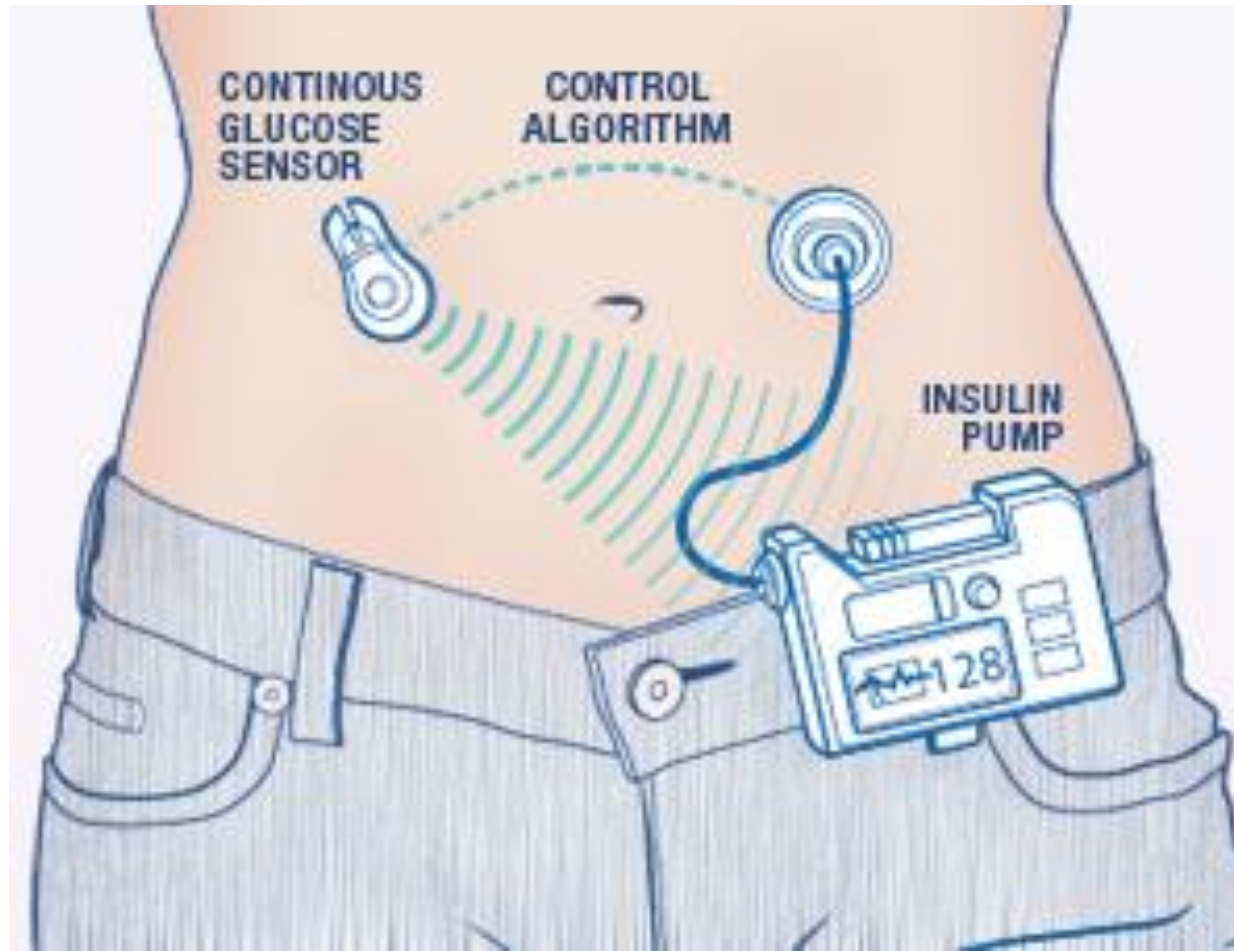


Glucose homeostasis

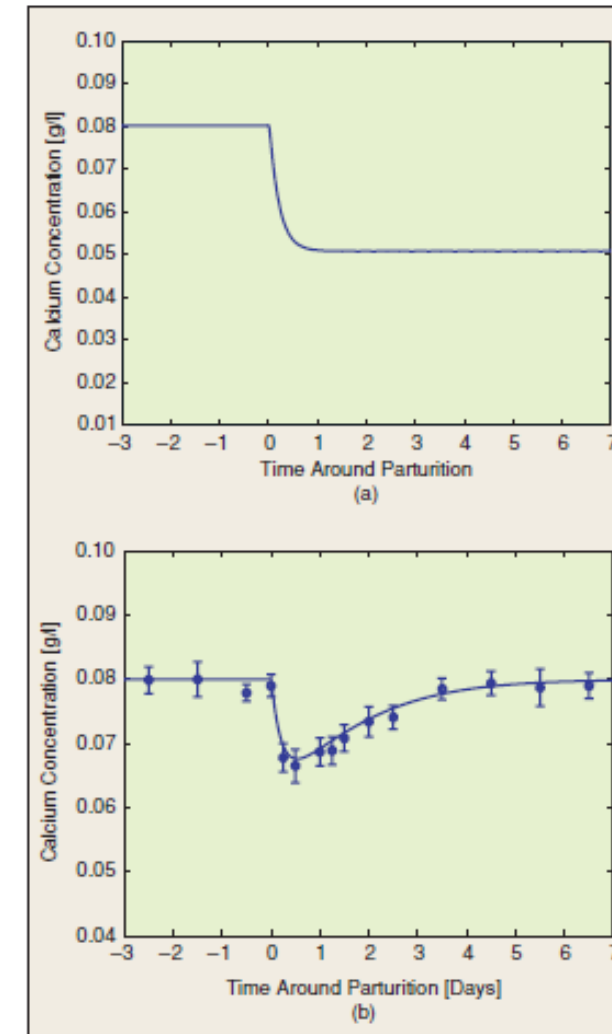
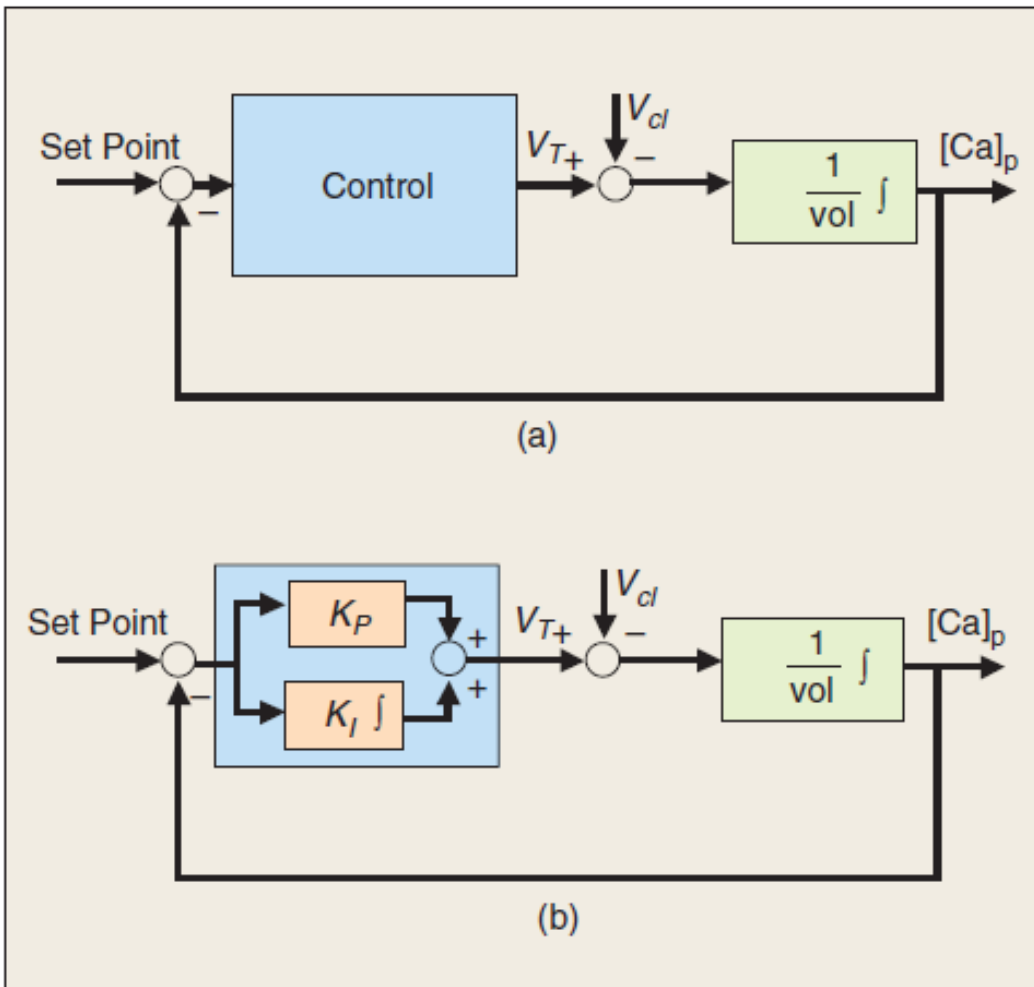




Closed Loop Systems: Future Treatment for Diabetes?



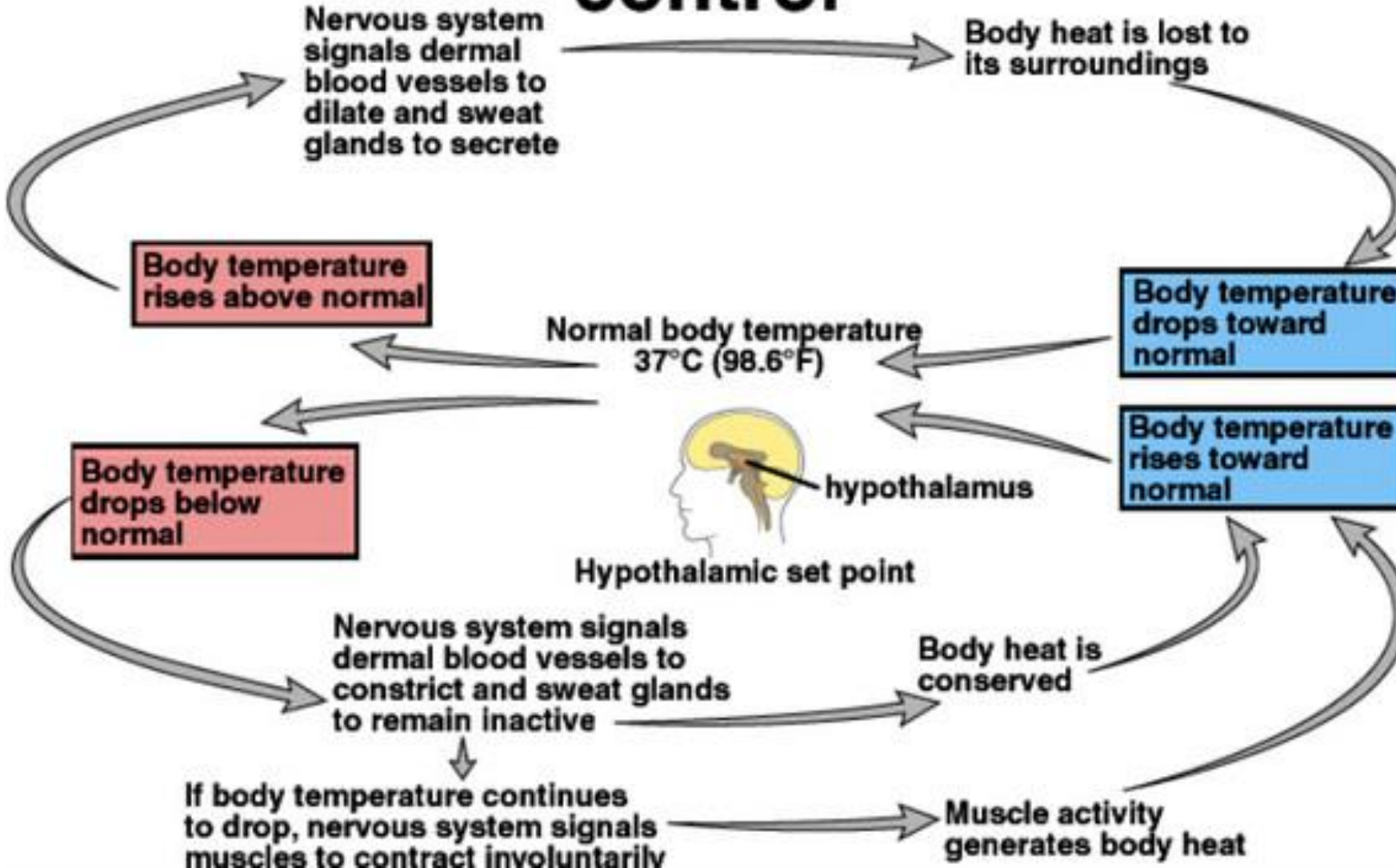
Calcium Homeostasis



$$\frac{d[Ca]_p}{dt} = \frac{1}{\text{vol}} (V_T(t) - V_{cl}(t))$$

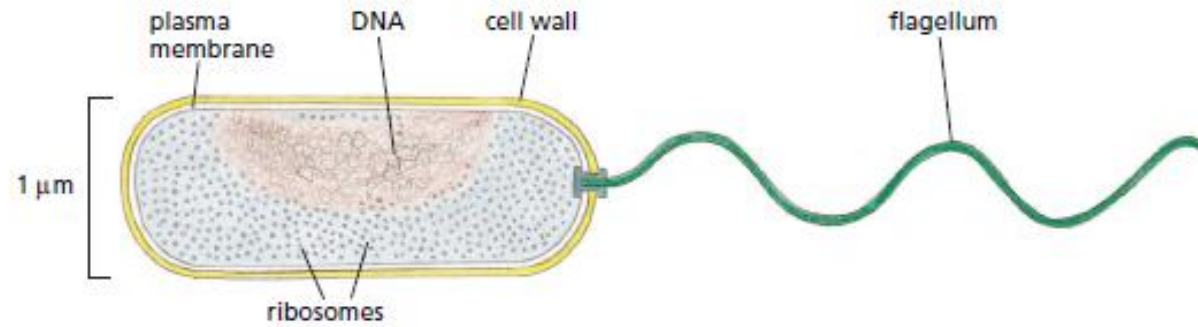
$$V_T = K_p e + K_I \int e$$

Homeostasis and temperature control

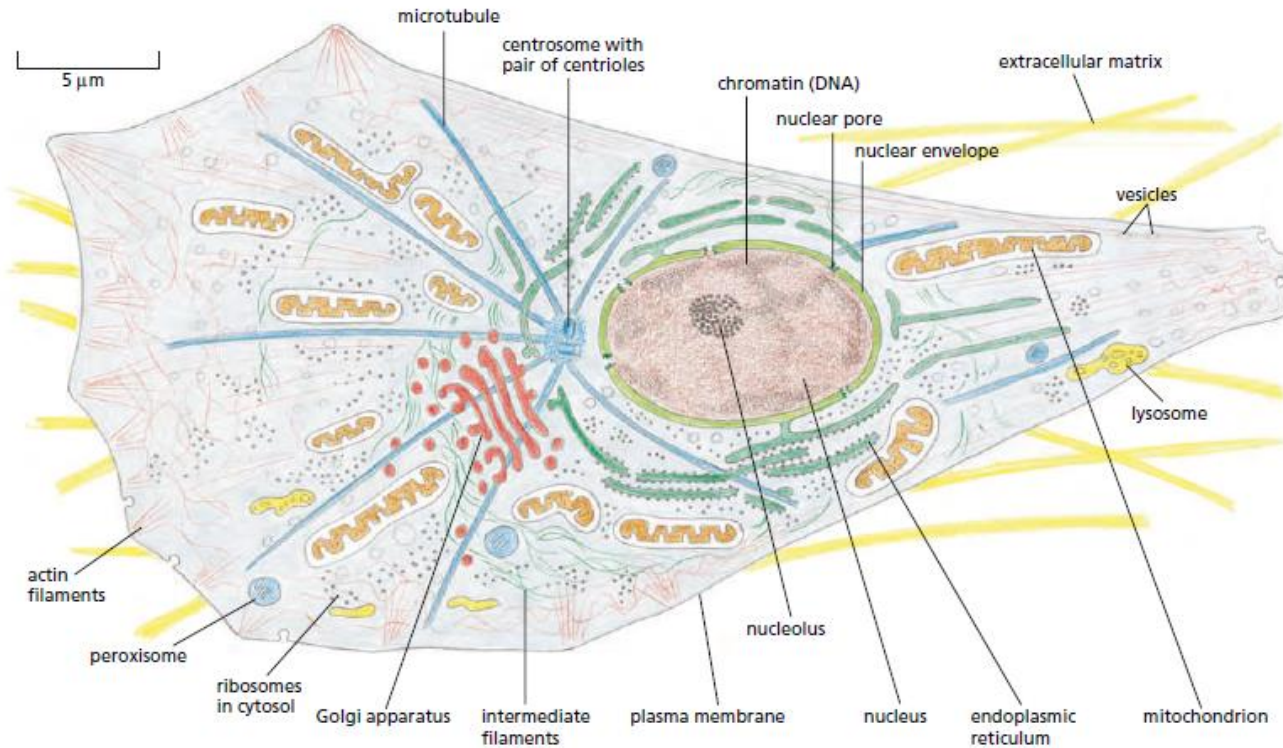


From Physiology to Cell Control System

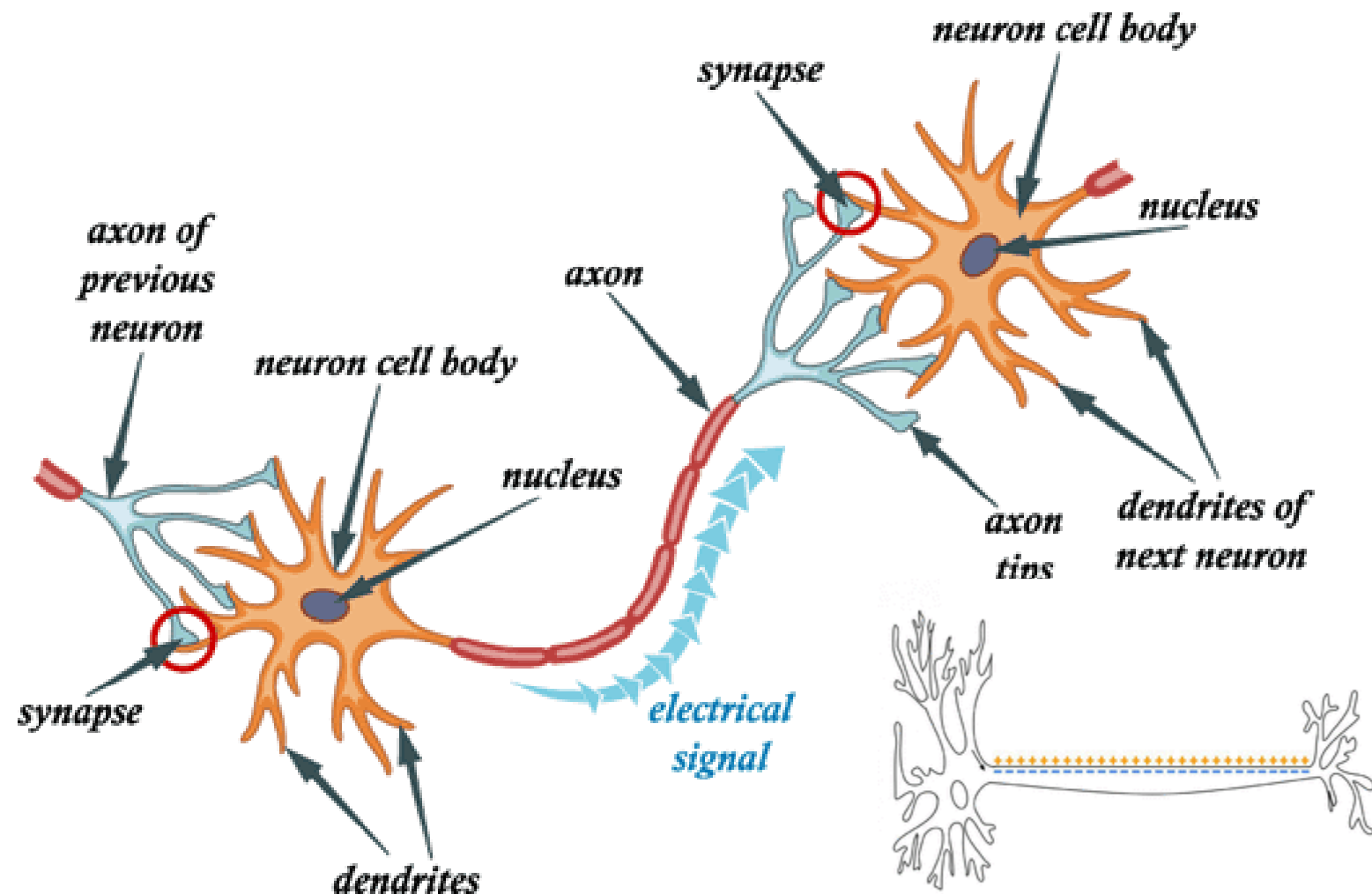
Bacterial cell



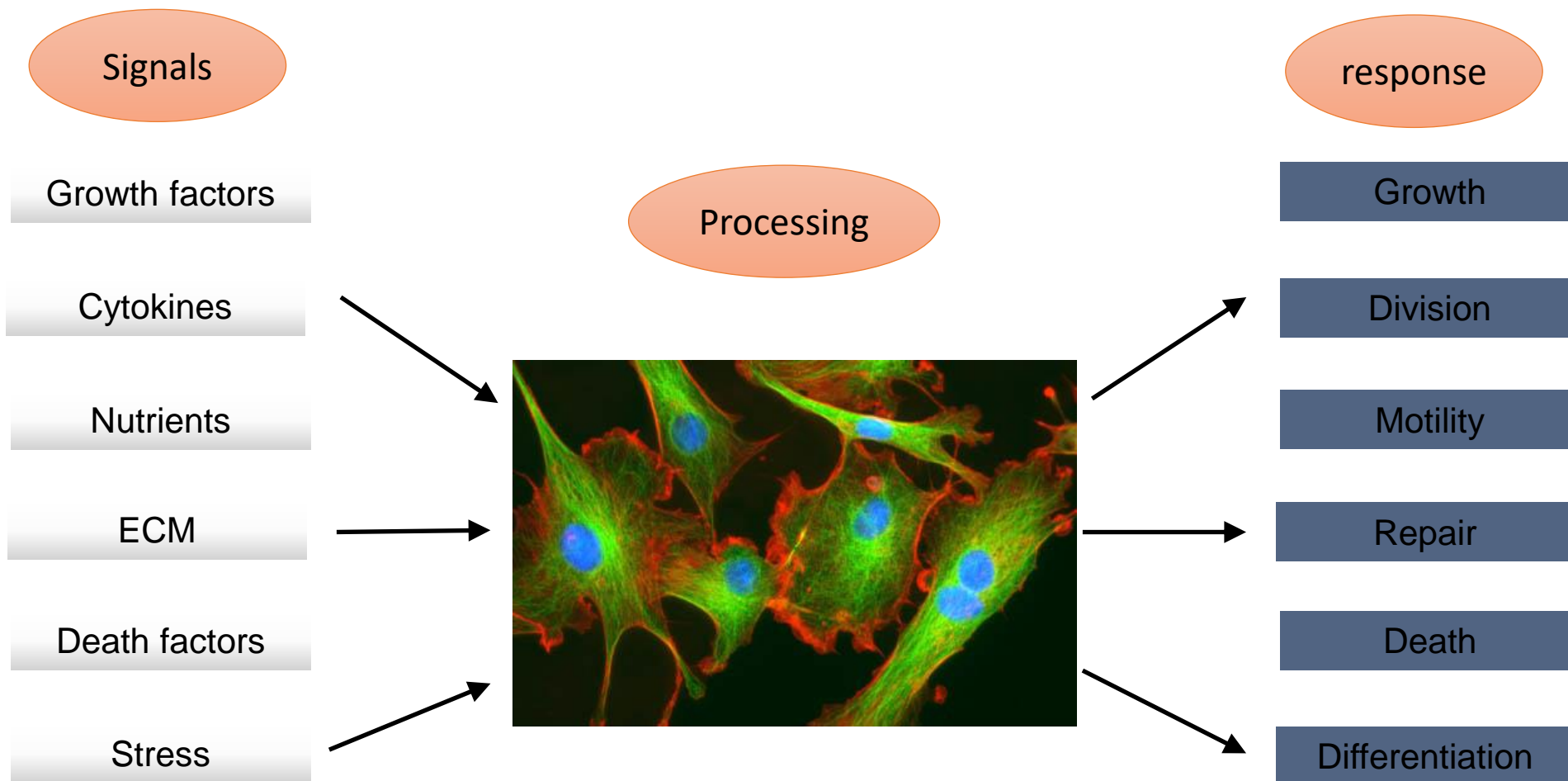
Animal cell



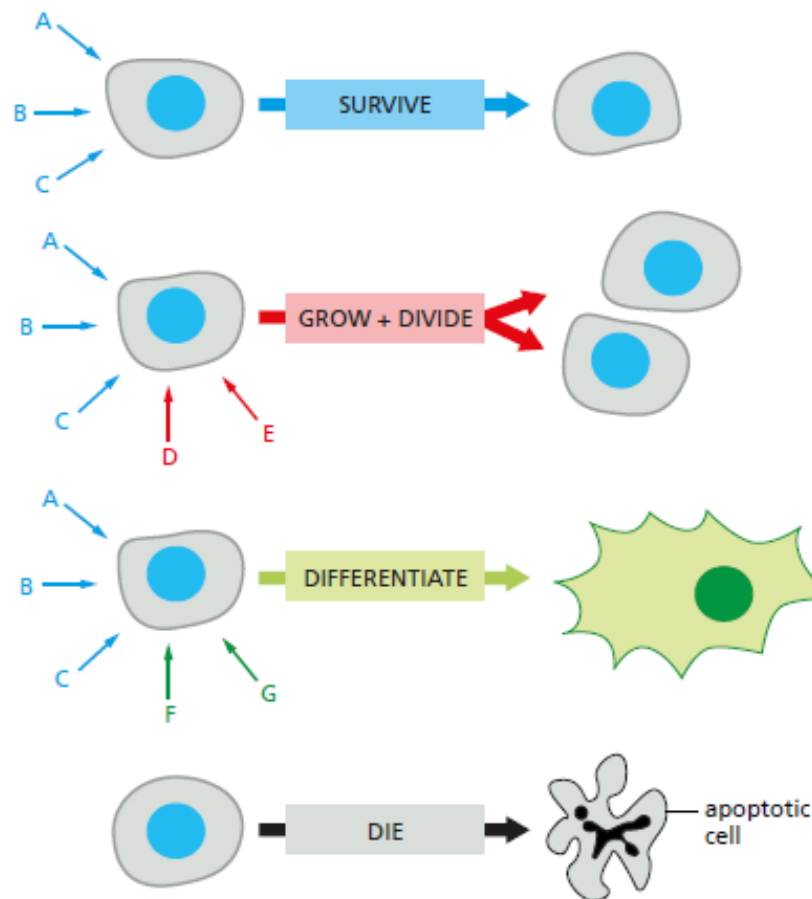
Neuron



Signals and System

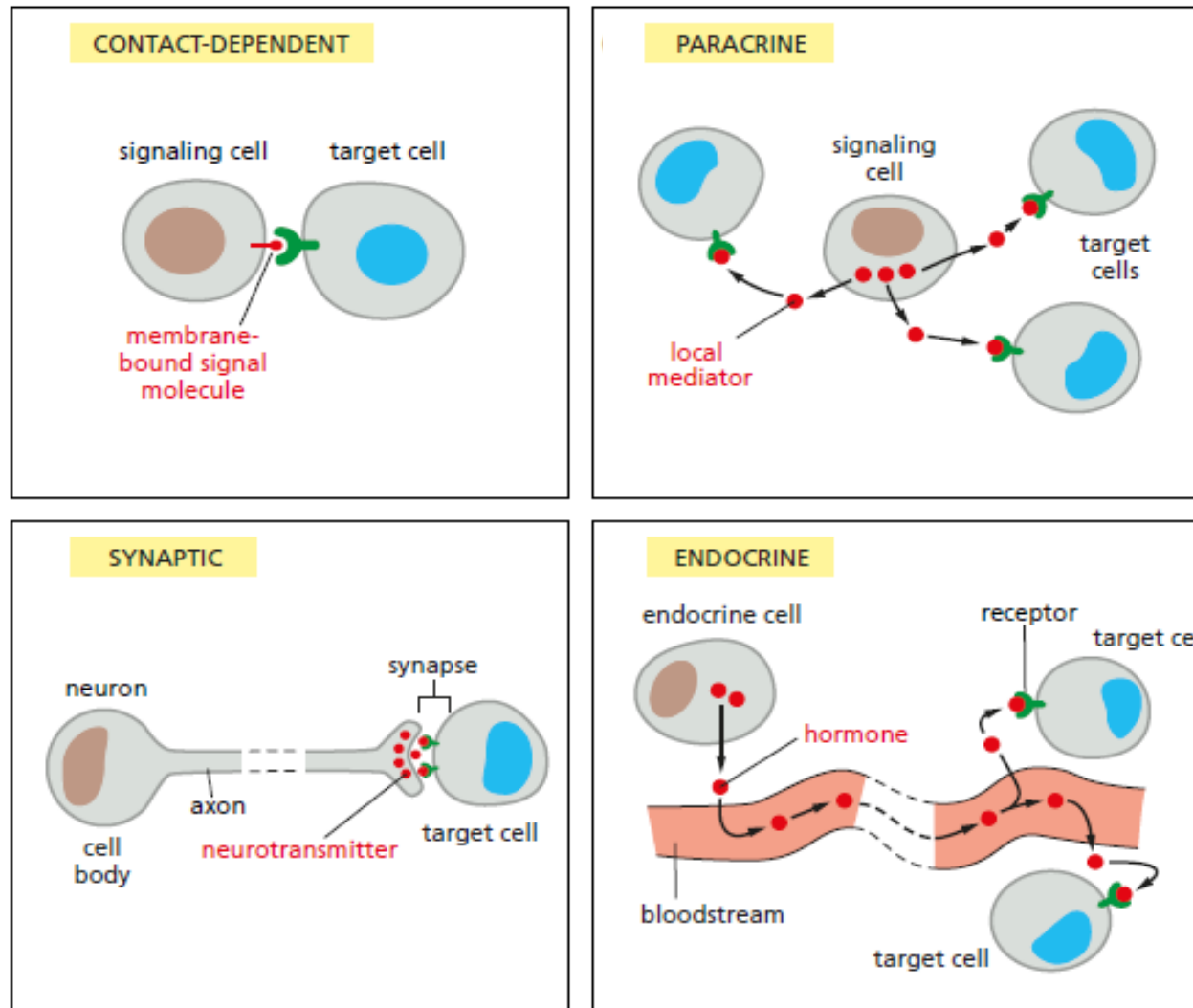


Each Cell Is Programmed to Respond to Specific Combinations of Extracellular Signals

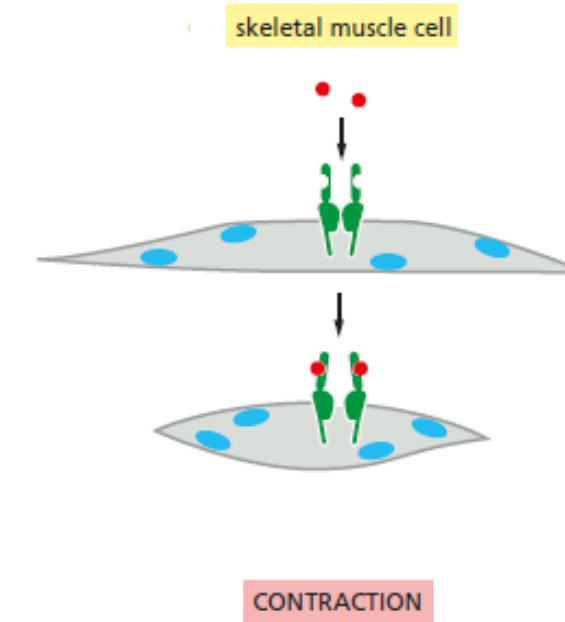
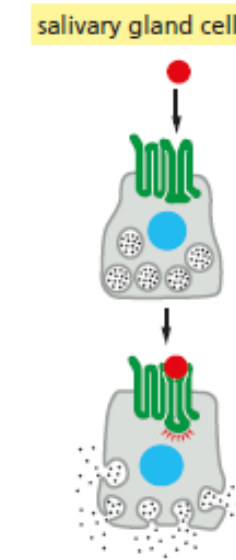
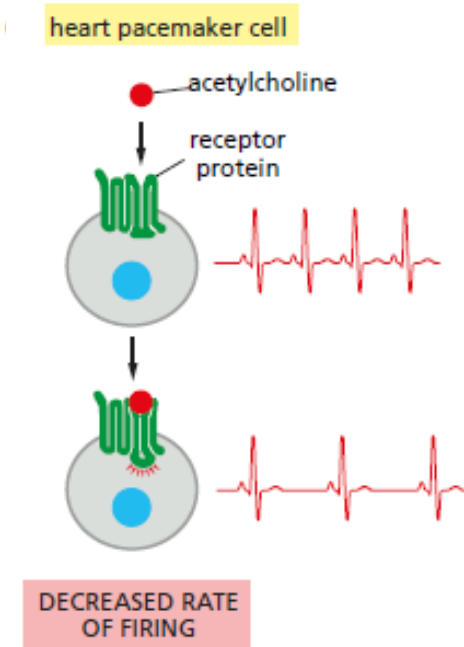
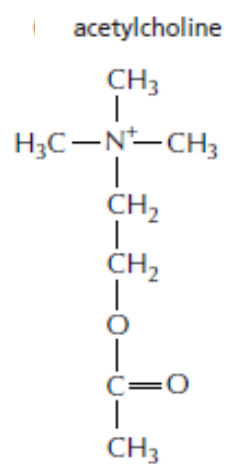


One of the key challenges is to determine how a cell integrates all of this signaling information in order to make decisions !!

Four forms of signals



Responses induced by the neurotransmitter acetylcholine

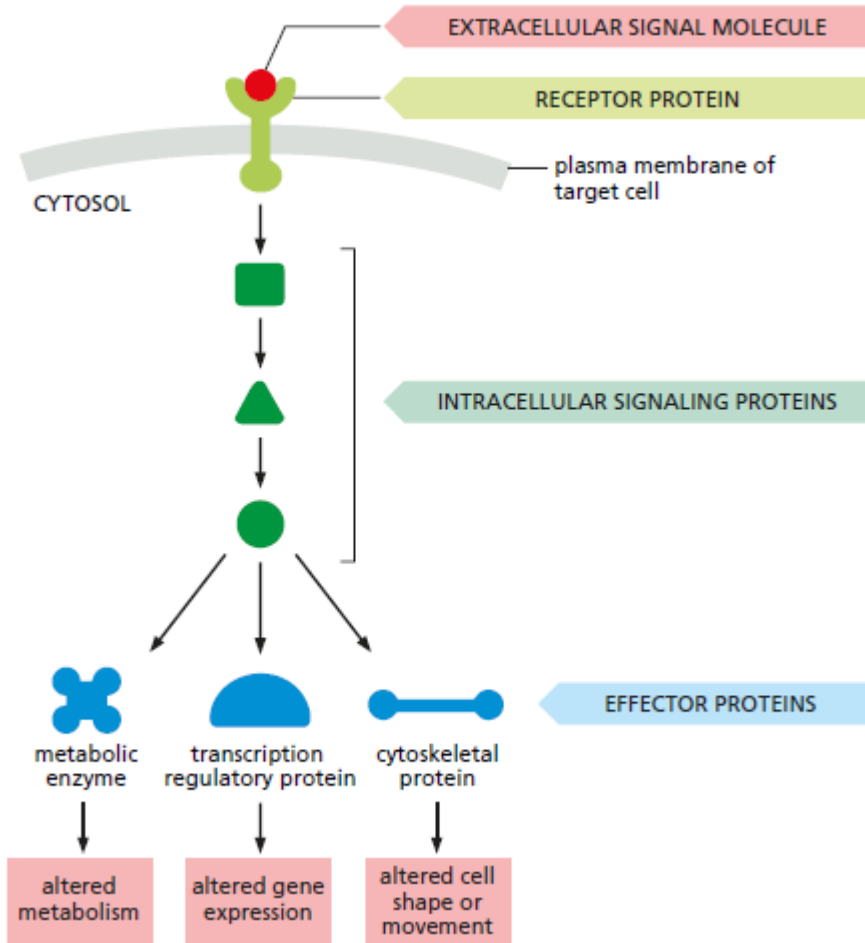


DECREASED RATE
OF FIRING

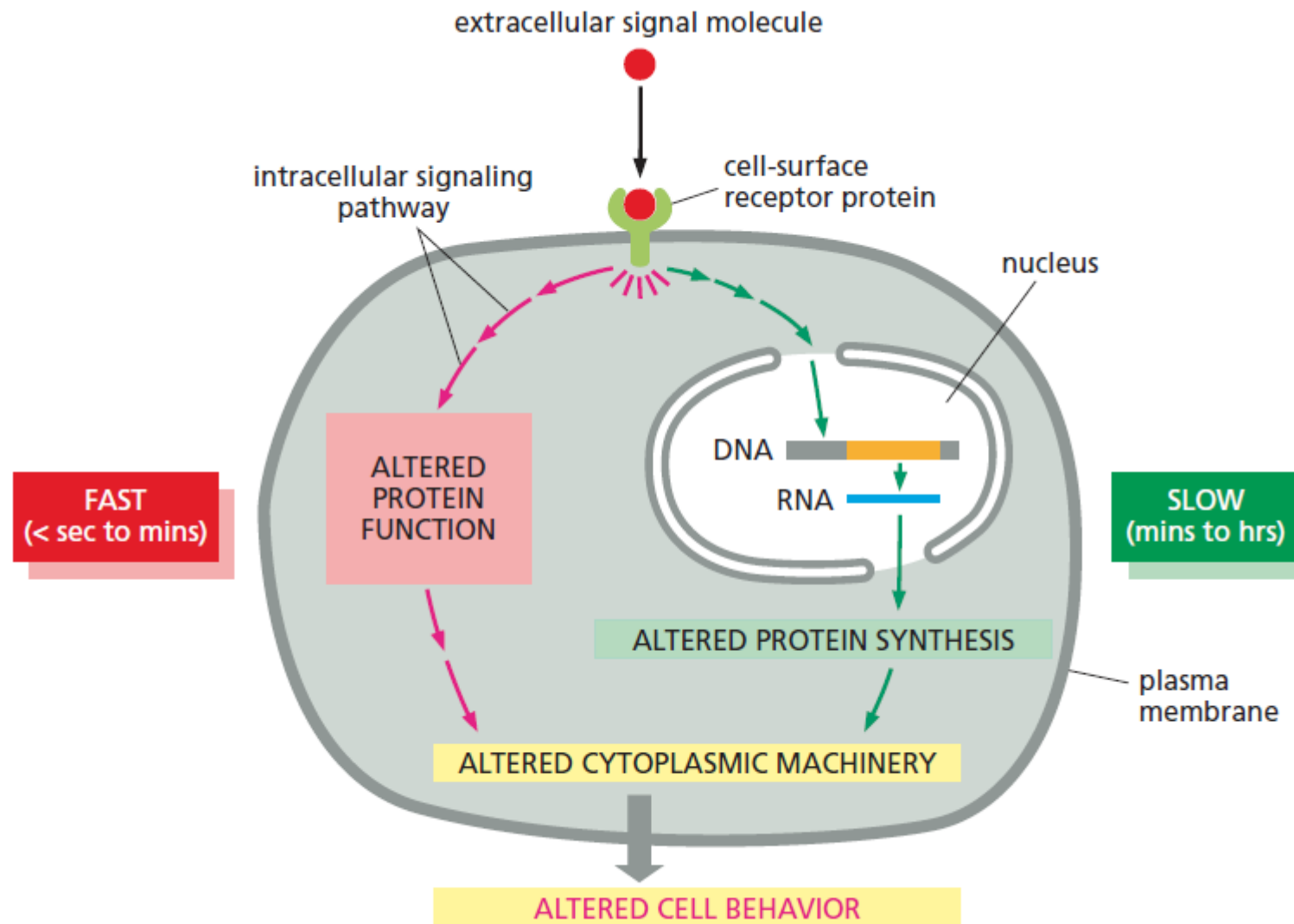
SECRETION

CONTRACTION

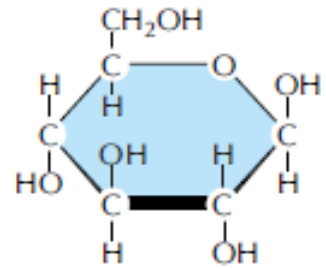
A simple intracellular signaling pathway activated by an extracellular signal molecule



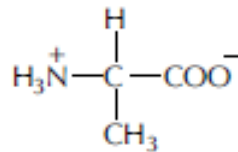
Extracellular signals can act slowly or rapidly



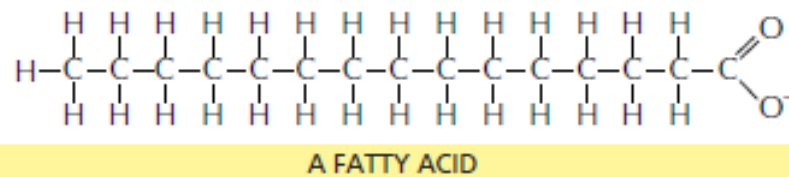
System components



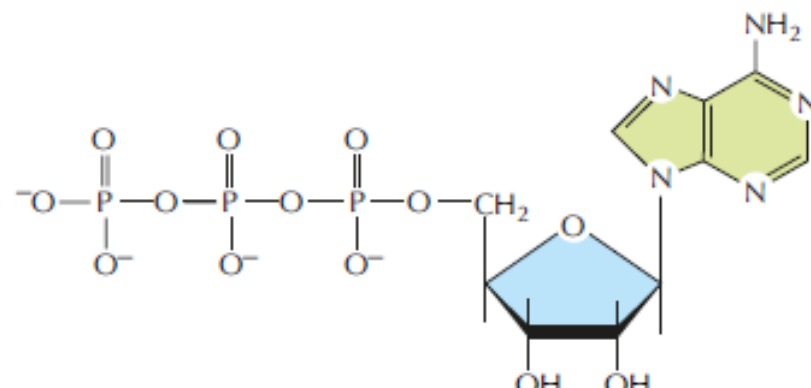
A SUGAR



AN AMINO ACID



A FATTY ACID



A NUCLEOTIDE

small organic building blocks
of the cell

SUGARS

FATTY ACIDS

AMINO ACIDS

NUCLEOTIDES

larger organic molecules
of the cell

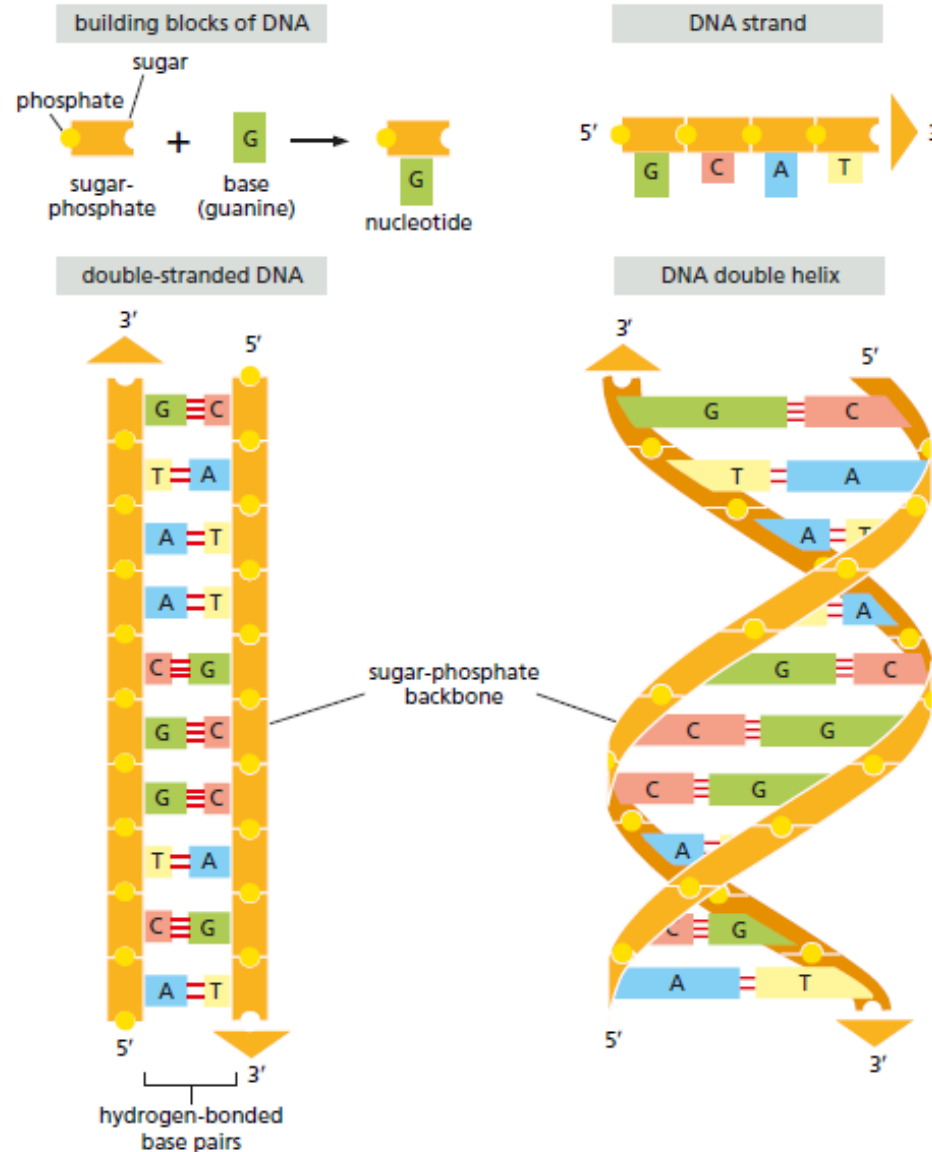
POLYSACCHARIDES, GLYCOGEN,
AND STARCH (IN PLANTS)

FATS AND MEMBRANE LIPIDS

PROTEINS

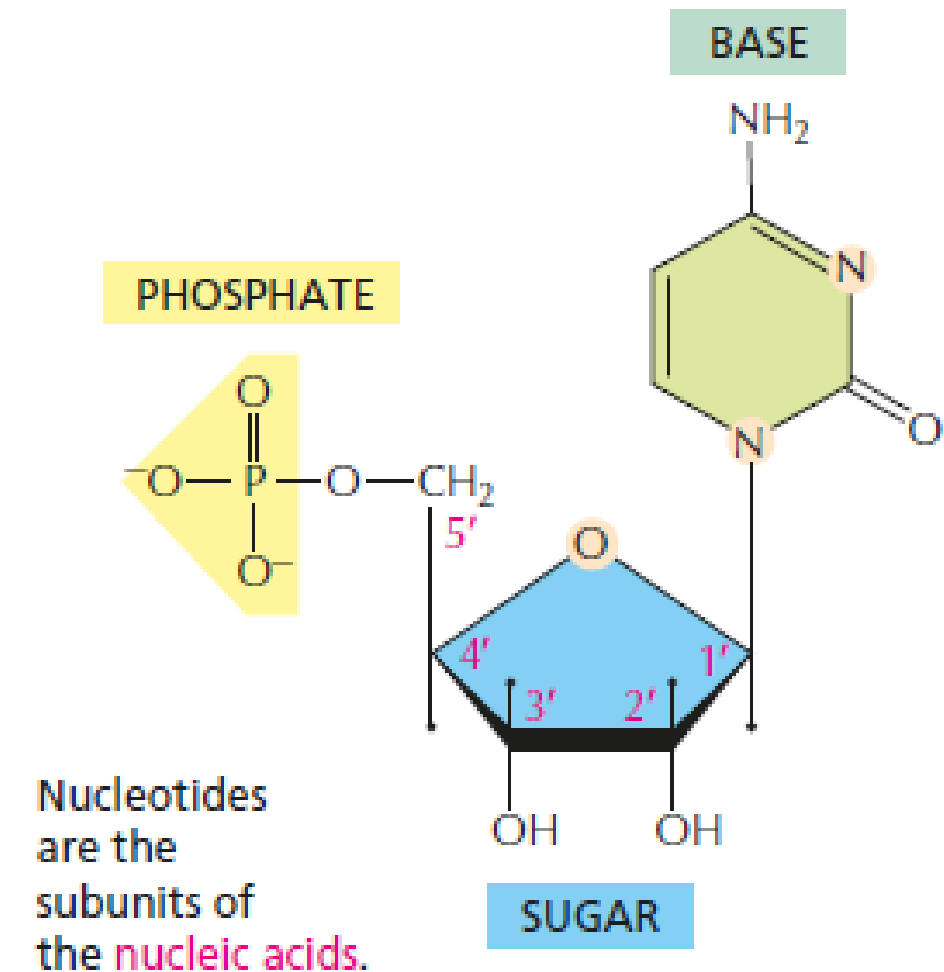
NUCLEIC ACIDS

DNA and its building blocks

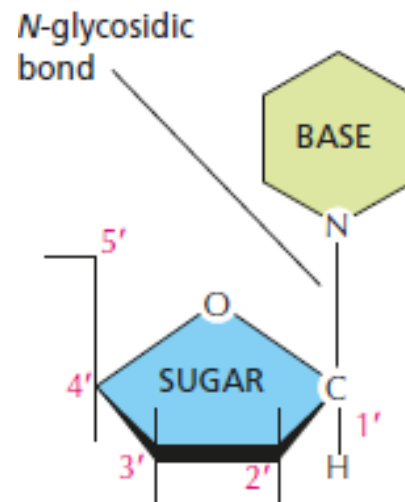


Nucleotides

A nucleotide consists of a nitrogen-containing base, a five-carbon sugar, and one or more phosphate groups.



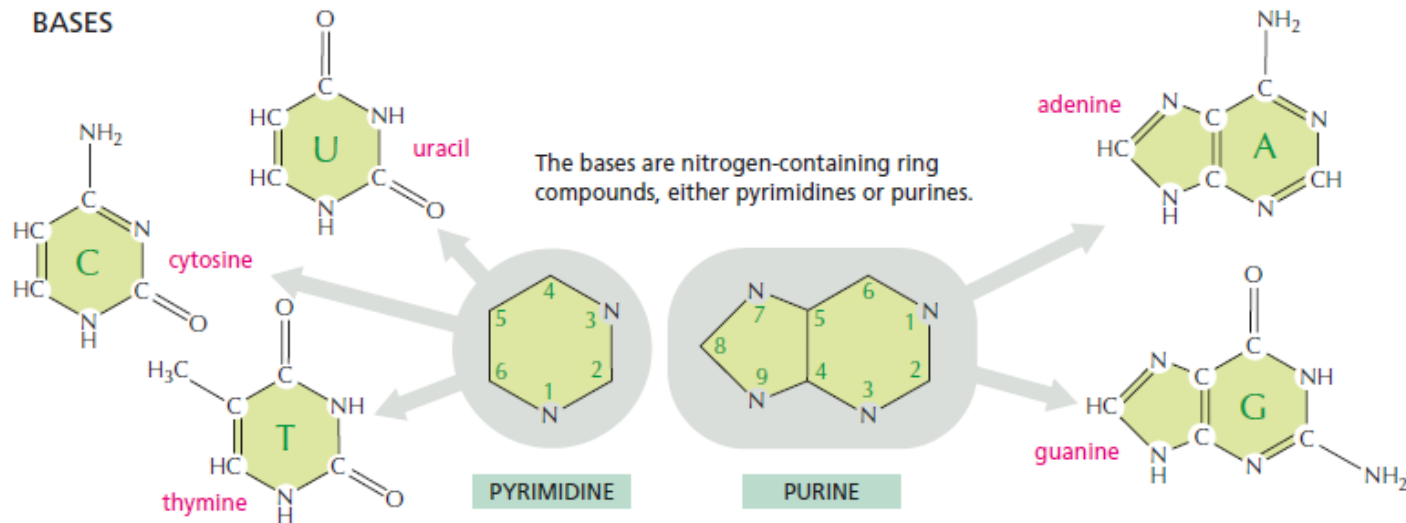
BASE–SUGAR LINKAGE



The base is linked to the same carbon (C1) used in sugar–sugar bonds.

Nucleotides

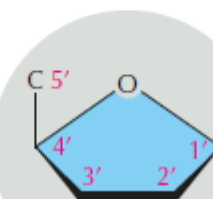
BASES



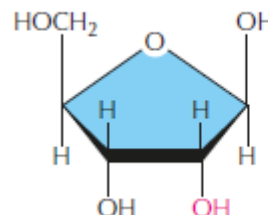
SUGARS

PENTOSE

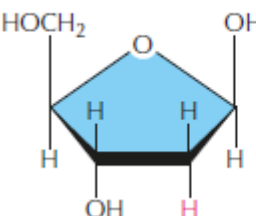
a five-carbon sugar



two kinds of pentoses are used



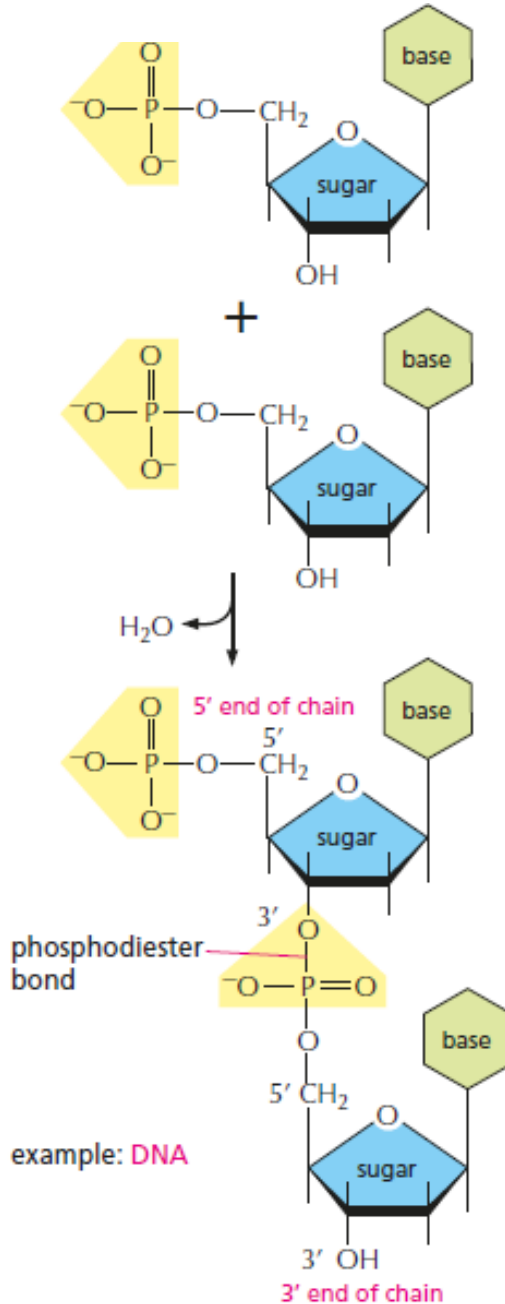
β -D-ribose
used in ribonucleic acid (RNA)



β -D-2-deoxyribose
used in deoxyribonucleic acid (DNA)

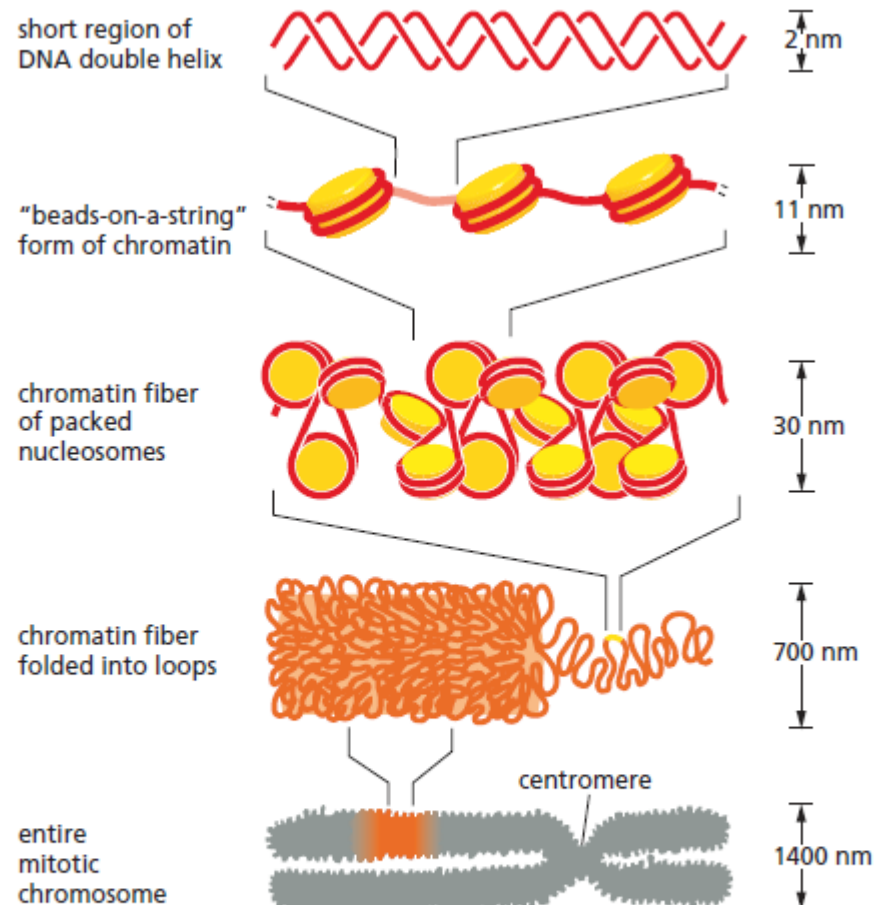
Each numbered carbon on the sugar of a nucleotide is followed by a prime mark; therefore, one speaks of the "5-prime carbon," etc.

Nucleic Acids

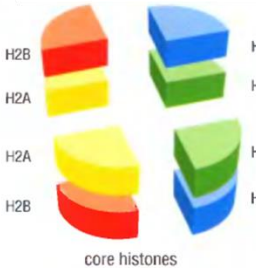
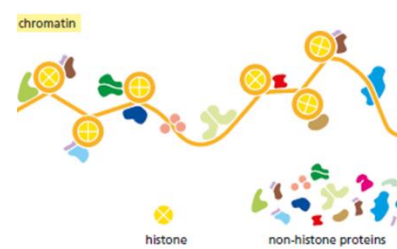


Nucleotides are joined together by phosphodiester bonds between 5' and 3' carbon atoms of the sugar ring, via a phosphate group, to form nucleic acids. The linear sequence of nucleotides in a nucleic acid chain is commonly abbreviated by a one-letter code, such as AGCTTACA, with the 5' end of the chain at the left.

The organization of Chromosomes



NET RESULT: EACH DNA MOLECULE HAS BEEN
PACKAGED INTO A MITOTIC CHROMOSOME THAT
IS 10,000-FOLD SHORTER THAN ITS FULLY
EXTENDED LENGTH

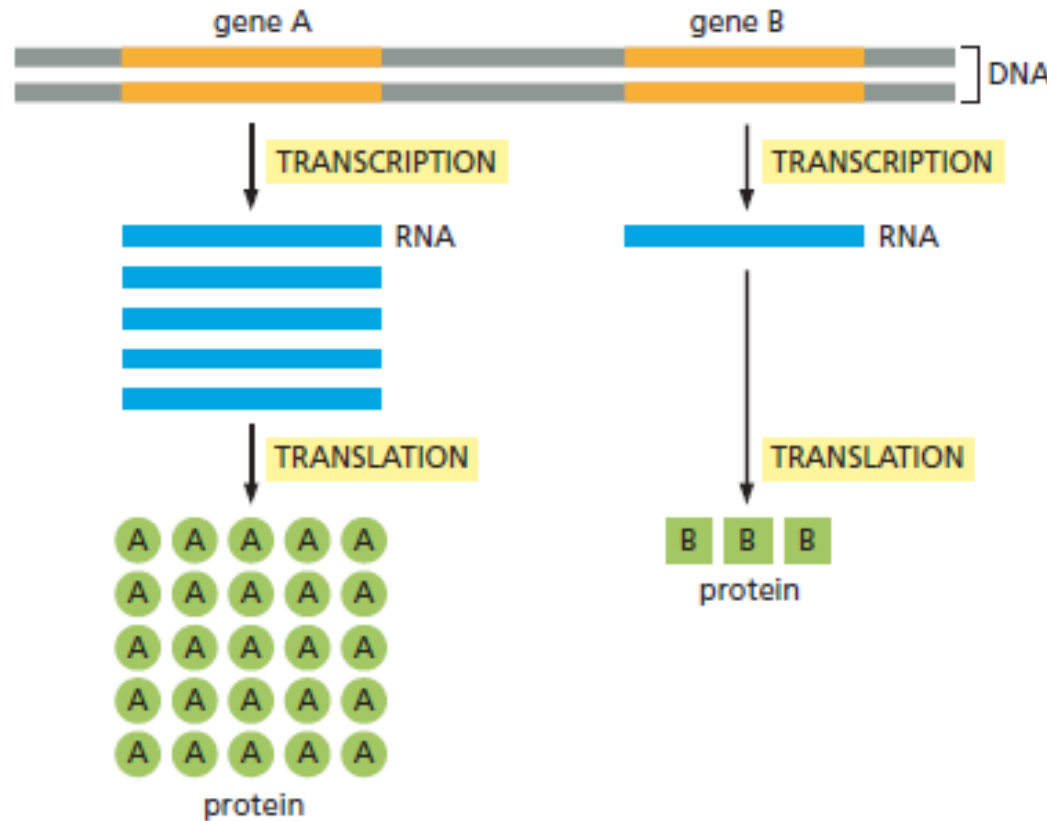


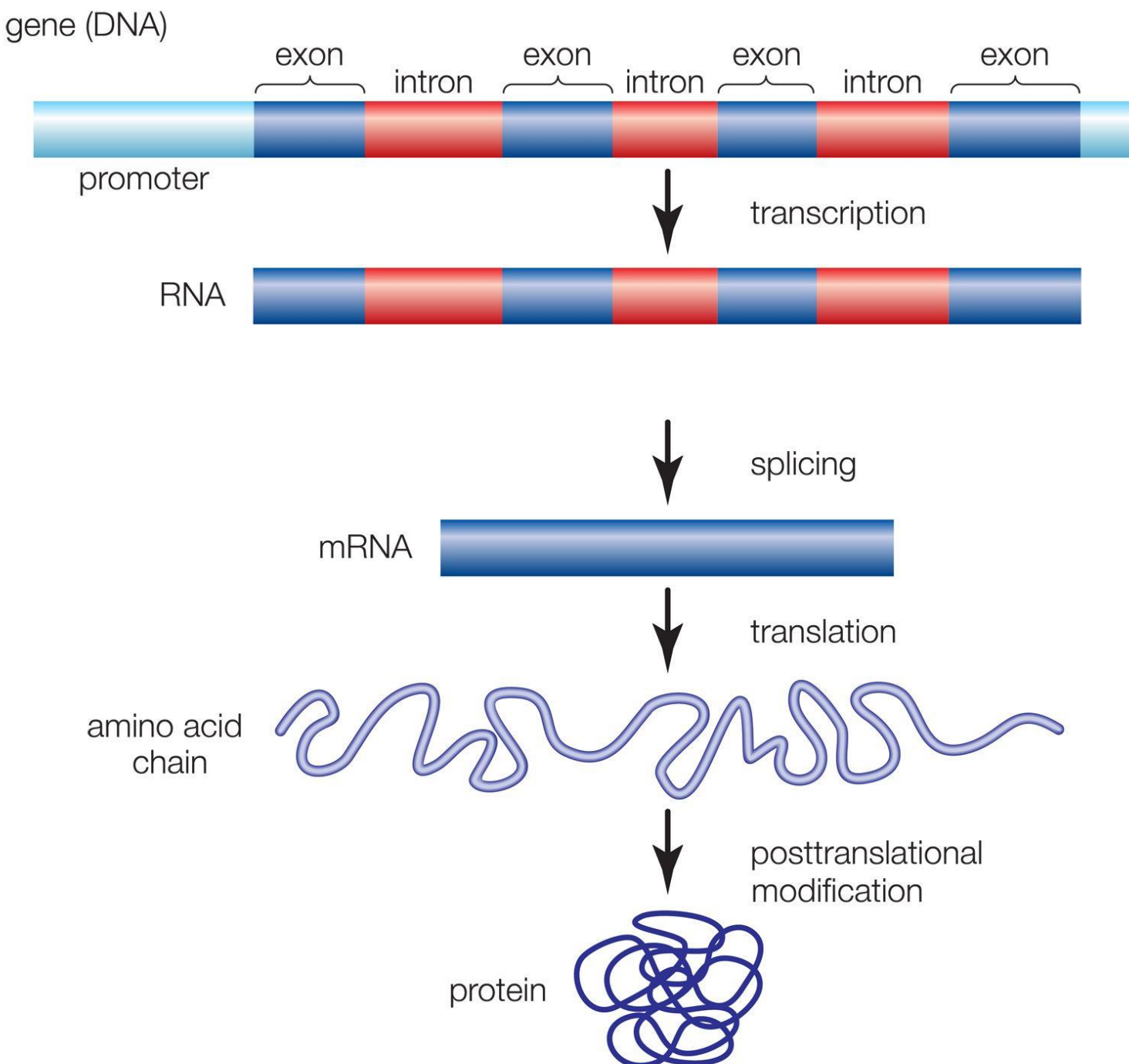
beads on a string - Nucleosome

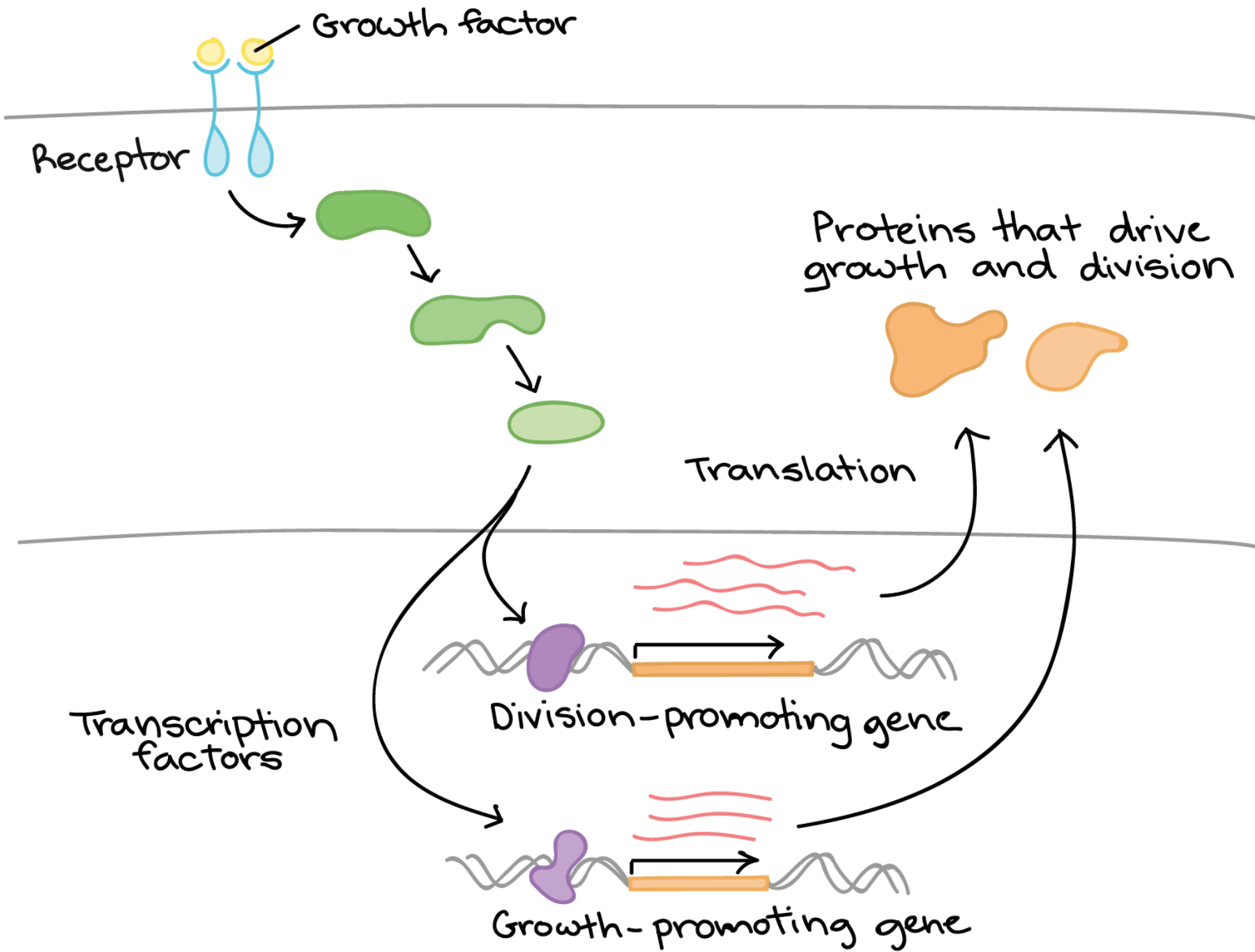
147 nucleotide pairs long makes 1.7 turns around each protein core



How Cells Read the Genome

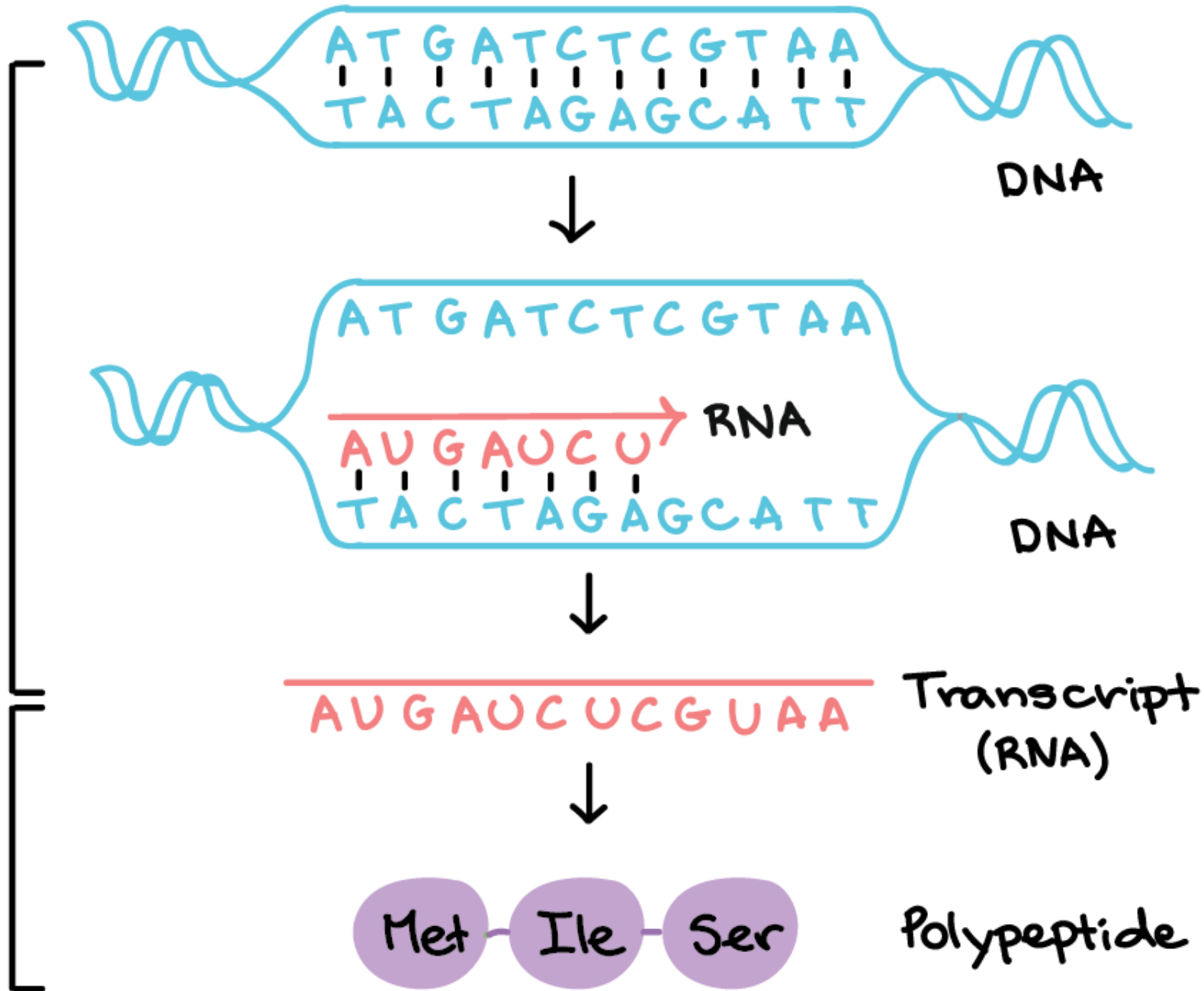






Transcription

Translation



From RNA to protein (Translation)

AGA	AGG	GCA	CGA	GCC	CGC	GCG	GGG	GAC	AAC	UGC	GAA	CAA	GGG	CAC	AUC	CUG	AAA	UUA	UUG	CUA	CUU	AGC	AGU	CCA	UCA	ACA	GUA	GUC	UAA
GCU	CGU	GAU	AAU	UGU	GAG	CAG	GGU	CAU	AUU	CUU	AAG	AUG	UUU	CCG	UCG	ACG	UUC	CCU	UCU	ACU	UGG	UAC	GUG	UAG	UAC	GUU	UGA		
Ala	Arg	Asp	Asn	Cys	Glu	Gln	Gly	His	Ile	Leu	Lys	Met	Phe	Pro	Ser	Thr	Trp	Tyr	Val								stop		
A	R	D	N	C	E	Q	G	H	I	L	K	M	F	P	S	T	W	Y	V										

The nucleotide sequence of an mRNA is translated into the amino acid sequence of a protein via the **genetic code**

Each group of three consecutive nucleotides in RNA is called a **codon**

Amino acids

AMINO ACID		SIDE CHAIN		AMINO ACID		SIDE CHAIN	
Aspartic acid	Asp	D	negative	Alanine	Ala	A	nonpolar
Glutamic acid	Glu	E	negative	Glycine	Gly	G	nonpolar
Arginine	Arg	R	positive	Valine	Val	V	nonpolar
Lysine	Lys	K	positive	Leucine	Leu	L	nonpolar
Histidine	His	H	positive	Isoleucine	Ile	I	nonpolar
Asparagine	Asn	N	uncharged polar	Proline	Pro	P	nonpolar
Glutamine	Gln	Q	uncharged polar	Phenylalanine	Phe	F	nonpolar
Serine	Ser	S	uncharged polar	Methionine	Met	M	nonpolar
Threonine	Thr	T	uncharged polar	Tryptophan	Trp	W	nonpolar
Tyrosine	Tyr	Y	uncharged polar	Cysteine	Cys	C	nonpolar

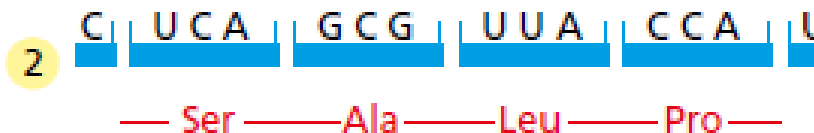
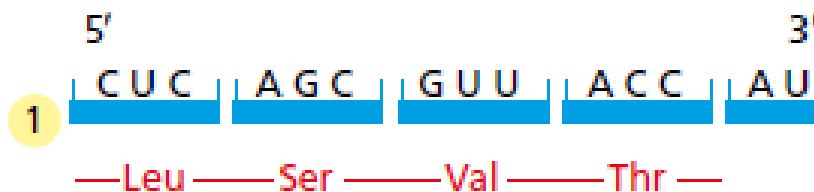
POLAR AMINO ACIDS

NONPOLAR AMINO ACIDS

Six amino acids (CHIMSV), the first letter of the amino acid name is unique

Phonetically suggestive - RFYW: aRginine, Fenylalanine, tYrosine, tWiptophan.

The RNA Message Is Decoded in Ribosomes



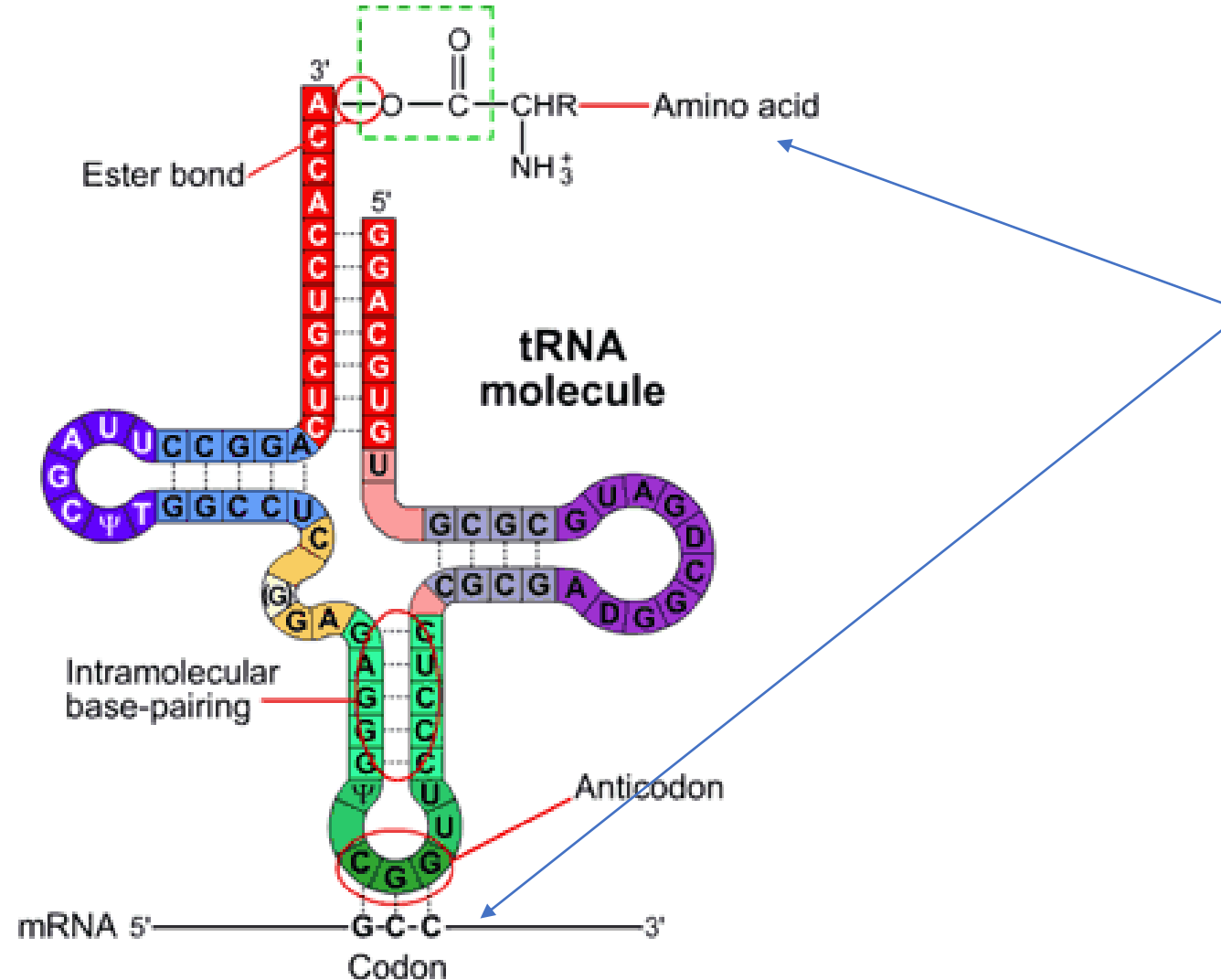
The three possible reading frames in protein synthesis

However, only one of the three possible reading frames in an mRNA encodes the required protein.

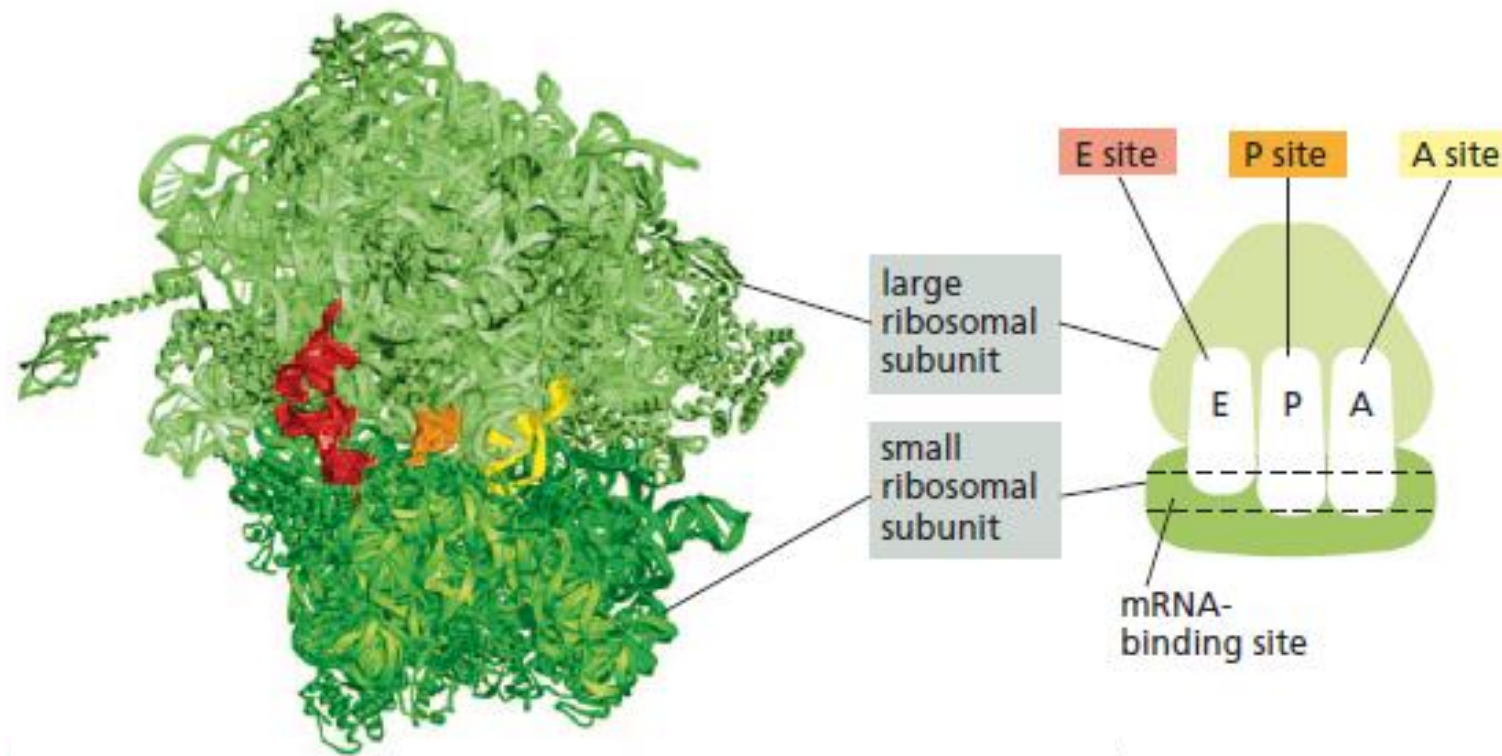
To maintain the correct reading frame and to ensure accuracy (about 1 mistake every 10,000 amino acids), protein synthesis is performed in the ribosome

The match-making is done by tRNA

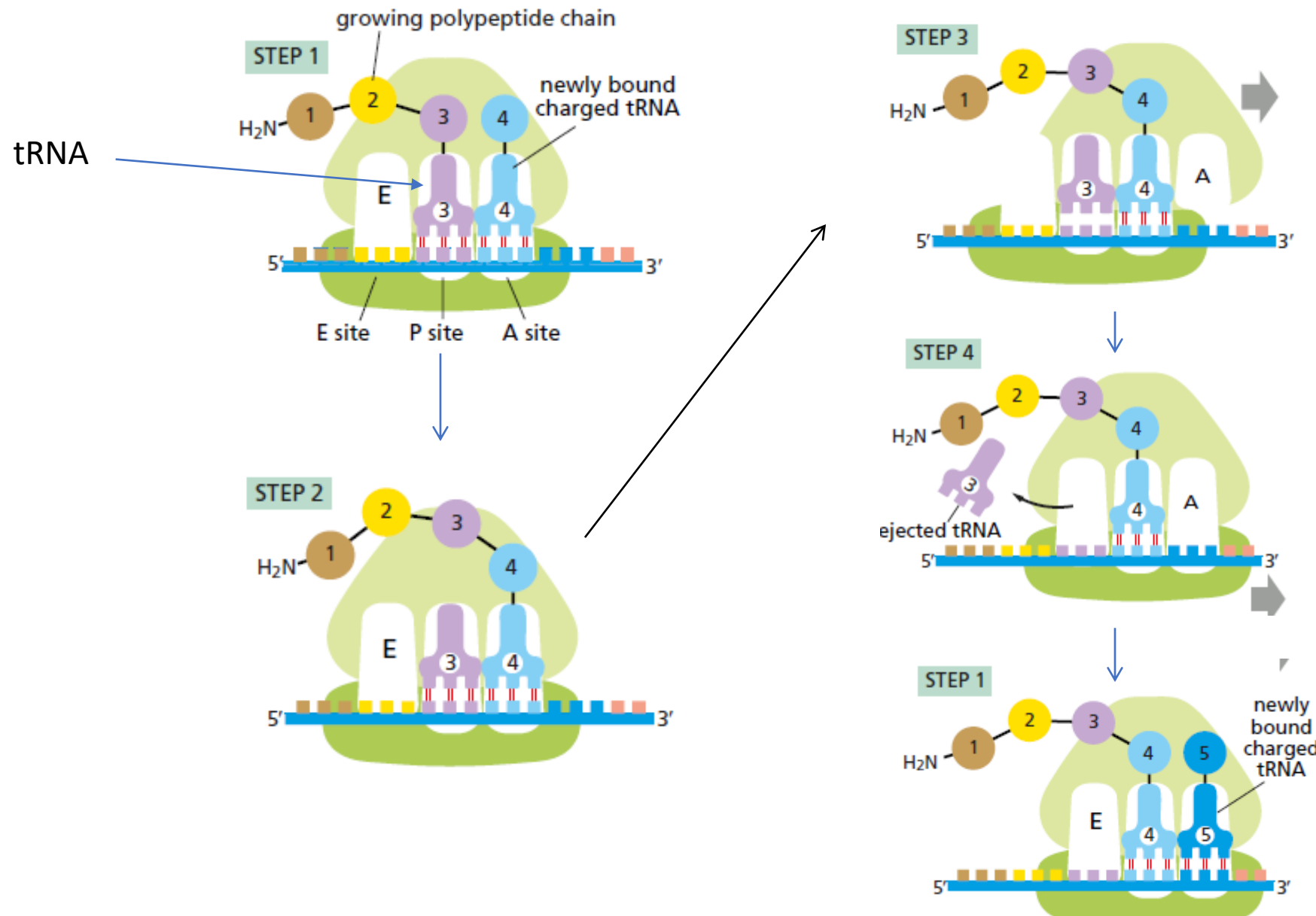
- tRNA recognize the codon through anticodon to bring correct amino acid for peptide bond formation
- There are tRNAs for each amino acids



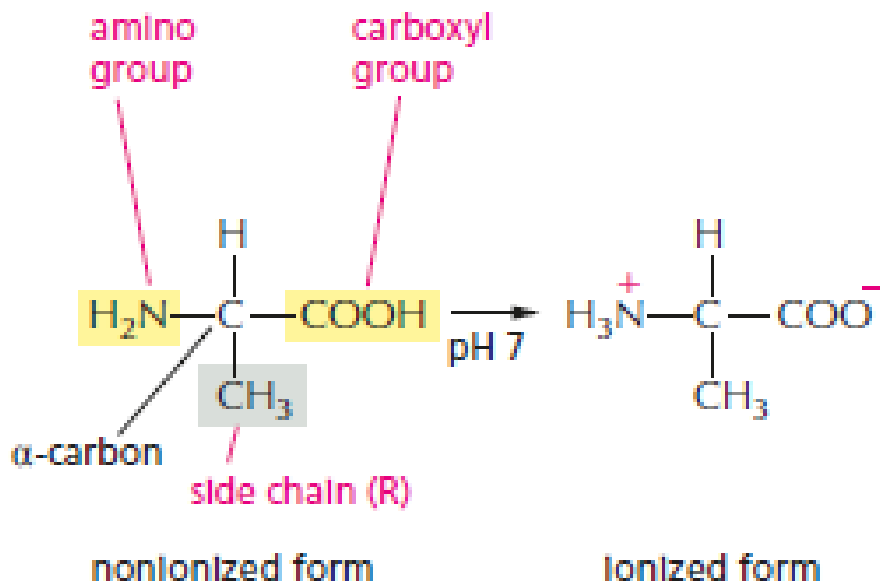
Each ribosome has a binding site for mRNA and three binding sites for tRNA



Translating an mRNA molecule

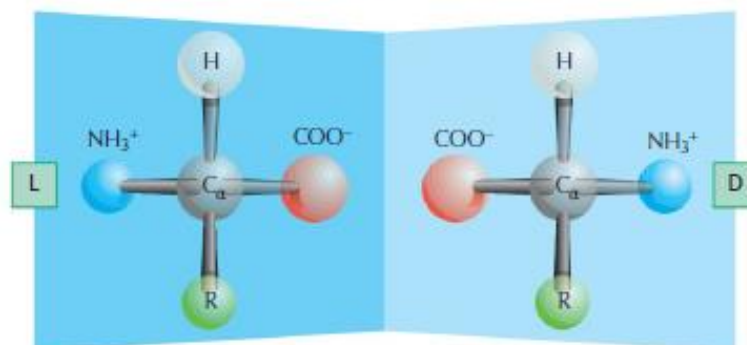


Amino acids



OPTICAL ISOMERS

The α -carbon atom is asymmetric, which allows for two mirror images (or stereo-isomers), L and D.



Proteins consist exclusively of L-amino acids.

FAMILIES OF AMINO ACIDS

The common amino acids are grouped according to whether their side chains are

acidic
basic
uncharged polar
nonpolar

These 20 amino acids are given both three-letter and one-letter abbreviations.

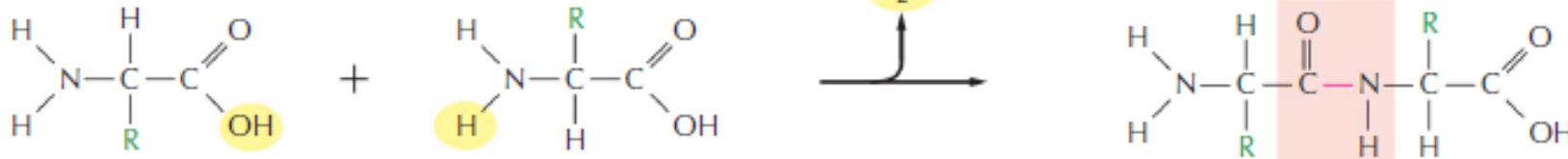
Thus: alanine = Ala = A

Proteins

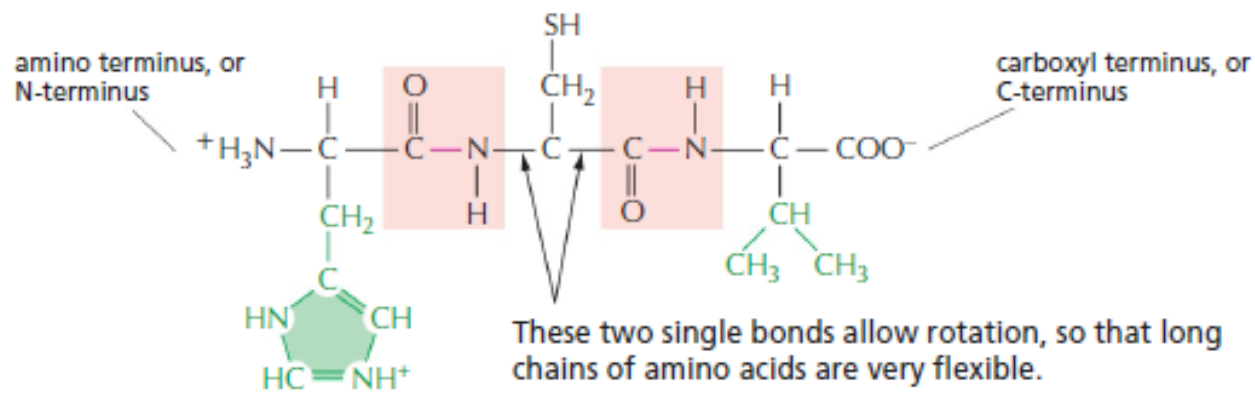
PEPTIDE BONDS

In proteins, amino acids are commonly joined together by an amide linkage, called a peptide bond.

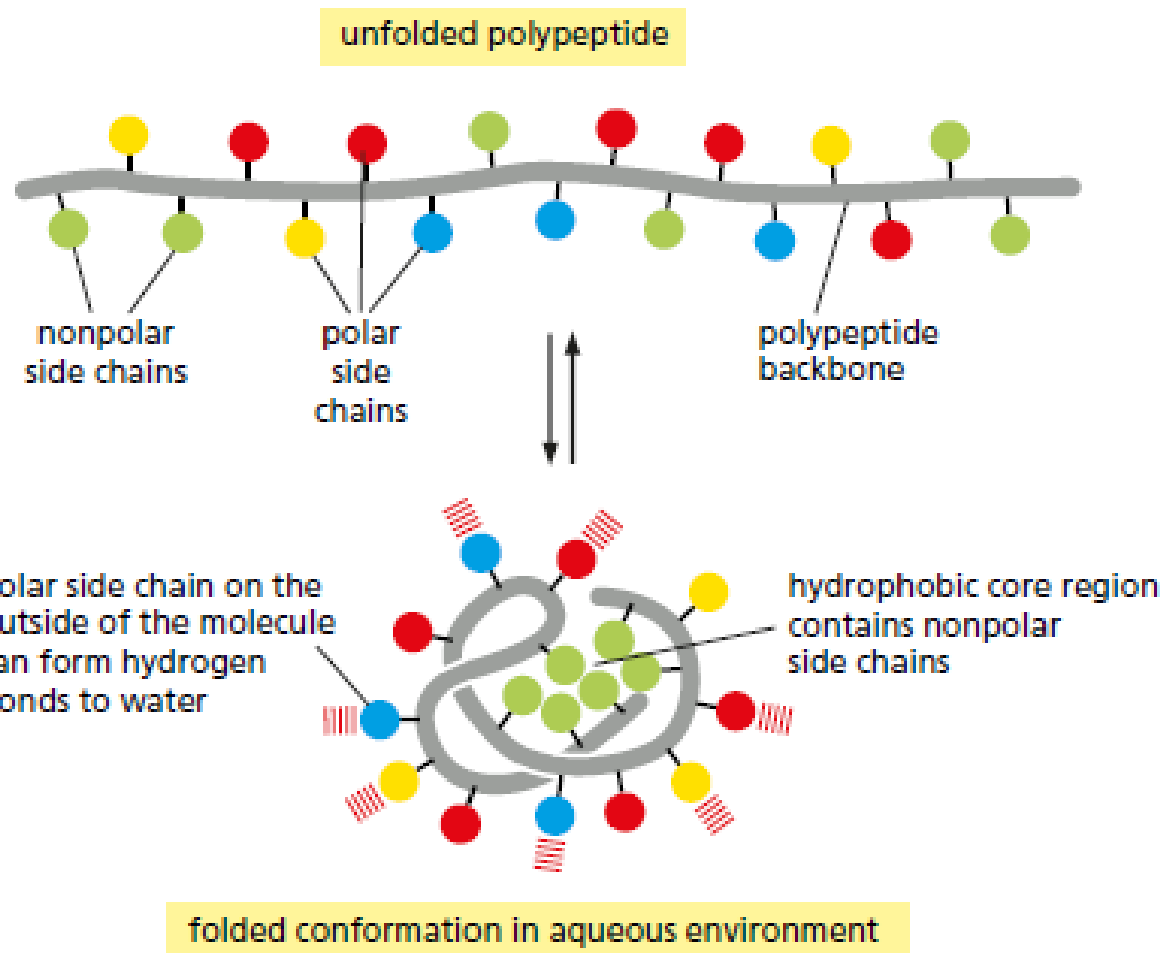
The four atoms in each peptide bond (red box) form a rigid planar unit. There is no rotation around the C-N bond.



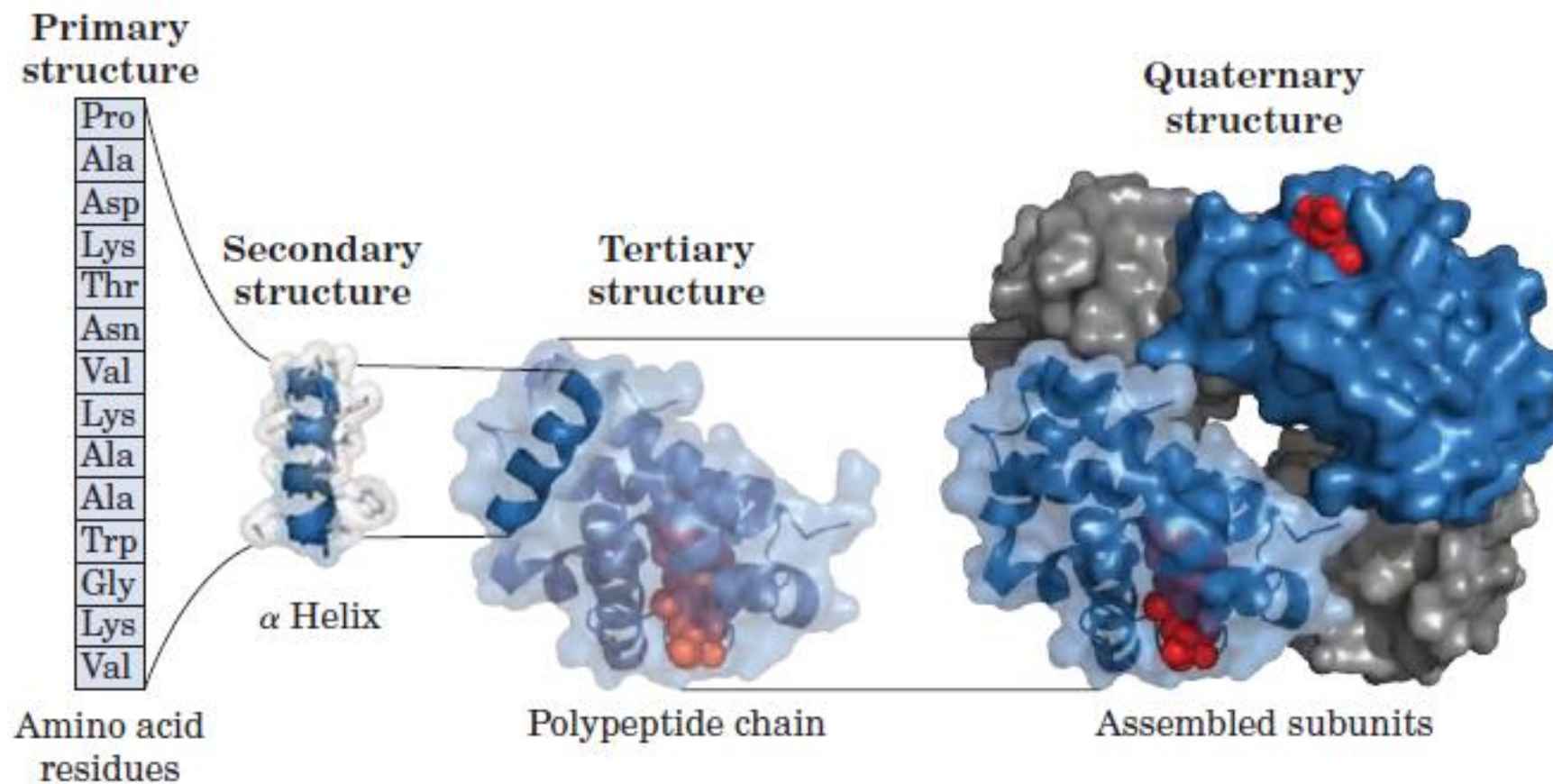
Proteins are long polymers of amino acids linked by peptide bonds, and they are always written with the N-terminus toward the left. **Peptides** are shorter, usually fewer than 50 amino acids long. The sequence of this tripeptide is histidine-cysteine-valine.



How a protein folds into a compact conformation



The Structure of Proteins



The Frequency Dependence of Osmo-Adaptation in *Saccharomyces cerevisiae*

Jerome T. Mettetal,¹ Dale Muzzey,^{1,2} Carlos Gómez-Uribe,^{1,3} Alexander van Oudenaarden^{1*}

The propagation of information through signaling cascades spans a wide range of time scales, including the rapid ligand-receptor interaction and the much slower response of downstream gene expression. To determine which dynamic range dominates a response, we used periodic stimuli to measure the frequency dependence of signal transduction in the osmo-adaptation pathway of *Saccharomyces cerevisiae*. We applied system identification methods to infer a concise predictive model. We found that the dynamics of the osmo-adaptation response are dominated by a fast-acting negative feedback through the kinase Hog1 that does not require protein synthesis. After large osmotic shocks, an additional, much slower, negative feedback through gene expression allows cells to respond faster to future stimuli.

The mechanisms cells use to sense and respond to environmental changes include complicated systems of biochemical reactions that occur with rates spanning a wide dynamic range. Reactions can be fast, such as association and dissociation between a ligand and its receptor (<1 s), or slow, such as protein synthesis (>10³ s). Although a system may comprise hundreds of reactions, often only a few of them dictate the system dynamics. Unfortunately, identification of the dominant processes is often difficult, and many models instead incorporate knowledge of all reactions in the system. Although occasionally successful (1–4), this exhaustive approach often suffers from missing information, such as unknown interactions or parameters.

Here, we used systems-engineering tools to study how oscillatory signals propagate through a signal transduction cascade, which allowed us to identify and to model concisely the interactions that dominate system dynamics. The cornerstone of this approach is to measure the cascade output in response to input signals oscillating at a range of frequencies (5, 6). By comparing the frequency response of the wild-type network to that of mutants, the molecular underpinnings of network dynamics can be determined. Studies of neural and other physiological systems have used systems theory (6), and control theory has also been applied to cellular networks (7–14).

We focused on the high-osmolarity glycerol (HOG) mitogen-activated protein kinase (MAPK) cascade in the budding yeast *Saccharomyces cerevisiae*. This cascade forms a core module of the hyperosmotic shock-response system and is particularly well suited to frequency-response analysis for several reasons. First, both the input

(extracellular osmolyte concentration) and output (activity of the MAPK Hog1) of the network are easily measured and manipulated. Second, the molecular components of the network have been well studied, which facilitates connecting dynamic models with molecular events. Finally, the system contains multiple negative-feedback loops that operate on different time scales (4, 15, 16). It is still unclear which negative-feedback loop or loops dominate the signaling dynamics and whether the different feedback loops have distinct biological functions. We determined the properties of the main negative-feedback loops in

the HOG network and arrived at a concise predictive model of the signaling dynamics. Furthermore, by analyzing the system's dynamics over a range of osmotic-shock strengths, we begin to understand how the multiple-feedback architecture might be beneficial for osmotic homeostasis in fluctuating environments.

After a hyperosmotic shock, membrane proteins trigger a signal transduction cascade that culminates in the activation of the MAPK Hog1, which is primarily cytoplasmic before the osmotic shock (17, 18). When activated, Hog1 accumulates in the nucleus (Fig. 1A), where it activates a broad transcriptional response to osmotic stress (19). Constitutively active phosphatases dephosphorylate and deactivate Hog1, which leads to its export from the nucleus. When osmotic balance is restored, through changes either to the extracellular environment or to the intracellular osmolyte concentration, cascade activity ceases, and the Hog1 nuclear enrichment decreases (Fig. 1A). To estimate the amount of phosphorylated Hog1 in living cells, we simultaneously monitored the cellular localization of Hog1-YFP, a yellow fluorescent protein fused to Hog1, and Nrd1-RFP, a red fluorescent protein fused to a strictly nuclear protein. To quantify Hog1 nuclear localization, we define the function, $R(t) = (\langle YFP \rangle_{\text{nucleus}} / \langle YFP \rangle_{\text{cell}})_{\text{population}}$, as the ratio (averaged over many cells) of mean YFP pixel intensities in the nucleus and the whole cell [(Fig. 1A), red circles].

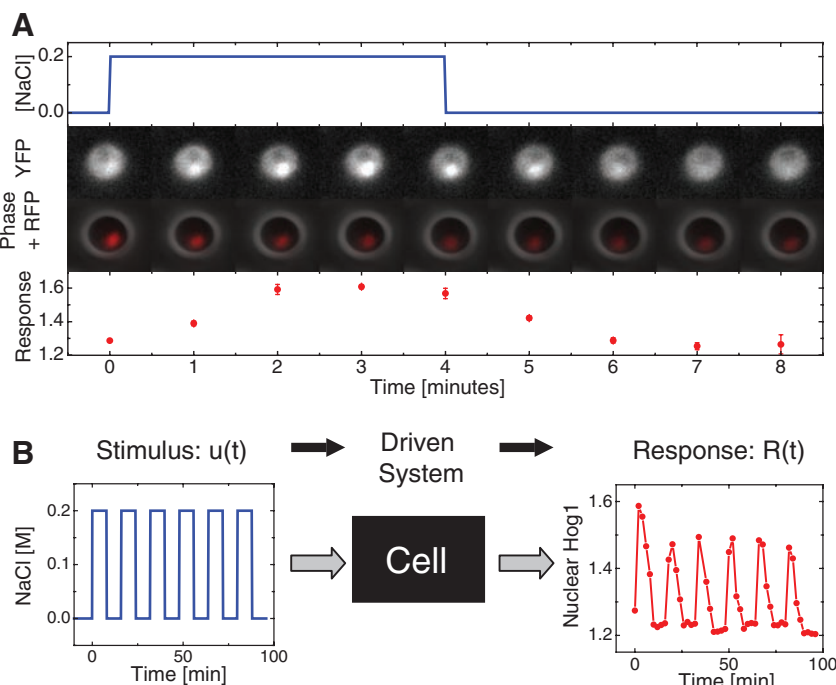


Fig. 1. Enrichment of Hog1 nuclear localization is driven by pulsed salt shocks. **(A)** Localization of the fusion protein Hog1-YFP and the nuclear marker Nrd1-RFP by fluorescence microscopy. We applied and removed NaCl (0.2 M) as shown by the blue line. The population average translocation response (red circles) was defined by the ratio of average YFP fluorescence in the nucleus to the average whole-cell YFP fluorescence. **(B)** Oscillations of Hog1-YFP translocation in a population of cells (red circles) in response to square-wave oscillations in the input of extracellular NaCl (blue line).

¹Department of Physics, Massachusetts Institute of Technology, Cambridge, MA 02139, USA. ²Harvard University Graduate Biophysics Program, Harvard Medical School, Boston, MA 02115, USA. ³Harvard-MIT Division of Health Sciences and Technology, Massachusetts Institute of Technology, Cambridge, MA 02139, USA.

*To whom correspondence should be addressed: E-mail: avano@mit.edu

Cells were periodically shocked in a flow chamber (fig. S1) in which a computer-actuated valve supplied square-wave pulses of medium, with and without 0.2 M NaCl [(Fig. 1B), blue line]. Localization of fluorescent proteins was concurrently imaged [(Fig. 1B), red circles]. Using Fourier analysis (20), we approximated both the input and output signals as sine waves oscillating with a period $T_0 = 2\pi/\omega$ and quantified the output signal by the magnitude of the amplitude (A) at the driving frequency ω and the relative phase

shift $\phi(\omega)$ (Fig. 2A) (21). We measured the response of the system to square-wave stimuli with periods ranging from $T_0 = 2$ min to $T_0 = 128$ min (fig. S2). These responses were analyzed to obtain so-called Bode plots (Fig. 2, B and C) (20), representing the frequency-dependent amplitude $A(\omega)$ and phase $\phi(\omega)$.

We used linear-systems theory to develop a predictive model for the response to arbitrary osmotic input signals $u(t)$ (20). We fitted a general second-order linear time-invariant (LTI)

Fig. 2. Fourier analysis, model fits, and model predictions of Hog1 nuclear enrichment. **(A)** Illustration of the input (NaCl concentration, blue line), the network response (Hog1-YFP translocation, red circles), and the sine wave (black line) corresponding to the Fourier component of the response at the driving frequency ω . This Fourier component is described by three parameters: $A(\omega)$ (green) representing the amplitude of the oscillations, $\phi(\omega)$ (brown) representing the phase delay between the input and the response oscillations, and $y_0(\omega)$ (red) representing the signal offset. **(B)** Measurement of the Fourier amplitude $A(\omega)$ (green dots) over a range of driving frequencies along with model fit (green line). **(C)** Phase of the response measured relative to the driving signal (brown dots) along with model prediction of the phase (brown line). **(D)** Response of the system to a step increase of 0.2 M NaCl compared with the step response predicted by the model. The “low Pbs2” data (boxes) are gathered from the Pbs2 underexpressing mutant strain and were used to generate the model fit [gray line in (B)] and model predictions [gray lines in (C) and (D)].

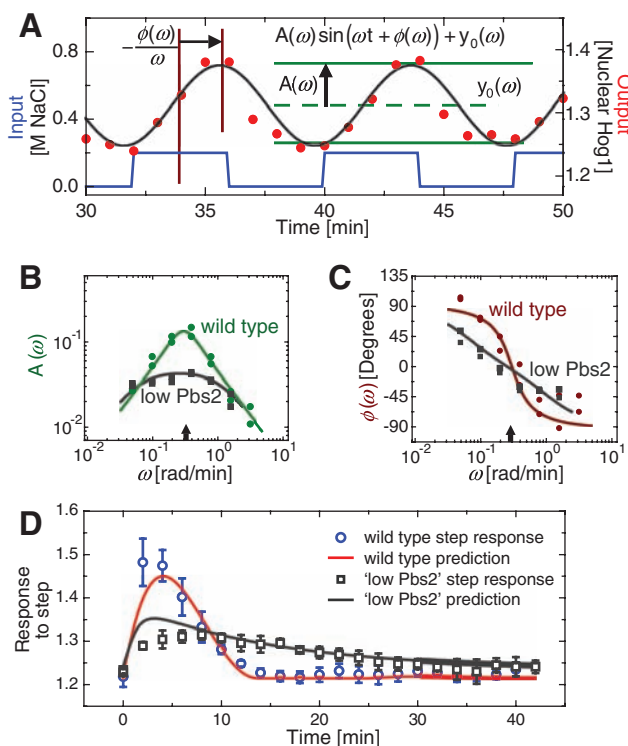


Fig. 3. Network topology implied by pulsed-input analysis corresponds to biological network. **(A)** Diagrammatic representation of the mechanistic model shows two linear negative-feedback responses: one dependent on Hog1 activity with strength β and a second independent of Hog1 activity with strength α . The intracellular osmotic pressure was modeled as an integrator, whereas the MAPK signal transduction pathway was modeled by the linear impulse-response function. The output of circumscribed plus-sign symbols is simply the sum of its inputs. **(B)** The osmo-adaptation network structure. With the induction of osmotic stress, cells increase or decrease their export rate of glycerol through the transmembrane protein Fps1, which is modified by Hog1-independent and Hog1-dependent mechanisms. In addition, under high osmotic stresses, active nuclear Hog1 is known to modify the expression of glycerol-producing proteins over longer time scales. ΔP represents the difference between internal and external pressure relative to its optimal value.

model to the data in Fig. 2B and used the extracted parameters and a simple nonlinear element (20, 22) to predict the response to a step input of 0.2 M NaCl. The model accurately predicted both the response amplitude and the time required to return to basal activity [(Fig. 2D), blue circles].

Because our model was not instructed by knowledge of the underlying biology, we sought to explore how it is similar to and different from the canonical molecular model of the hyperosmotic-shock response. Thus, we converted our LTI model into a model that is more readily interpreted in terms of biological processes (20):

$$\begin{aligned} \dot{y} &= (A_0 u - x) - \gamma y \\ \dot{x} &= \alpha(A_0 u - x) + \beta y \end{aligned} \quad (1)$$

This model contains two negative-feedback loops, which act to reduce the difference, $(A_0 u - x)$, between the stimulus $A_0 u$ and the internal-state variable x . Fig. 3A shows a schematic of the model, and Fig. 3B shows the canonical bio-

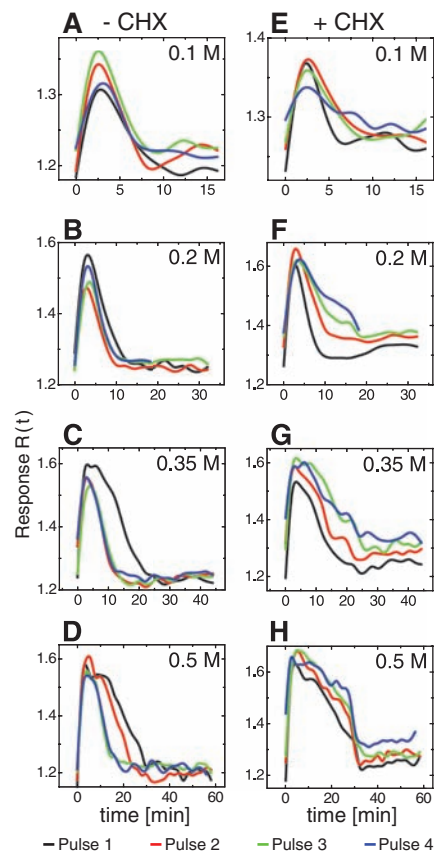


Fig. 4. Gene expression facilitates response to subsequent pulses. Consecutive-pulse responses were compared for cells treated with **(A)** 0.1 M NaCl, 16-min period (i.e., 8 min at 0.1 M followed by 8 min at 0.0 M); **(B)** 0.2 M NaCl, 32-min period; **(C)** 0.35 M NaCl, 45-min period; and **(D)** 0.5 M NaCl, 60-min period. **(E) to (H)** Similarly treated cells also exposed to cycloheximide.

chemical mechanisms that regulate the osmotic-shock response. Because of the high degree of correspondence between our derived model and the extensive Hog1 literature, we interpret the state variable, x , as the intracellular osmolyte concentration and y as enrichment of phosphorylated Hog1 above its baseline level. Thus, interpreted in biological terms, our model predicts that one feedback pathway depends on Hog1-induced glycerol accumulation (i.e., βy changes x through the activity of the observable y), whereas a second glycerol-accumulating pathway is Hog1-independent [i.e., $\alpha(A_0 u - x)$ changes x independently of y].

To gauge the relative strength of the two feedbacks, we applied the same Fourier technique to a mutant strain expressing a reduced amount of Pbs2, the MAPK kinase that phosphorylates Hog1 (Fig. 3B). Because Hog1 is not activated as highly after a hyperosmotic shock in this strain, we can effectively isolate Hog1-dependent feedback from Hog1-independent feedback by comparing the response dynamics (fig. S4) to those of the wild-type strain. Bode plots for this strain were different from those of the wild-type strain (Fig. 2, B and C). Matching the LTI model to the $A(\omega)$ data alone yielded a good fit [(Fig. 2B), black squares], as well as an accurate prediction for the $\phi(\omega)$ data [(Fig. 2C), black squares] and the step response [(Fig. 2D), boxes]. The latter prediction [(Fig. 2D), gray line] reproduced both the reduced maximum response and the slower response dynamics observed in this strain. This suggests that the Hog1-dependent feedback loop plays a major role in rapidly regulating the osmotic-shock response (20).

We compared our model with known biological details of the hyperosmotic-shock response (4, 15, 16). Yeast regulate their intracellular osmolyte concentration through two parallel mechanisms. In a Hog1-independent manner, the membrane protein Fps1 quickly (<2 min) responds by decreasing the glycerol-export rate (23, 24), thereby leading to glycerol retention. Further, active Hog1 increases expression of the glycerol-producing proteins Gpd1 and Gpp2. This raises the intracellular glycerol level over longer time scales (>30 min) (25).

Although the topology of our derived model corresponds closely to that of the known biological system (Fig. 3, A and B), dynamic differences suggest that the current view of the MAPK's

role in osmotic regulation is incomplete. Cells begin to recover from the NaCl pulse within 5 min and are finished responding within 15 min. Both of these time scales are faster than required for gene expression, which is typically greater than 15 min (4). This suggests that both feedback loops in our model control the rapid accumulation of glycerol, consistent with previous reports (23, 24, 26).

Our model suggests that gene expression plays a minimal role in the hyperosmotic-shock response, yet the expression of hundreds of genes changes in response to hyperosmotic shock. We hypothesized that gene expression may be more important as a longer-time scale feedback in this system, so we looked for pulse-to-pulse variability in the response of cells stimulated with periodic pulses of NaCl (fig. S5). Cells were shocked either in the absence (Fig. 4, A to D) or presence (Fig. 4, E to H) of cycloheximide, a small molecule that inhibits protein synthesis. As predicted by the initial data, cells responded very similarly to an initial pulse of osmolyte regardless of their ability to synthesize new proteins (Fig. 4, black lines). Nevertheless, we found that cells stimulated multiple times recovered from each subsequent pulse faster in the absence of cycloheximide and slower in its presence, revealing a longer-time scale component absent from our earlier data. These results suggest that nontranscriptional feedback mediates short-time scale osmolyte accumulation (4, 16, 26, 27), whereas gene expression plays a role in osmolyte production only on longer time scales and for more intense shocks. Accordingly, we found that stronger shocks cause cells to increase their rate of glycerol production (fig. S6) in a manner that depends on gene expression, which permits faster recovery to subsequent fluctuations (28).

These results demonstrate the promise of applying engineering principles to cellular networks, particularly when predicting the response of the system to dynamic stimuli. In more complex systems, measuring the activity level of all relevant state-space variables could help with determining the effective network structure.

References and Notes

- J. J. Tyson, K. Chen, B. Novak, *Nat. Rev. Mol. Cell Biol.* **2**, 908 (2001).
- B. M. Slepchenko, J. C. Schaff, I. Macara, L. M. Loew, *Trends Cell Biol.* **13**, 570 (2003).
- H. Kitano, A. Funahashi, Y. Matsuo, K. Oda, *Nat. Biotechnol.* **23**, 961 (2005).
- E. Klipp, B. Nordlander, R. Kruger, P. Gennemark, S. Hohmann, *Nat. Biotechnol.* **23**, 975 (2005).
- A. V. Oppenheim, A. S. Willsky, I. T. Young, *Signals and Systems* (Prentice-Hall, Englewood Cliffs, NJ, 1983).
- D. T. Westwick, R. E. Kearney, *Identification of Nonlinear Physiological Systems* (IEEE Press, Hoboken, NJ, 2003).
- M. A. Savageau, *Biochemical Systems Analysis: A Study of Function and Design in Molecular Biology* (Addison-Wesley, Reading, MA, 1976).
- S. M. Block, J. E. Segall, H. C. Berg, *Cell* **31**, 215 (1982).
- T. M. Yi, Y. Huang, M. I. Simon, J. Doyle, *Proc. Natl. Acad. Sci. U.S.A.* **97**, 4649 (2000).
- W. Vance, A. Arkin, J. Ross, *Proc. Natl. Acad. Sci. U.S.A.* **99**, 5816 (2002).
- M. Samoilov, A. Arkin, J. Ross, *J. Phys. Chem. A* **106**, 10205 (2002).
- B. P. Ingalls, *J. Phys. Chem. B* **108**, 1143 (2004).
- E. D. Sontag, *Eur. J. Control* **11**, 396 (2005).
- O. Lipan, W. H. Wong, *Proc. Natl. Acad. Sci. U.S.A.* **102**, 7063 (2005).
- S. Hohmann, *Microbiol. Mol. Biol. Rev.* **66**, 300 (2002).
- P. Gennemark, B. Nordlander, S. Hohmann, D. Wedelin, *In Silico Biol.* **6**, 193 (2006).
- P. Ferrigno, F. Posas, D. Koepf, H. Saito, P. A. Silver, *EMBO J.* **17**, 5606 (1998).
- V. Reiser, H. Ruis, G. Ammerer, *Mol. Biol. Cell* **10**, 1147 (1999).
- F. Posas et al., *J. Biol. Chem.* **275**, 17249 (2000).
- Details are available in the supporting materials on Science Online.
- In principle, both the input and output signals also contain higher-frequency components. Nevertheless, here we focus on the driving frequency alone in order to simplify analysis while obtaining significant information about the signal's strength and timing.
- The linear model is related to measured outputs using the formulas $R_{\text{model}}(t) = f_{\text{nl}}[y(t)] + R_0$ and $f_{\text{nl}}(y) = y(t) + ly(t)$ (fig. S3).
- K. Luyten et al., *EMBO J.* **14**, 1360 (1995).
- M. J. Tamas et al., *Mol. Microbiol.* **31**, 1087 (1999).
- J. Albertyn, S. Hohmann, J. M. Thevelein, B. A. Prior, *Mol. Cell. Biol.* **14**, 4135 (1994).
- M. Thorsen et al., *Mol. Biol. Cell* **17**, 4400 (2006).
- M. Proft, K. Struhl, *Cell* **118**, 351 (2004).
- M. Krantz et al., *Eukaryot. Cell* **3**, 1381 (2004).
- We thank J. Falvo, R. Tsien, and E. O'Shea for suggesting and providing Nrd1-RFP as a nuclear marker and E. Sontag, S. Hohmann, K. Maclean, and A. Raj for helpful discussions. Supported by NSF grant PHY-0548484 and NIH grants R01-GM068957 and 5 R90 DK071511-01, NSF Graduate Research Fellowships to J.T.M. and D.M., and an MIT-Merck Graduate Fellowship to C.G.-U.

Supporting Online Material

www.sciencemag.org/cgi/content/full/319/5862/482/DC1

Materials and Methods

SOM Text

Figs. S1 to S7

Table S1

References

10 October 2007; accepted 11 December 2007

10.1126/science.1151582

The Frequency Dependence of Osmo-Adaptation in *Saccharomyces cerevisiae*

Jerome T. Mettetal, Dale Muzzey, Carlos Gómez-Uribe and Alexander van Oudenaarden

Science 319 (5862), 482-484.
DOI: 10.1126/science.1151582

ARTICLE TOOLS

<http://science.sciencemag.org/content/319/5862/482>

SUPPLEMENTARY MATERIALS

<http://science.sciencemag.org/content/suppl/2008/01/24/319.5862.482.DC1>

RELATED CONTENT

<http://science.sciencemag.org/content/sci/319/5862/417.full>
<http://stke.sciencemag.org/content/sigtrans/1/4/ec39.abstract>
<http://stke.sciencemag.org/contenthttp://stke.sciencemag.org/cgi/content/abstract/sigtrans;1/4/ec39>

REFERENCES

This article cites 22 articles, 10 of which you can access for free
<http://science.sciencemag.org/content/319/5862/482#BIBL>

PERMISSIONS

<http://www.sciencemag.org/help/reprints-and-permissions>

Use of this article is subject to the [Terms of Service](#)

Science (print ISSN 0036-8075; online ISSN 1095-9203) is published by the American Association for the Advancement of Science, 1200 New York Avenue NW, Washington, DC 20005. The title *Science* is a registered trademark of AAAS.

American Association for the Advancement of Science

Universal features of sensory system

- ↳ Adaptation (sniffer)
- ↳ Ability to sense relative changes

Incoherent feed forward loop

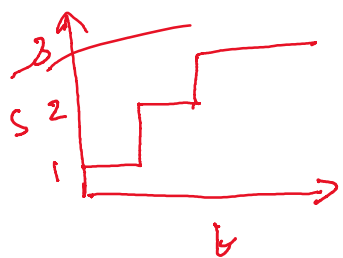
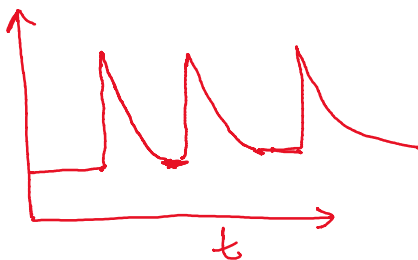
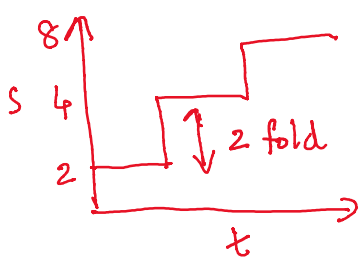


Weber's law

$$\Delta x = k \cdot x_0 \quad (x_0 = \text{initial})$$

\downarrow

$\Delta x \Rightarrow \text{difference}$



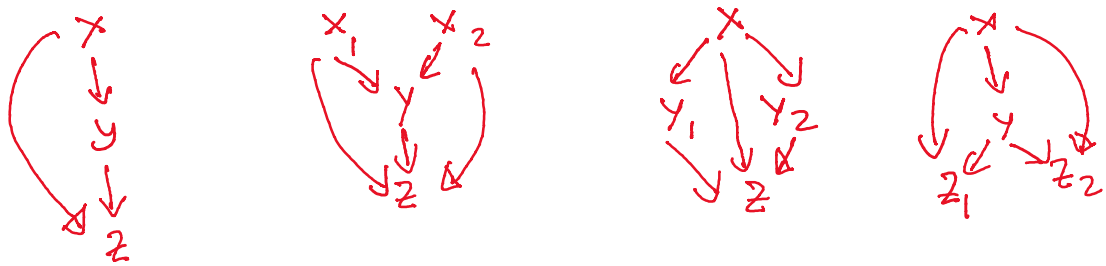
Adaptation is a requirement for fold detection

$$\frac{dz}{dt} = k_z \cdot \left(\frac{x}{y} \right) - k_{dz} \cdot z \quad [\text{fold detection}]$$

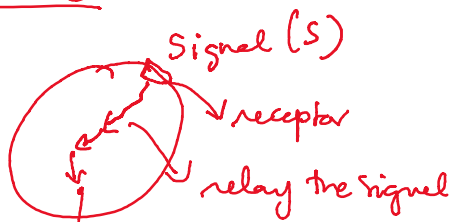
$$\frac{dx}{dt} = k_x \cdot x - k_{dx} \cdot z \cdot y \quad [\text{Adaptation}]$$

Fold detection \rightarrow Adaptation

3 Component System



Signalling

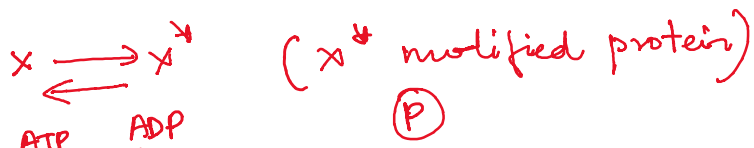
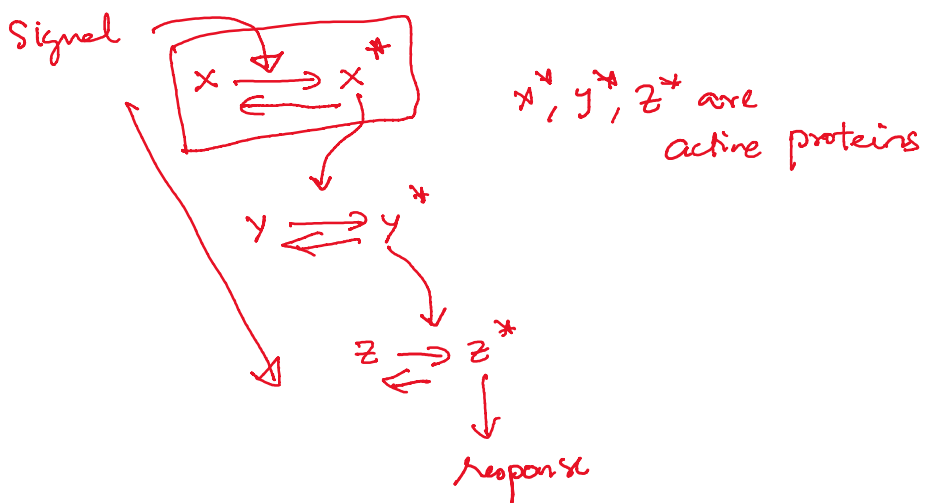


final response

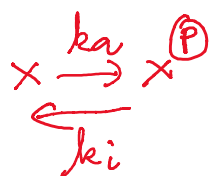
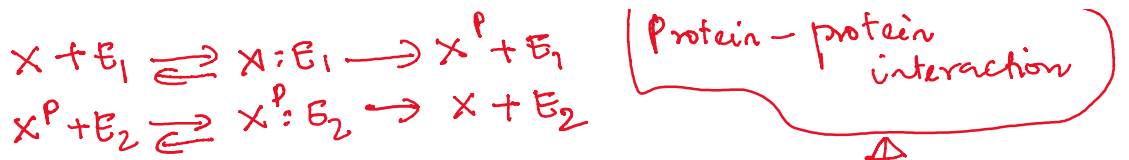
↳ protein which is synthesized (slow)
(S)

↳ protein localization

↳ protein becomes active/inactive
(fast)



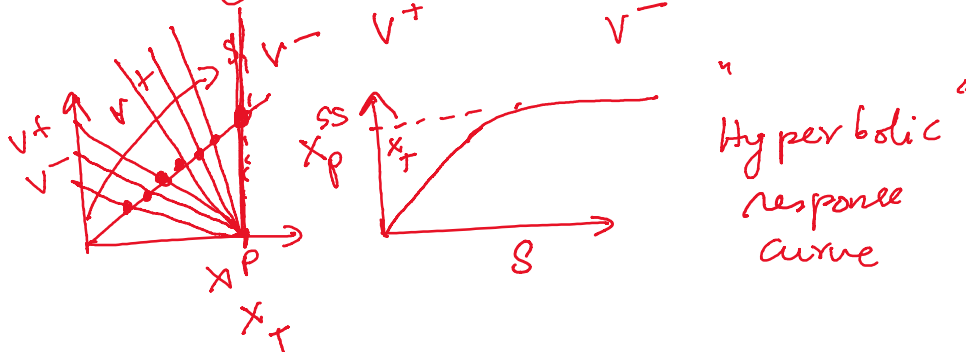
$x \xrightarrow{\text{E}_1} x^*$
 $x^* \xrightarrow{\text{E}_2} x$
 E_1, E_2 are enzymes



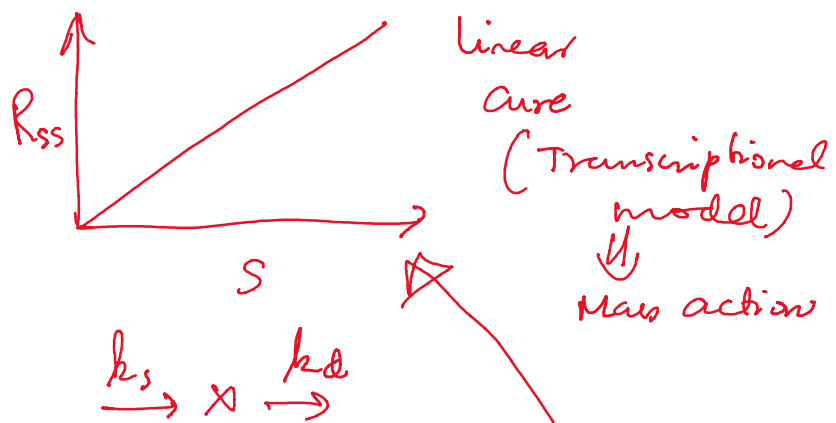
$$\frac{dx^P}{dt} = k_a \cdot x - k_i \cdot x^P$$

$x_T \Rightarrow$ total concentration of X
 $x_T = x + x^P$ (mass balance)

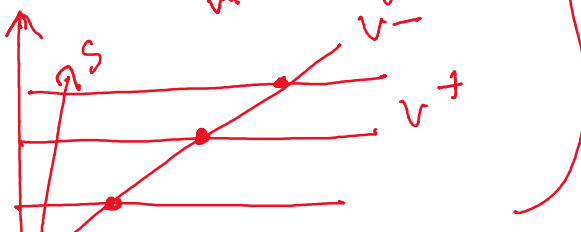
$$\frac{dx^P}{dt} = k_a \cdot (x_T - x^P) - k_i \cdot x^P$$



Protein-DNA interaction



$$\frac{dx}{dt} = k_s - k_d \cdot x$$



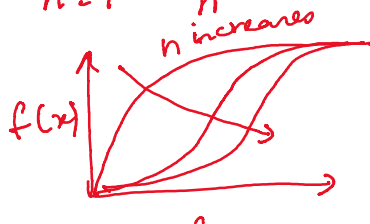


$$f(x) = \frac{s^n}{s^n + K^n} \quad (\text{Hill function})$$

$n > 1 \Rightarrow$ ultrasensitive

$n \ll 1 \Rightarrow$ Subsensitive

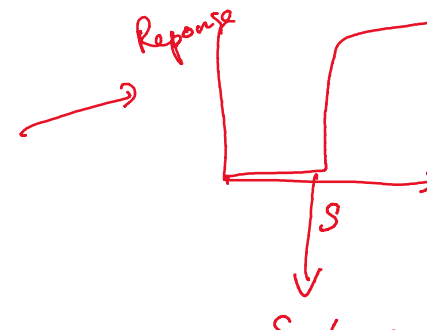
$n = 1$ hyperbolic



Molecular mechanism \Rightarrow Switch-like characteristics

ON/OFF (Buzzer)

Toggle switches



Kinetics

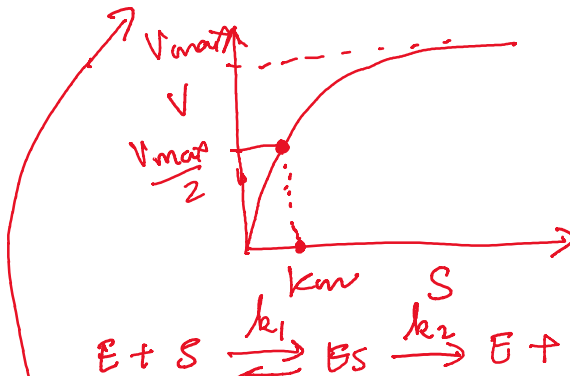
Mass action

↓
Hill function (Transcriptional activation/inactivation)

↓
Michaelis-Menten kinetics (Hill function with $n = 1$)

$$V = \frac{V_{\max} \cdot S}{K_m + S}$$

(Enzyme kinetics)



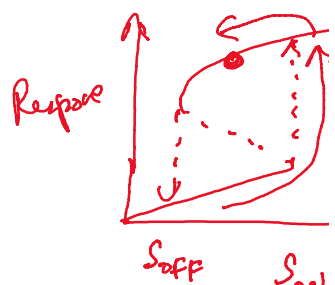
$$V_{\max} = k_2 \cdot C_T$$

S = Substrate

(protein) \Rightarrow protein-protein graph

(Metabolite)

e.g.: glucose \Rightarrow metabolic g



$$\frac{d[\text{ES}]}{dt} = (k_2) (\text{E})(\text{s}) - k_{-1} \cdot [\text{ES}] - k_1 \cdot [\text{ES}]$$

$$\frac{d[\text{s}^P]}{dt} = k_1 \cdot [\text{ES}] \quad E_T = E + [\text{ES}]$$

$$V_{\max} = k_2 \cdot E_T \quad K_m = \frac{k_1 + k_2}{k_{-1}}$$

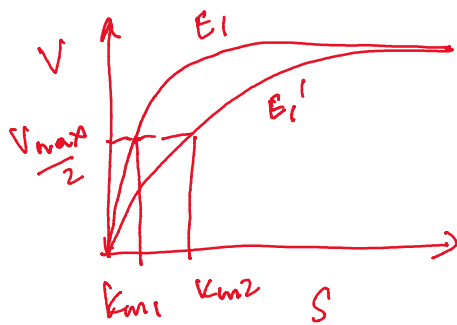
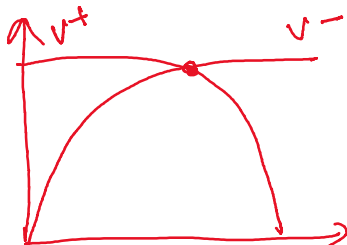


$$\frac{dx^P}{dt} = k_a \cdot \frac{(x_T - x^P)}{K_m + (x_T - x^P)} - k_i \cdot \frac{x^P}{K_m + x^P}$$

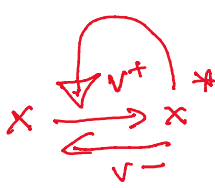
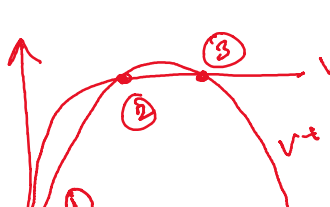
$x_T = x + x^P$

$$\frac{dx^P}{dt} = k_a \cdot (x_T - x^P) - k_i \cdot x^P$$

Goldbeter model (1981)



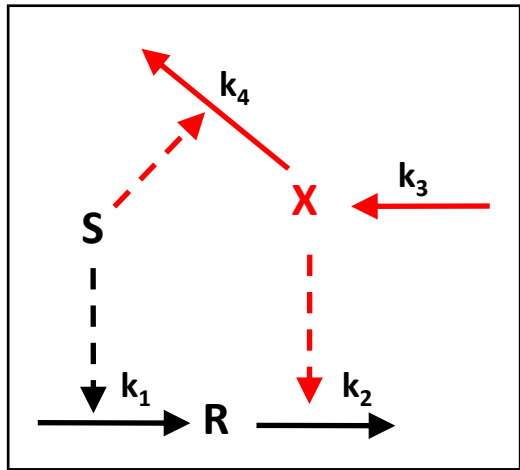
Lisman model (1985)



v^z auto phosphorylating kinase

~~Ca²⁺~~ → (Ca²⁺)^{in brain})
①, ③ stable ⇒ Distable
② Unstable
↓
Calmodulin kinase

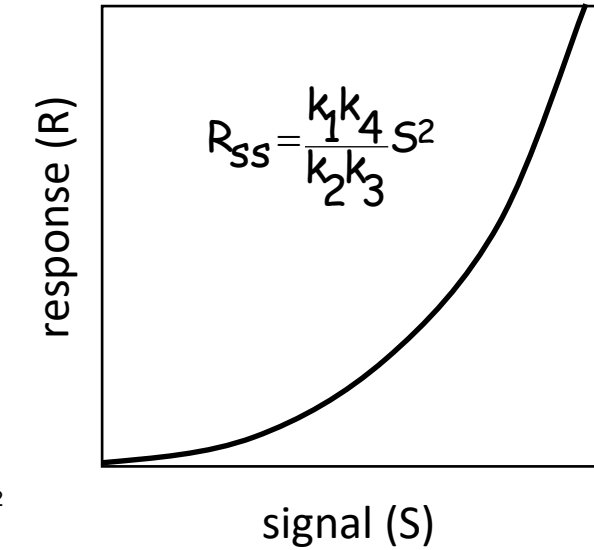
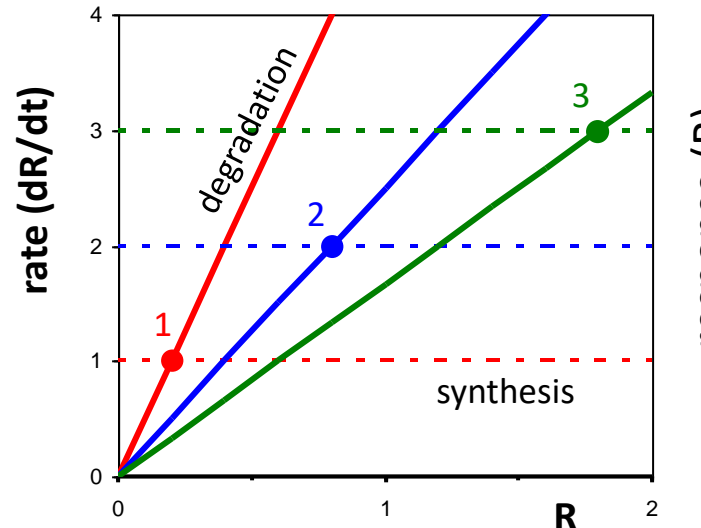
More examples for ultrasensitivity: two linear modules



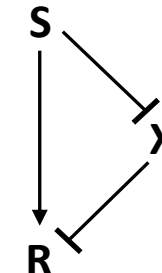
$$\frac{dR}{dt} = k_1 \cdot S - k_2 \cdot X \cdot R$$

$$\frac{dX}{dt} = k_3 - k_4 \cdot S \cdot X$$

$$\begin{aligned} \text{synthesis} &= k_1 S \\ \text{degradation} &= k_2 \cdot X \cdot R = k_2 \frac{k_3}{k_4 \cdot S} R \end{aligned}$$

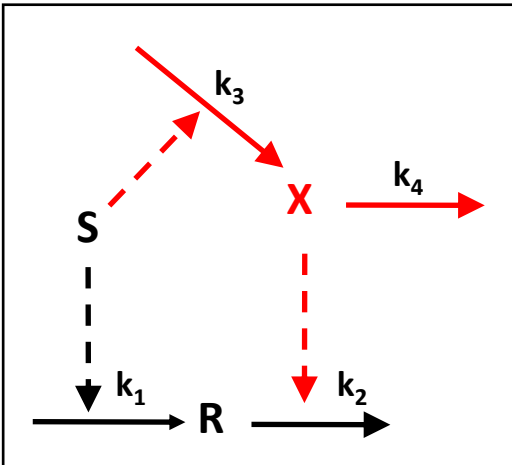


Coherent feed-forward loop



Two linear modules: adaptation

fast arm
slow arm



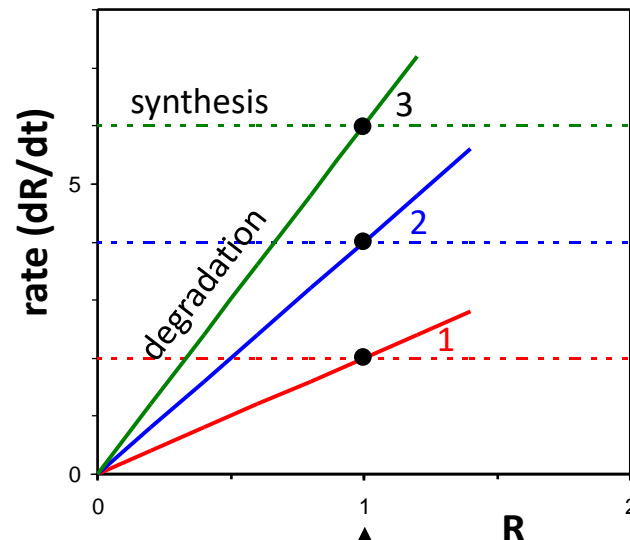
$$\frac{dR}{dt} = k_1 S - k_2 X R$$

$$\frac{dX}{dt} = k_3 S - k_4 X$$

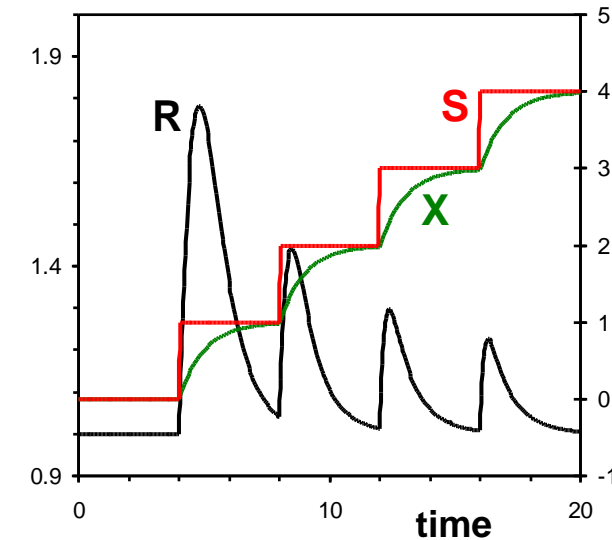
$$R_{ss} = \frac{k_1 k_4}{k_2 k_3} \quad X_{ss} = \frac{k_3 S}{k_4}$$

$$\text{synthesis} = k_1 S$$

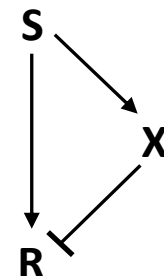
$$\text{degradation} = k_2 X R = k_2 \frac{k_3 S}{k_4} R$$



Perfect
adaptation



Incoherent feed-forward loop



The Incoherent Feedforward Loop Can Provide Fold-Change Detection in Gene Regulation

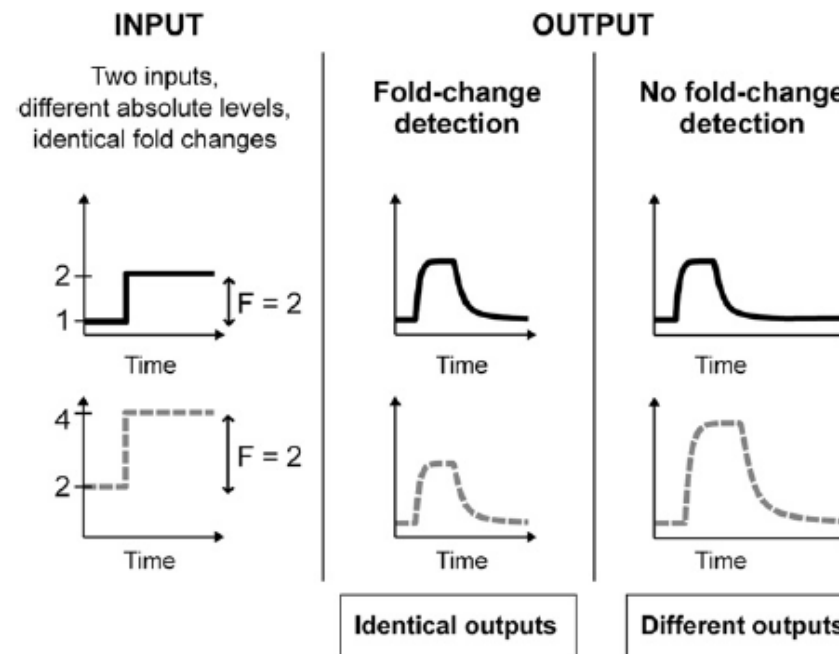
Lea Goentoro,¹ Oren Shoval,² Marc W. Kirschner,^{1,*} and Uri Alon^{2,*}

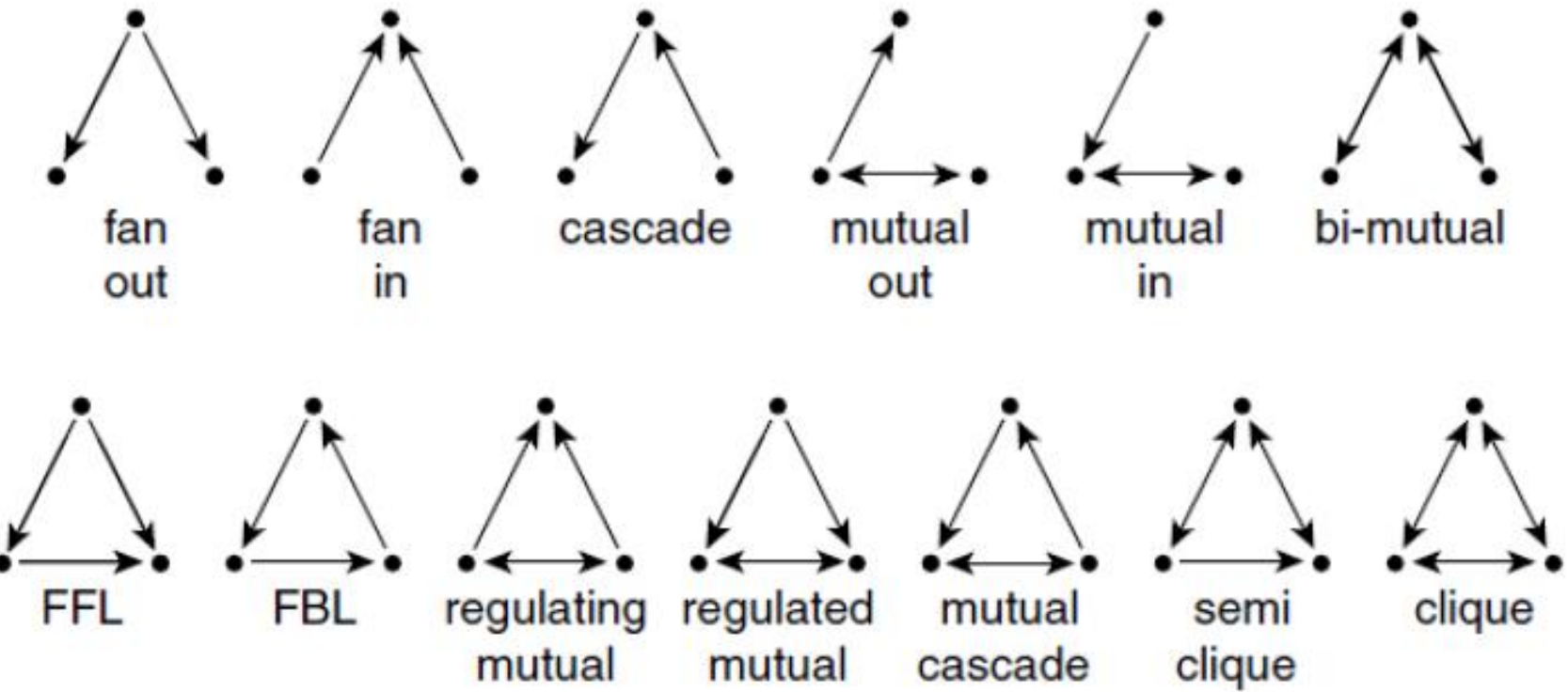
¹Department of Systems Biology, Harvard Medical School, Boston, MA 02115, USA

²Department of Molecular Cell Biology, Weizmann Institute of Science, Rehovot 76100, Israel

*Correspondence: marc@hms.harvard.edu (M.W.K.), uralon@weizmann.ac.il (U.A.)

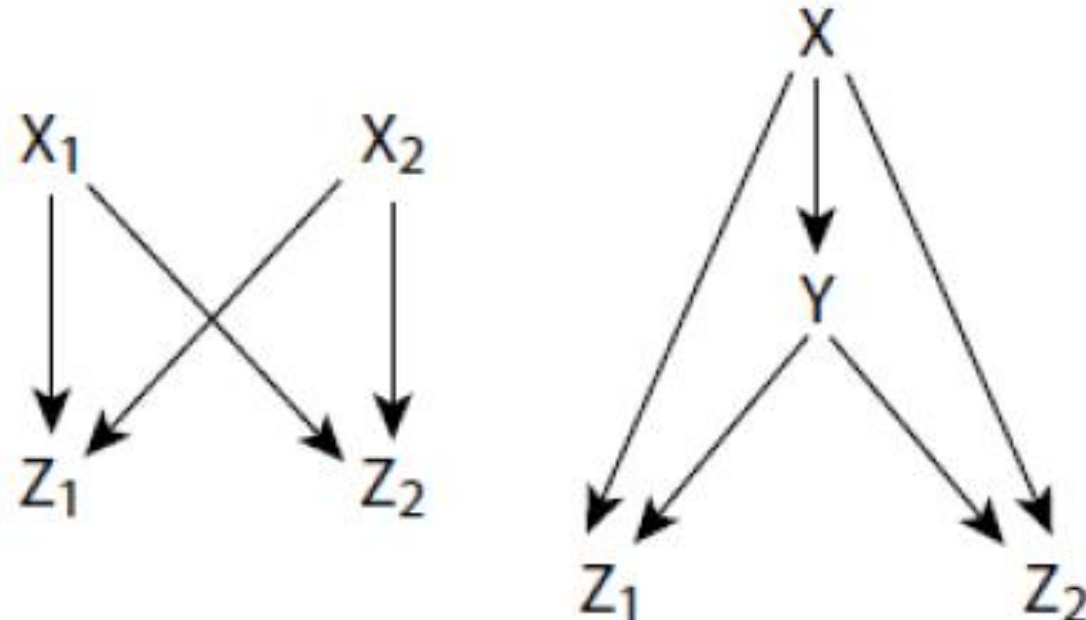
DOI 10.1016/j.molcel.2009.11.018





There are 199 possible four-node subgraphs, 9364 five-node subgraphs, and so on

THE MULTI-OUTPUT FEEDFORWARD LOOP

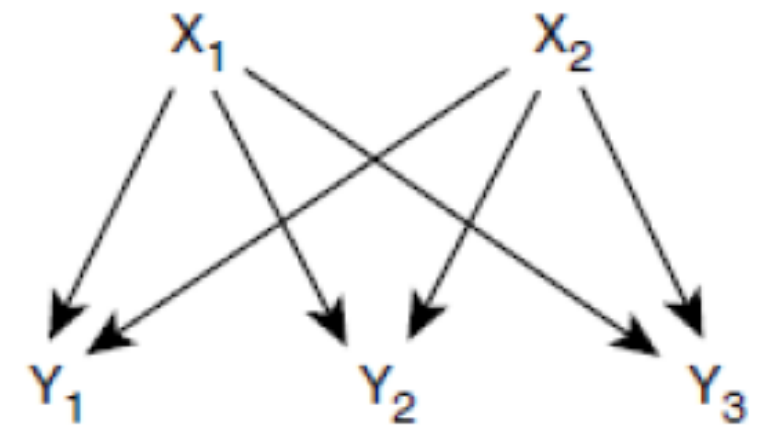
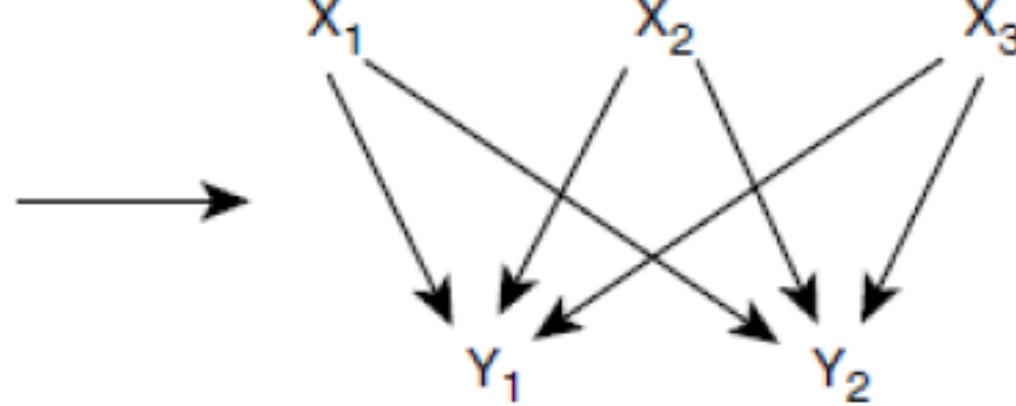
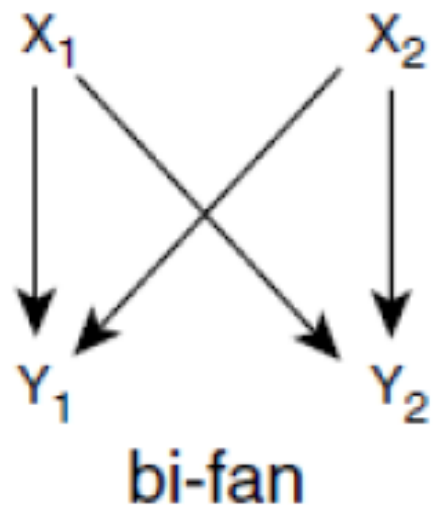


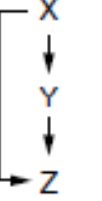
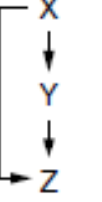
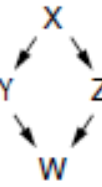
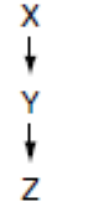
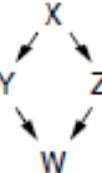
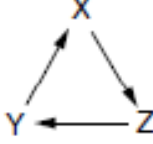
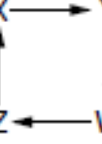
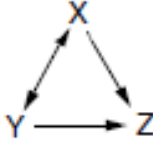
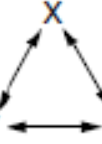
Bi-Fan

Two-output
Feedforward Loop

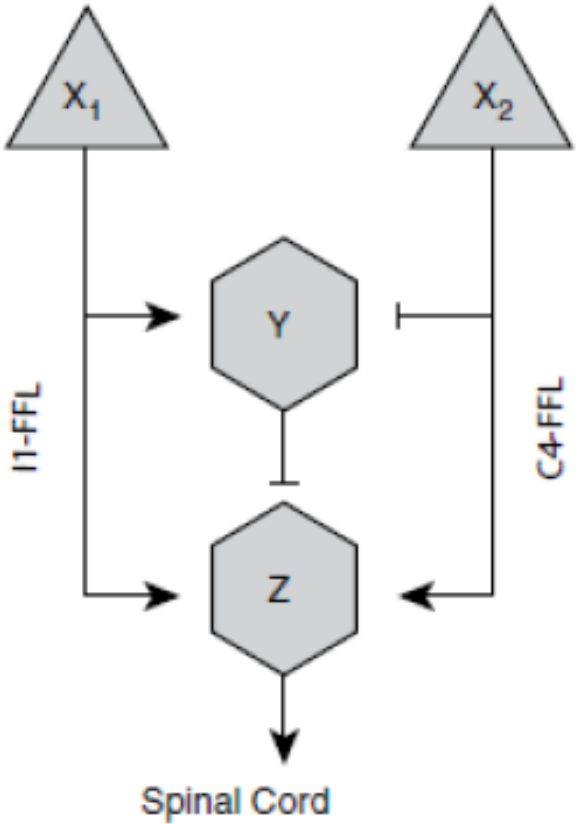
There are 199 possible four-node subgraphs – two most common!

SIGNAL INTEGRATION BY BI-FANS



Transcription networks	 Feedforward loop	 Bi-fan	
Neurons	 Feedforward loop	 Bi-fan	 Diamond
Food webs	 Cascade	 Diamond	
Electronic circuits (fractional multipliers)	 Three-node feedback loop	 Bi-fan	 Four-node feedback loop
Social Networks	 Regulating mutual	 Semi-Clique	 Clique

This circuit explains why there are two types of pain.

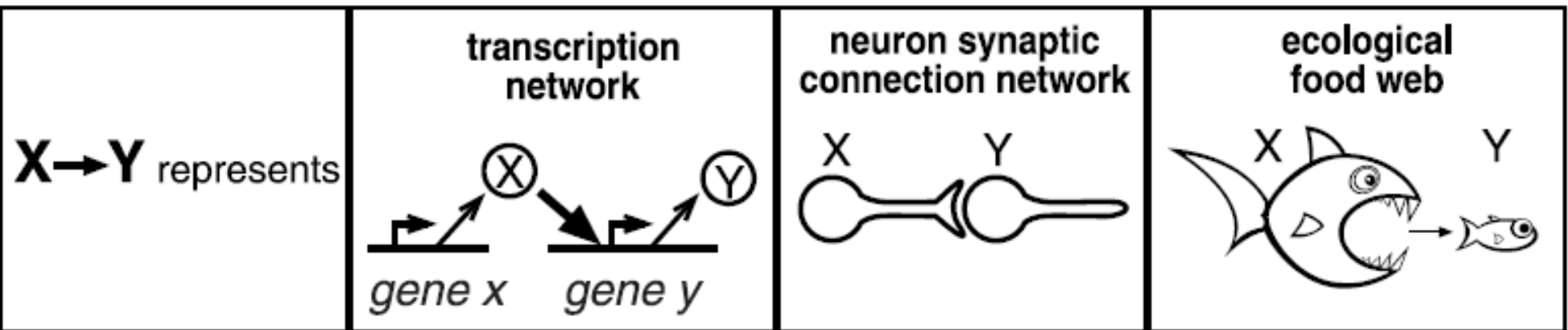


Neuron X_1 sits just below the skin and fires in response to painful stimuli. It excites neuron Z which projects up the spinal cord, sending a pain message to the brain. But neuron X_1 also excites neuron Y which inhibits Z . This is an I1-FFL, a pulse generator. As a result, neuron Z fires for a while and is then silenced. You feel a sharp pain, as if you've been poked by a needle.

The second input neuron is X_2 , located under the skin in the same region as X_1 . X_2 also excites neuron Z , and the message is sent up to the brain. But X_2 inhibits Y , forming a type-4 coherent FFL. You feel a throbbing, continuous pain, like a burn or abrasion. This circuit starts to fire only after a delay

The two circuits can interact, and we often intentionally force them to. Suppose you have a continuous, throbbing pain – say, an insect bite. How can you stop the throbbing? Briefly stimulate X_1 , which shuts the system down for a while. And that is precisely what we often do in such circumstances, we scratch hard right around the bite to dull the pain, and the slow chronic pain pathway is shut down for up to a few minutes.

A

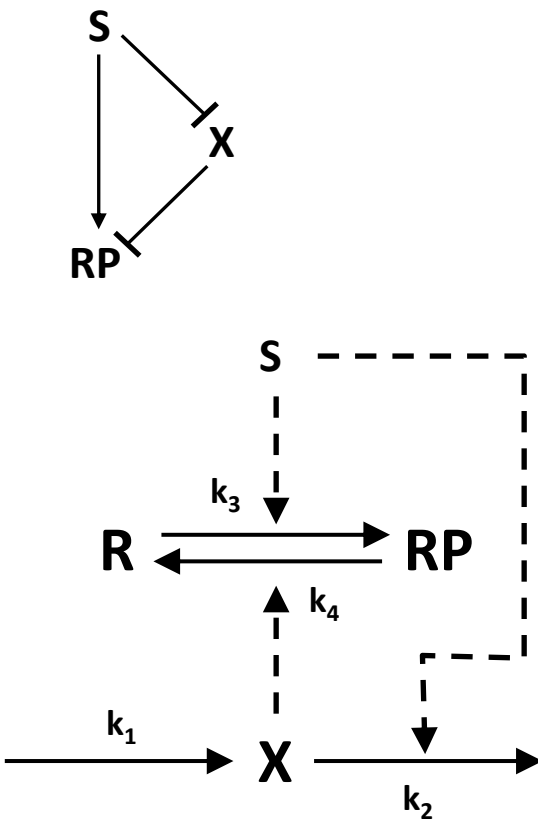


Signalling: Protein-Protein interactions

(protein phosphorylation-dephosphorylation cycle)

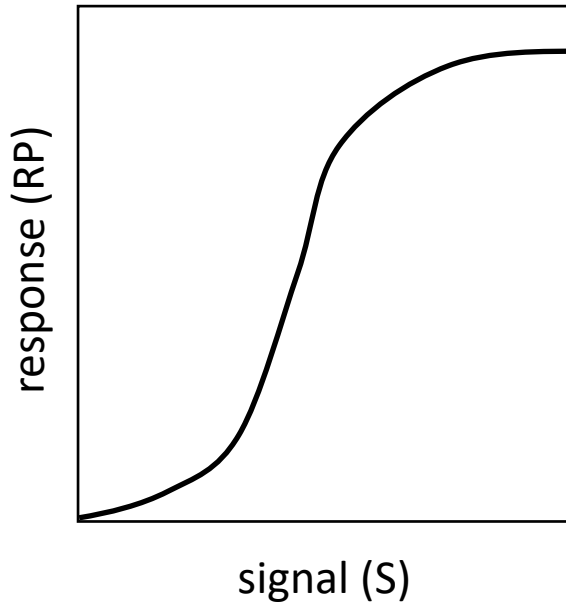
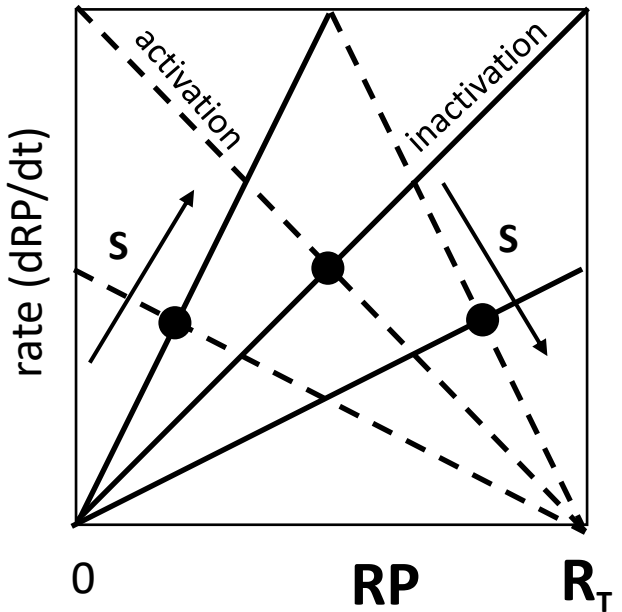
Check the online notes for introduction

Two modules: linear & saturation



Activation: $k_3 \cdot S \cdot (R_T - RP)$

Inactivation: $k_4 \cdot X \cdot RP = k_4 \cdot \frac{k_1}{k_2 \cdot S} \cdot RP$



$$\frac{d RP}{dt} = k_3 \cdot S \cdot (R_T - RP) - k_4 \cdot X \cdot RP$$

$$\frac{d X}{dt} = k_1 - k_2 \cdot S \cdot X$$

$$X_{ss} = \frac{k_1}{k_2 \cdot S}$$

$$RP_{ss} = \frac{k_3 \cdot S^2 \cdot R_T}{k_3 \cdot S^2 + k_4 \cdot k_1 / k_2}$$

ultrasensitivity

Coherent feed-forward loop

An amplified sensitivity arising from covalent modification in biological systems

(protein modification/metabolic regulation/switch mechanism/enzyme cascades)

ALBERT GOULD BETER[†] AND DANIEL E. KOSHLAND, JR.

Department of Biochemistry, University of California, Berkeley, California 94720

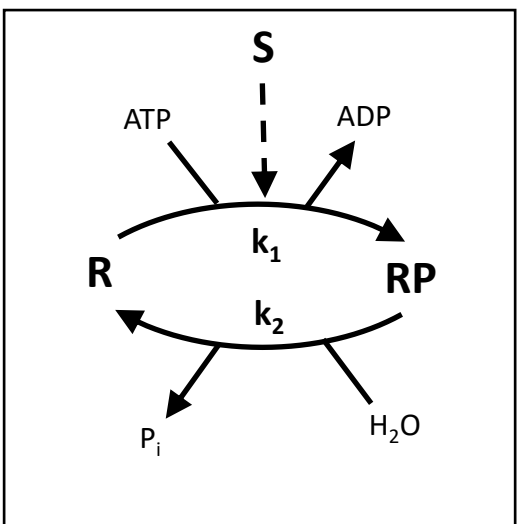
Contributed by Daniel E. Koshland, Jr., August 11, 1981



S = protein-kinase

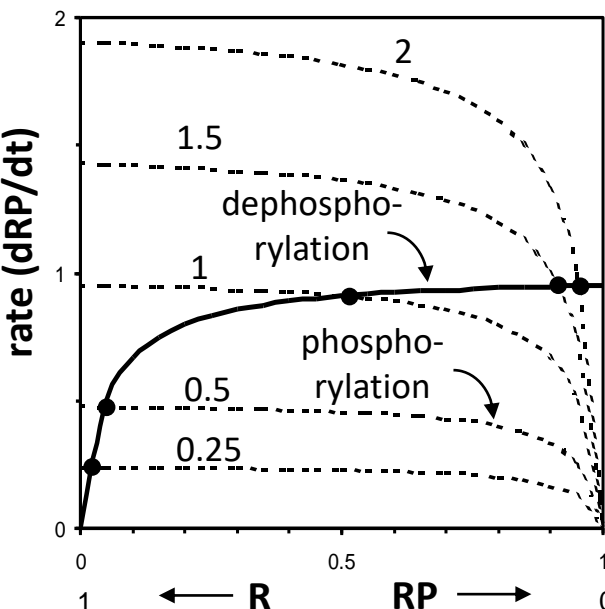
R = unP'd protein

RP = P'd protein

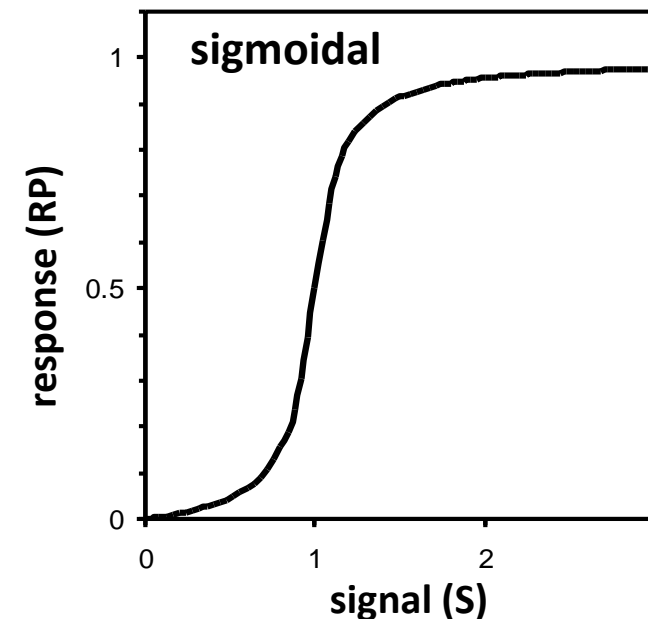


$$\frac{dR_P}{dt} = \frac{k_1 S (R_T - R_P)}{K_{m1} + R_T - R_P} - \frac{k_2 R_P}{K_{m2} + R_P}$$

phosphorylation dephosphorylation



Signal-response
curve



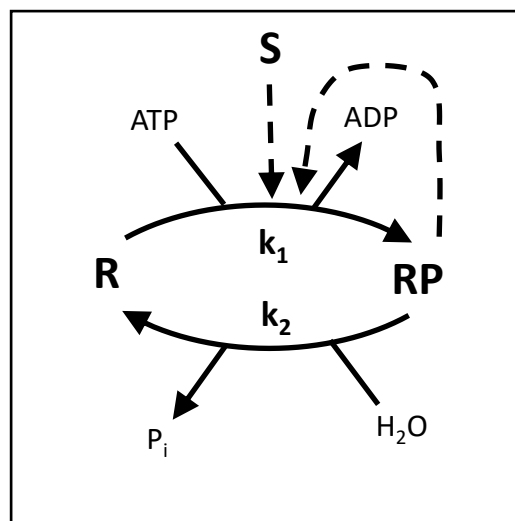
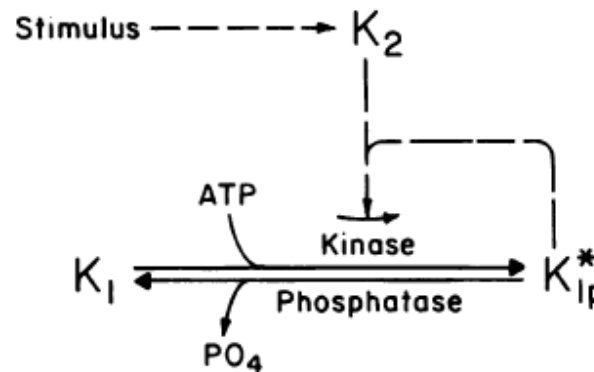
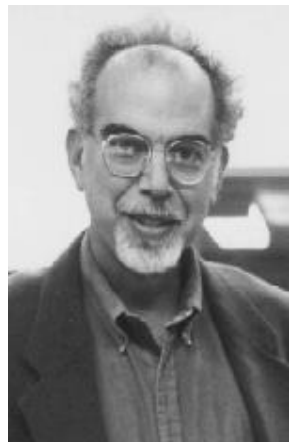
zero order ultrasensitivity

A mechanism for memory storage insensitive to molecular turnover: A bistable autophosphorylating kinase

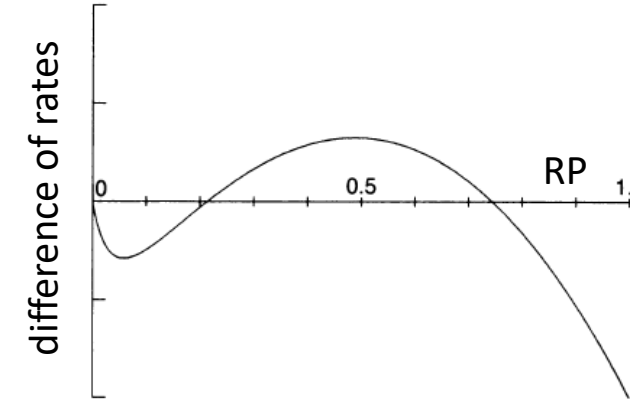
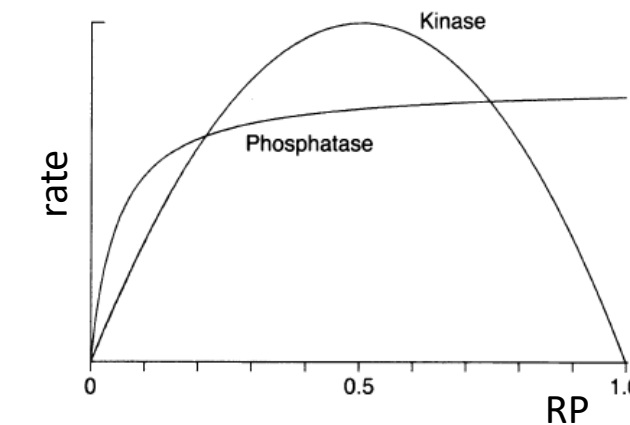
(long-term memory/nervous system/protein phosphorylation)

JOHN E. LISMAN

Department of Biology, Brandeis University, Waltham, MA 02254

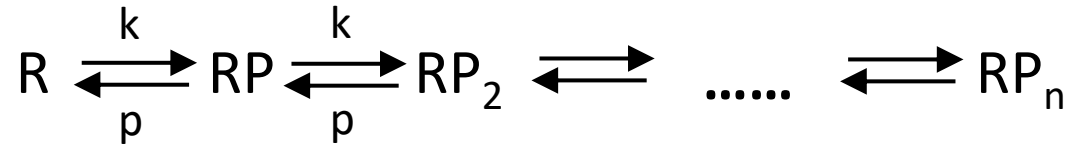


autocatalytic
Goldbeter-Koshland
mechanism



Multi-site phosphorylation

(distributed & ordered)



$$RP = \frac{k}{p} R \quad RP_2 = \frac{k}{p} RP = \frac{k^2}{p^2} R \quad \dots \dots$$

$$R_T = R + RP + RP_2 + \dots = R(1 + K + K^2 + \dots) \quad \text{where } K = k/p$$

for n=2

$$R = \frac{R_T}{1 + K + K^2} \quad RP = K \cdot R = \frac{K \cdot R_T}{1 + K + K^2} \quad RP_2 = K^2 \cdot R = \frac{K^2 \cdot R_T}{1 + K + K^2}$$

REPORTS

Cl concentrations in the Sajama ice core, and to a number of other pedological and geomorphological features indicative of long-term dry climates (8, 11–14, 18). This decline in human activity around the Altiplano paleolakes is seen in most caves, with early and late occupations separated by largely sterile mid-Holocene sediments. However, a few sites, including the caves of Tulan-67 and Tulan-68, show that people did not completely disappear from the area. All of the sites of sporadic occupation are located near wetlands in valleys, near large springs, or where lakes turned into wetlands and subsistence resources were locally still available despite a generally arid climate (7, 8, 19, 20).

Archaeological data from surrounding areas suggest that the Silencio Arqueológico applies best to the most arid areas of the central Andes, where aridity thresholds for early societies were critical. In contrast, a weaker expression is to be expected in the more humid highlands of northern Chile (north of 20°S, such as Salar Huasco) and Peru (21). In northwest Argentina, the Silencio Arqueológico is found in four of the six known caves (22) [see review in (23)]. It is also found on the coast of Peru in sites that are associated with ephemeral streams (24). The southern limit in Chile and northwest Argentina has yet to be explored.

References and Notes

1. T. Dillehay, *Science* **245**, 1436 (1989).
2. D. J. Meltzer et al., *Am. Antiq.* **62**, 659 (1997).
3. T. F. Lynch, C. M. Stevenson, *Quat. Res.* **37**, 117 (1992).
4. D. H. Sandweiss et al., *Science* **281**, 1830 (1998).
5. L. Núñez, M. Grosjean, I. Cartajena, in *Interhemispheric Climate Linkages*, V. Markgraf, Ed. (Academic Press, San Diego, CA 2001), pp. 105–117.
6. M. A. Geyh, M. Grosjean, L. Núñez, U. Schotterer, *Quat. Res.* **52**, 143 (1999).
7. J. L. Betancourt, C. Latorre, J. A. Rech, J. Quade, K. Rylander, *Science* **289**, 1542 (2000).
8. M. Grosjean et al., *Global Planet. Change* **28**, 35 (2001).
9. C. Latorre, J. L. Betancourt, K. A. Rylander, J. Quade, *Geol. Soc. Am. Bull.* **114**, 349 (2002).
10. Charcoal in layers containing triangular points has been ^{14}C dated at Tuina-1, Tuina-5, Tambillo-1, San Lorenzo-1, and Tuyajto-1 between 13,000 and 9000 cal yr B.P. (table S1 and fig. S1).
11. P. A. Baker et al., *Science* **291**, 640 (2001).
12. G. O. Seltzer, S. Cross, P. Baker, R. Dunbar, S. Fritz, *Geology* **26**, 167 (1998).
13. L. G. Thompson et al., *Science* **282**, 1858 (1998).
14. M. Grosjean, *Science* **292**, 2391 (2001).
15. E. P. Tonni, written communication.
16. M. T. Alberdi, written communication.
17. J. Fernandez et al., *Geoarchaeology* **6**, 251 (1991).
18. The histogram of middens is processed from (9).
19. M. Grosjean, L. Núñez, I. Cartajena, B. Messerli, *Quat. Res.* **48**, 239 (1997).
20. The term Silencio Arqueológico describes the mid-Holocene collapse of human population at those archaeological sites of the Atacama Desert that are vulnerable to multicentennial or millennial-scale drought. The term Silencio Arqueológico does not conflict with the presence of humans at sites that are not susceptible to climate change, such as in spring and river oases that drain large (Pleistocene) aquifers or at sites where wetlands were created during the arid middle Holocene, such as Tulan-67, Tulan-68, and Laguna Miscanti.
21. M. Aldenderfer, *Science* **241**, 1828 (1988).
22. A mid-Holocene hiatus is found at Inca Cueva 4, Huachichocana 3, Pintocamayoc, and Yavi, whereas occupation continued at the oases of Susques and Quebrada Seca.
23. L. Núñez et al., *Estud. Atacameños* **17**, 125 (1999).
24. D. H. Sandweiss, K. A. Maaesch, D. G. Anderson, *Science* **283**, 499 (1999).
25. Grants from the National Geographic Society (5836-96), the Swiss National Science Foundation (21-57073), and Fondo Nacional de Desarrollo Científico y Tecnológico (1930022) and comments by J. P. Bradbury, B. Meggers, G. Seltzer, and D. Stanford are acknowledged.

Supporting Online Material

www.sciencemag.org/cgi/content/full/298/5594/821/DC1
Figs. S1 to S3
Tables S1 and S2

22 July 2002; accepted 9 September 2002

Network Motifs: Simple Building Blocks of Complex Networks

R. Milo,¹ S. Shen-Orr,¹ S. Itzkovitz,¹ N. Kashtan,¹ D. Chklovskii,² U. Alon^{1*}

Complex networks are studied across many fields of science. To uncover their structural design principles, we defined "network motifs," patterns of interconnections occurring in complex networks at numbers that are significantly higher than those in randomized networks. We found such motifs in networks from biochemistry, neurobiology, ecology, and engineering. The motifs shared by ecological food webs were distinct from the motifs shared by the genetic networks of *Escherichia coli* and *Saccharomyces cerevisiae* or from those found in the World Wide Web. Similar motifs were found in networks that perform information processing, even though they describe elements as different as biomolecules within a cell and synaptic connections between neurons in *Ceenorhabditis elegans*. Motifs may thus define universal classes of networks. This approach may uncover the basic building blocks of most networks.

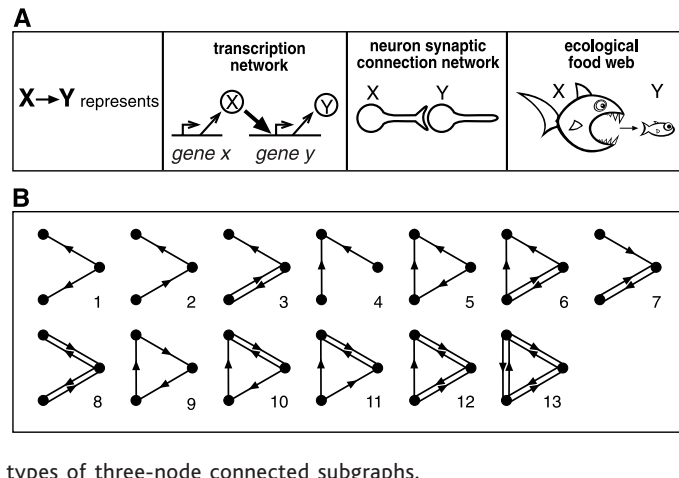
Many of the complex networks that occur in nature have been shown to share global statistical features (1–10). These include the "small world" property (1–9) of short paths between any two nodes and highly clustered connections. In addition, in many natural networks, there are a few nodes with many more connections than the average node has. In these types

of networks, termed "scale-free networks" (4, 6), the fraction of nodes having k edges, $p(k)$, decays as a power law $p(k) \sim k^{-\gamma}$ (where γ is often between 2 and 3). To go beyond these global features would require an understanding of the basic structural elements particular to each class of networks (9). To do this, we developed an algorithm for detecting network motifs: recurring, significant patterns of interconnections. A detailed application to a gene regulation network has been presented (11). Related methods were used to test hypotheses on social networks (12, 13). Here we generalize this approach to virtually any type of connectivity graph and find the striking appearance of

¹Departments of Physics of Complex Systems and Molecular Cell Biology, Weizmann Institute of Science, Rehovot, Israel 76100. ²Cold Spring Harbor Laboratory, Cold Spring Harbor, NY 11724, USA.

*To whom correspondence should be addressed. E-mail: urialon@weizmann.ac.il

Fig. 1. (A) Examples of interactions represented by directed edges between nodes in some of the networks used for the present study. These networks go from the scale of biomolecules (transcription factor protein X binds regulatory DNA regions of a gene to regulate the production rate of protein Y), through cells (neuron X is synaptically connected to neuron Y, (X feeds on Y), to organisms (X



motifs in networks representing a broad range of natural phenomena.

We started with networks where the interactions between nodes are represented by directed edges (Fig. 1A). Each network was scanned for all possible n -node subgraphs (in the present study, $n = 3$ and 4), and the number of occurrences of each subgraph was recorded. Each network contains numerous types of n -node subgraphs (Fig. 1B). To focus on those that are likely to be important, we compared the real network to suitably randomized networks (12–16) and only selected patterns appearing in the real network at numbers significantly higher than those in the randomized networks (Fig. 2). For a stringent comparison, we used randomized networks that have the same single-node characteristics as does the real network: Each node in the randomized networks has the same

number of incoming and outgoing edges as the corresponding node has in the real network. The comparison to this randomized ensemble accounts for patterns that appear only because of the single-node characteristics of the network (e.g., the presence of nodes with a large number of edges). Furthermore, the randomized networks used to calculate the significance of n -node subgraphs were generated to preserve the same number of appearances of all ($n - 1$)-node subgraphs as in the real network (17, 18). This ensures that a high significance was not assigned to a pattern only because it has a highly significant subpattern. The “network motifs” are those patterns for which the probability P of appearing in a randomized network an equal or greater number of times than in the real network is lower than a cutoff value (here $P = 0.01$). Patterns that are functionally important but not

statistically significant could exist, which would be missed by our approach.

We applied the algorithm to several networks from biochemistry (transcriptional gene regulation), ecology (food webs), neurobiology (neuron connectivity), and engineering (electronic circuits, World Wide Web). The network motifs found are shown in Table 1. Transcription networks are biochemical networks responsible for regulating the expression of genes in cells (11, 19). These are directed graphs, in which the nodes represent genes (Fig. 1A). Edges are directed from a gene that encodes for a transcription factor protein to a gene transcriptionally regulated by that transcription factor. We analyzed the two best characterized transcriptional regulation networks, corresponding to organisms from different kingdoms: a eukaryote (the yeast *Saccharomyces cerevisiae*) (20) and a bacterium (*Escherichia coli*) (11, 19). The two transcription networks show the same motifs: a three-node motif termed “feed-forward loop” (11) and a four-node motif termed “bi-fan.” These motifs appear numerous times in each network (Table 1), in nonhomologous gene systems that perform diverse biological functions. The number of times they appear is more than 10 standard deviations greater than their mean number of appearances in randomized networks. Only these subgraphs, of the 13 possible different three-node subgraphs (Fig. 1B) and 199 different four-node subgraphs, are significant and are therefore considered network motifs. Many other three- and four-node subgraphs recur throughout the networks, but at numbers that are less than the mean plus 2 standard deviations of their appearance in randomized networks.

We next applied the algorithm to ecosystem food webs (21, 22), in which nodes represent groups of species. Edges are directed from a node representing a predator to the node representing its prey. We analyzed data collected by different groups at seven distinct ecosystems (22), including both aquatic and terrestrial habitats. Each of the food webs displayed one or two three-node network motifs and one to five four-node network motifs. One can define the “consensus motifs” as the motifs shared by networks of a given type. Five of the seven food webs shared one three-node motif, and all seven shared one four-node motif (Table 1). In contrast to the three-node motif (termed “three chain”), the three-node feedforward loop was underrepresented in the food webs. This suggests that direct interactions between species at a separation of two layers [as in the case of omnivores (23)] are selected against. The bi-parallel motif indicates that two species that are prey of the same predator both tend to share the same prey. Both network motifs may thus represent general tendencies of food webs (21, 22).

We next studied the neuronal connectivity network of the nematode *Caenorhabditis elegans* (24). Nodes represent neurons (or neuron

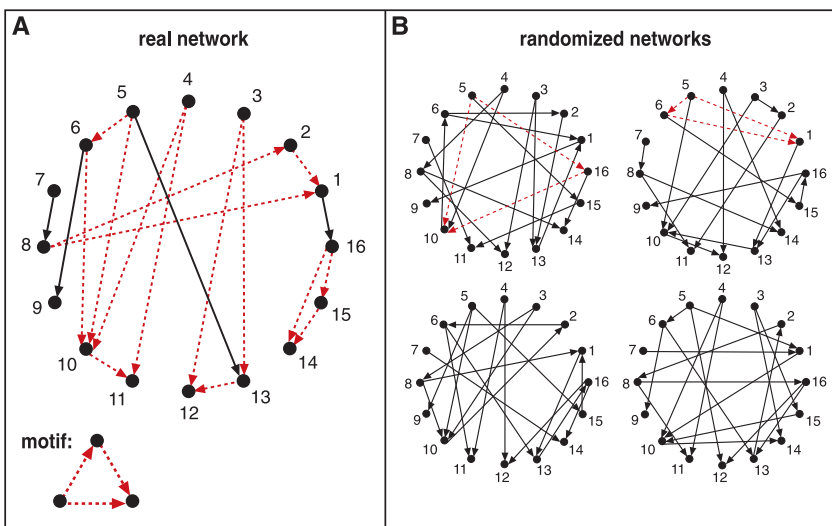
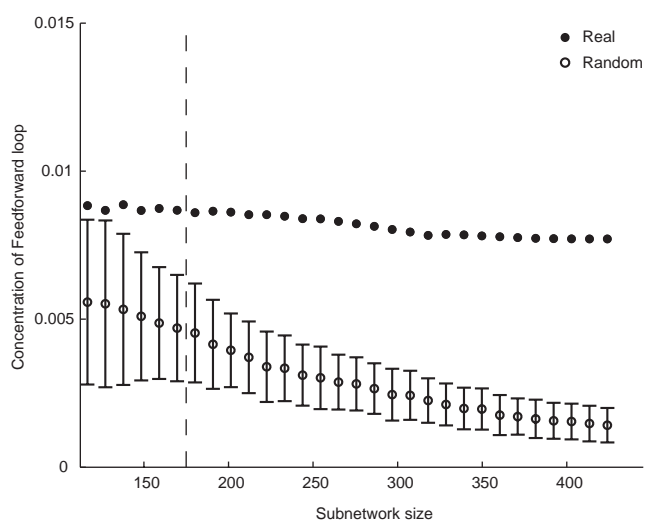


Fig. 2. Schematic view of network motif detection. Network motifs are patterns that recur much more frequently (A) in the real network than (B) in an ensemble of randomized networks. Each node in the randomized networks has the same number of incoming and outgoing edges as does the corresponding node in the real network. Red dashed lines indicate edges that participate in the feedforward loop motif, which occurs five times in the real network.

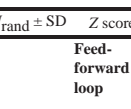
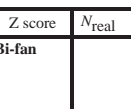
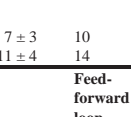
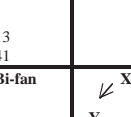
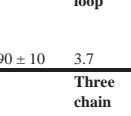
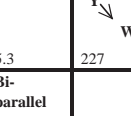
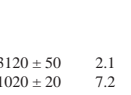
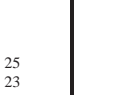
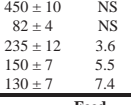
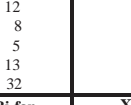
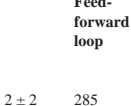
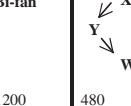
Fig. 3. Concentration C of the feedforward loop motif in real and randomized subnetworks of the *E. coli* transcription network (11). C is the number of appearances of the motif divided by the total number of appearances of all connected three-node subgraphs (Fig. 1B). Subnetworks of size S were generated by choosing a node at random and adding to it n nodes connected by an incoming or outgoing edge, until S nodes were obtained, and then including all of the edges between these S nodes present in the full network. Each of the subnetworks was randomized (17, 18) (shown are mean and SD of 400 subnetworks of each size).



classes), and edges represent synaptic connections between the neurons. We found the feed-forward loop motif in agreement with anatomical observations of triangular connectivity structures (24). The four-node motifs include the bi-fan and the bi-parallel (Table 1). Two of these motifs (feedforward loop and bi-fan) were

also found in the transcriptional gene regulation networks. This similarity in motifs may point to a fundamental similarity in the design constraints of the two types of networks. Both networks function to carry information from sensory components (sensory neurons/transcription factors regulated by biochemical signals) to ef-

Table 1. Network motifs found in biological and technological networks. The numbers of nodes and edges for each network are shown. For each motif, the numbers of appearances in the real network (N_{real}) and in the randomized networks ($N_{\text{rand}} \pm \text{SD}$, all values rounded) (17, 18) are shown. The P value of all motifs is $P < 0.01$, as determined by comparison to 1000 randomized networks (100 in the case of the World Wide Web). As a qualitative measure of statistical significance, the Z score = $(N_{\text{real}} - N_{\text{rand}})/\text{SD}$ is shown. NS, not significant. Shown are motifs that occur at least $U = 4$ times with completely different sets of nodes. The networks are as follows (18): transcription interactions between regulatory proteins and genes in the bacterium *E. coli* (11) and the yeast *S. cerevisiae* (20); synaptic connections between neurons in *C. elegans*, including neurons connected by at least five synapses (24); trophic interactions in ecological food webs (22), representing pelagic and benthic species (Little Rock Lake), birds, fishes, invertebrates (Ythan Estuary), primarily larger fishes (Chesapeake Bay), lizards (St. Martin Island), primarily invertebrates (Skipwith Pond), pelagic lake species (Bridge Brook Lake), and diverse desert taxa (Coachella Valley); electronic sequential logic circuits parsed from the ISCAS89 benchmark set (7, 25), where nodes represent logic gates and flip-flops. Presented are all five partial scans of forward-logic chips and three digital fractional multipliers in the benchmark set; and World Wide Web hyperlinks between Web pages in a single domain (4) (only three-node motifs are shown). e, multiplied by the power of 10 (e.g., $1.46e6 = 1.46 \times 10^6$).

Network	Nodes	Edges	N_{real}	$N_{\text{rand}} \pm \text{SD}$	Z score	N_{real}	$N_{\text{rand}} \pm \text{SD}$	Z score	N_{real}	$N_{\text{rand}} \pm \text{SD}$	Z score	
Gene regulation (transcription)							Feed-forward loop		Bi-fan			
<i>E. coli</i>	424	519	40	7 ± 3	10	203	47 ± 12	13				
<i>S. cerevisiae</i> *	685	1,052	70	11 ± 4	14	1812	300 ± 40	41				
Neurons							Feed-forward loop		Bi-fan			
<i>C. elegans</i> †	252	509	125	90 ± 10	3.7	127	55 ± 13	5.3	227	35 ± 10	20	
Food webs							Three chain		Bi-parallel			
Little Rock	92	984	3219	3120 ± 50	2.1	7295	2220 ± 210	25				
Ythan	83	391	1182	1020 ± 20	7.2	1357	230 ± 50	23				
St. Martin	42	205	469	450 ± 10	NS	382	130 ± 20	12				
Chesapeake	31	67	80	82 ± 4	NS	26	5 ± 2	8				
Coachella	29	243	279	235 ± 12	3.6	181	80 ± 20	5				
Skipwith	25	189	184	150 ± 7	5.5	397	80 ± 25	13				
B. Brook	25	104	181	130 ± 7	7.4	267	30 ± 7	32				
Electronic circuits (forward logic chips)							Feed-forward loop		Bi-fan			
s15850	10,383	14,240	424	2 ± 2	285	1040	1 ± 1	1200	480	2 ± 1	335	
s38584	20,717	34,204	413	10 ± 3	120	1739	6 ± 2	800	711	9 ± 2	320	
s38417	23,843	33,661	612	3 ± 2	400	2404	1 ± 1	2550	531	2 ± 2	340	
s9234	5,844	8,197	211	2 ± 1	140	754	1 ± 1	1050	209	1 ± 1	200	
s13207	8,651	11,831	403	2 ± 1	225	4445	1 ± 1	4950	264	2 ± 1	200	
Electronic circuits (digital fractional multipliers)							Three-node feedback loop		Bi-fan			
s208	122	189	10	1 ± 1	9	4	1 ± 1	3.8	5	1 ± 1	5	
s420	252	399	20	1 ± 1	18	10	1 ± 1	10	11	1 ± 1	11	
s838‡	512	819	40	1 ± 1	38	22	1 ± 1	20	23	1 ± 1	25	
World Wide Web							Feedback with two mutual dyads		Fully connected triad			
nd.edu\$	325,729	1,46e6	1.1e5	2e3 ± 1e2	800	6.8e6	5e4 ± 4e2	15,000	1.2e6	1e4 ± 2e2	5000	

*Has additional four-node motif: $(X \rightarrow Z, W; Y \rightarrow Z, W; Z \rightarrow W)$, $N_{\text{real}} = 150$, $N_{\text{rand}} = 85 \pm 15$, $Z = 4$. †Has additional four-node motif: $(X \rightarrow Y, Z; Y \rightarrow Z; Z \rightarrow W)$, $N_{\text{real}} = 204$, $N_{\text{rand}} = 80 \pm 20$, $Z = 6$. The three-node pattern $(X \rightarrow Y, Z; Y \rightarrow Z; Z \rightarrow Y)$ also occurs significantly more than at random. It is not a motif by the present definition because it does not appear with completely distinct sets of nodes more than $U = 4$ times. ‡Has additional four-node motif: $(X \rightarrow Y, Z \rightarrow Y; W \rightarrow Z; Z \rightarrow X; W \rightarrow X)$, $N_{\text{real}} = 914$, $N_{\text{rand}} = 500 \pm 70$, $Z = 6$. §Has two additional three-node motifs: $(X \rightarrow Y, Z; Y \rightarrow Z; Z \rightarrow Y)$, $N_{\text{real}} = 3e5$, $N_{\text{rand}} = 1.4e3 \pm 6e1$, $Z = 6000$, and $(X \rightarrow Y, Z; Y \rightarrow Z)$, $N_{\text{real}} = 5e5$, $N_{\text{rand}} = 9e4 \pm 1.5e3$, $Z = 250$.

factors (motor neurons/structural genes). The feedforward loop motif common to both types of networks may play a functional role in information processing. One possible function of this circuit is to activate output only if the input signal is persistent and to allow a rapid deactivation when the input goes off (11). Indeed, many of the input nodes in the neural feedforward loops are sensory neurons, which may require this type of information processing to reject transient input fluctuations that are inherent in a variable or noisy environment.

We also studied several technological networks. We analyzed the ISCAS89 benchmark set of sequential logic electronic circuits (7, 25). The nodes in these circuits represent logic gates and flip-flops. These nodes are linked by directed edges. We found that the motifs separate the circuits into classes that correspond to the circuit's functional description. In Table 1, we present two classes, consisting of five forward-logic chips and three digital fractional multipliers. The digital fractional multipliers share three motifs, including three- and four-node feedback loops. The forward logic chips share the feed-forward loop, bi-fan, and bi-parallel motifs, which are similar to the motifs found in the genetic and neuronal information-processing networks. We found a different set of motifs in a network of directed hyperlinks between World Wide Web pages within a single domain (4). The World Wide Web motifs may reflect a design aimed at short paths between related pages. Application of our approach to nondirected networks shows distinct sets of motifs in networks of protein interactions and Internet router connections (18).

None of the network motifs shared by the food webs matched the motifs found in the gene regulation networks or the World Wide Web. Only one of the food web consensus motifs also appeared in the neuronal network. Different motif sets were found in electronic circuits with different functions. This suggests that motifs can define broad classes of networks, each with specific types of elementary structures. The motifs reflect the underlying processes that generated each type of network; for example, food webs evolve to allow a flow of energy from the bottom to the top of food chains, whereas gene regulation and neuron networks evolve to process information. Information processing seems to give rise to significantly different structures than does energy flow.

We further characterized the statistical significance of the motifs as a function of network size, by considering pieces of various sizes (subnetworks) of the full network. The concentration of motifs in the subnetworks is about the same as that in the full network (Fig. 3). In contrast, the concentration of the corresponding subgraphs in the randomized versions of the subnetworks decreases sharply with size. In analogy with statistical physics, the number of appearances of each motif in the real networks

REPORTS

appears to be an extensive variable (i.e., one that grows linearly with the system size). These variables are nonextensive in the randomized networks. The existence of such variables may be a unifying property of evolved or designed systems. The decrease of the concentration C with randomized network size S (Fig. 3) qualitatively agrees with exact results (2, 26) on Erdos-Renyi random graphs (random graphs that preserve only the number of nodes and edges of the real network) in which $C \sim 1/S$. In general, the larger the network is, the more significant the motifs tend to become. This trend can also be seen in Table 1 by comparing networks of different sizes. The network motif detection algorithm appears to be effective even for rather small networks (on the order of 100 edges). This is because three- or four-node subgraphs occur in large numbers even in small networks. Furthermore, our approach is not sensitive to data errors; for example, the sets of significant network motifs do not change in any of the networks upon addition, removal, or rearrangement of 20% of the edges at random.

In information-processing networks, the motifs may have specific functions as elementary computational circuits (11). More generally, they may be interpreted as structures that arise because of the special constraints under which the network has evolved (27). It is of value to detect and understand network motifs in order to gain insight into their dynamical behavior and to define classes of networks and network homologies. Our approach can be readily generalized to any type of network, including those with multiple “colors” of edges or nodes. It would be fascinating to see what types of motifs occur in other networks and to understand the processes that yield given motifs during network evolution.

References and Notes

1. S. H. Strogatz, *Nature* **410**, 268 (2001).
2. B. Bollobas, *Random Graphs* (Academic, London, 1985).
3. D. Watts, S. Strogatz, *Nature* **393**, 440 (1998).
4. A.-L. Barabasi, R. Albert, *Science* **286**, 509 (1999).
5. M. Newman, *Proc. Natl. Acad. Sci. U.S.A.* **98**, 404 (2001).
6. H. Jeong, B. Tombor, R. Albert, Z. N. Oltvai, A. L. Barabasi, *Nature* **407**, 651 (2000).
7. R. F. Cancho, C. Janssen, R. V. Sole, *Phys. Rev. E* **64**, 046119 (2001).
8. R. F. Cancho, R. V. Sole, *Proc. R. Soc. London Ser. B* **268**, 2261 (2001).
9. L. Amaral, A. Scala, M. Barthelemy, H. Stanley, *Proc. Natl. Acad. Sci. U.S.A.* **97**, 11149 (2000).
10. B. Huberman, L. Adamic, *Nature* **401**, 131 (1999).
11. S. Shen-Orr, R. Milo, S. Mangan, U. Alon, *Nature Genet.* **31**, 64 (2002).
12. P. Holland, S. Leinhardt, in *Sociological Methodology*, D. Heise, Ed. (Jossey-Bass, San Francisco, 1975), pp. 1–45.
13. S. Wasserman, K. Faust, *Social Network Analysis* (Cambridge Univ. Press, New York, 1994).
14. N. Guelzim, S. Bottani, P. Bourgine, F. Kepes, *Nature Genet.* **31**, 60 (2002).
15. M. Newman, S. Strogatz, D. Watts, *Phys. Rev. E* **64**, 6118 (2001).
16. S. Maslov, K. Sneppen, *Science* **296**, 910 (2002).
17. The randomized networks used for detecting three-node motifs preserve the numbers of incoming, outgoing, and double edges with both incoming and outgoing arrows for each node. The randomized networks used for detecting four-node motifs preserve the above characteristics as well as the numbers of all 13 three-node subgraphs as in the real network. Algorithms for constructing these randomized network ensembles are described (18). Additional information is available at www.weizmann.ac.il/mcb/UriAlon.
18. Methods are available as supporting material on *Science Online*.
19. D. Thieffry, A. M. Huerta, E. Perez-Rueda, J. Collado-Vides, *Bioessays* **20**, 433 (1998).
20. M. C. Costanzo *et al.*, *Nucleic Acids Res.* **29**, 75 (2001).
21. J. Cohen, F. Briand, C. Newman, *Community Food Webs: Data and Theory* (Springer, Berlin, 1990).
22. R. Williams, N. Martinez, *Nature* **404**, 180 (2000).
23. S. Pimm, J. Lawton, J. Cohen, *Nature* **350**, 669 (1991).
24. J. White, E. Southgate, J. Thomson, S. Brenner, *Philos. Trans. R. Soc. London Ser. B* **314**, 1 (1986).
25. F. Brglez, D. Bryan, K. Kozminski, *Proc. IEEE Int. Symp. Circuits Syst.*, 1929 (1989).
26. In Erdos-Renyi randomized networks with a fixed connectivity (2), the concentration of a subgraph with n nodes and k edges scales with network size as $C \sim S^{n-k-1}$ (thus, $C \sim 1/S$ for the feedforward loop of Fig. 3 where $n = k = 3$). The sole exception in Table 1 in which C should not vanish at large S is the three-chain pattern in food webs where $n = 3$ and $k = 2$.
27. D. Callaway, J. Hopcroft, J. Kleinberg, M. Newman, S. Strogatz, *Phys. Rev. E* **64**, 041902 (2001).
28. We thank S. Maslov and K. Sneppen for valuable discussions. We thank J. Collado-Vides, N. Martinez, R. Govindan, R. Durbin, L. Amaral, R. Cancho, S. Maslov, and K. Sneppen for kindly providing data, as well as D. Alon, E. Domany, M. Elowitz, I. Kanter, O. Hobart, M. Naor, D. Mukamel, A. Murray, S. Quake, R. Raz, M. Reigl, M. Surette, K. Sneppen, P. Sternberg, E. Winfree, and all members of our lab for comments. We thank Caltech and the Aspen Center for Physics for their hospitality during part of this work. We acknowledge support from the Israel Science Foundation, the Human Frontier Science Program, and the Minerva Foundation.

Supporting Online Material

www.sciencemag.org/cgi/content/full/298/5594/824/DC1
Methods
Table S1

1 May 2002; accepted 10 September 2002

Progression of Vertebrate Limb Development Through SHH-Mediated Counteraction of GLI3

Pascal te Welscher,¹ Aimée Zuniga,¹ Sanne Kuijper,² Thijs Drenth,¹ Hans J. Goedemans,¹ Frits Meijlink,² Rolf Zeller^{1*}

Distal limb development and specification of digit identities in tetrapods are under the control of a mesenchymal organizer called the polarizing region. *Sonic Hedgehog* (SHH) is the morphogenetic signal produced by the polarizing region in the posterior limb bud. Ectopic anterior SHH signaling induces digit duplications and has been suspected as a major cause underlying congenital malformations that result in digit polydactyly. Here, we report that the polydactyly of *Gl3*-deficient mice arises independently of SHH signaling. Disruption of one or both *Gl3* alleles in mouse embryos lacking *Shh* progressively restores limb distal development and digit formation. Our genetic analysis indicates that SHH signaling counteracts GLI3-mediated repression of key regulator genes, cell survival, and distal progression of limb bud development.

The *Hedgehog* (*Hh*) signaling pathway controls many key developmental processes during animal embryogenesis (1). In *Drosophila* embryos, all known functions of *Hh* signaling are mediated by the transcriptional effector *Cubitus interruptus* (*Ci*) (2). Several homologs of *Hh* and *Ci* have been identified in higher vertebrates. In particular, *Sonic Hedgehog* (SHH) and the *Ci* homolog GLI3 are required for vertebrate limb development (3–6). GLI3 acts first during the initiation of

limb bud development and before the activation of SHH signaling in posterior restriction of the basic helix-loop-helix transcription factor dHAND. dHAND in turn prevents *Gl3* expression from spreading posteriorly (Fig. 1A, panel 1) (7). In addition, GLI3 restricts the SHH-independent early expression of 5' *HoxD* genes and *Gremlin* to the posterior mesenchyme (8). Subsequently, dHAND functions in the activation of *Shh* expression (9). Limb bud morphogenesis is then controlled by reciprocal interactions of two signaling centers (Fig. 1A, panel 2): the polarizing region, an instructive organizer located in the posterior limb bud mesenchyme, and the apical ectodermal ridge (AER). SHH signaling by the polarizing region in combination with bone morphogenetic proteins

¹Department of Developmental Biology, Faculty of Biology, Utrecht University, Padualaan 8, NL-3584 CH Utrecht, Netherlands. ²Hubrecht Laboratorium, Uppsalalaan 8, NL-3584 CT Utrecht, Netherlands.

*To whom correspondence should be addressed. E-mail: R.Zeller@bio.uu.nl



Network Motifs: Simple Building Blocks of Complex Networks
R. Milo, S. Shen-Orr, S. Itzkovitz, N. Kashtan, D. Chklovskii and U. Alon (October 25, 2002)
Science **298** (5594), 824-827. [doi: 10.1126/science.298.5594.824]

Editor's Summary

This copy is for your personal, non-commercial use only.

Article Tools Visit the online version of this article to access the personalization and article tools:
<http://science.sciencemag.org/content/298/5594/824>

Permissions Obtain information about reproducing this article:
<http://www.sciencemag.org/about/permissions.dtl>

Science (print ISSN 0036-8075; online ISSN 1095-9203) is published weekly, except the last week in December, by the American Association for the Advancement of Science, 1200 New York Avenue NW, Washington, DC 20005. Copyright 2016 by the American Association for the Advancement of Science; all rights reserved. The title *Science* is a registered trademark of AAAS.

The Incoherent Feedforward Loop Can Provide Fold-Change Detection in Gene Regulation

Lea Goentoro,¹ Oren Shoval,² Marc W. Kirschner,^{1,*} and Uri Alon^{2,*}

¹Department of Systems Biology, Harvard Medical School, Boston, MA 02115, USA

²Department of Molecular Cell Biology, Weizmann Institute of Science, Rehovot 76100, Israel

*Correspondence: marc@hms.harvard.edu (M.W.K.), urialon@weizmann.ac.il (U.A.)

DOI 10.1016/j.molcel.2009.11.018

SUMMARY

Many sensory systems (e.g., vision and hearing) show a response that is proportional to the fold-change in the stimulus relative to the background, a feature related to Weber's Law. Recent experiments suggest such a fold-change detection feature in signaling systems in cells: a response that depends on the fold-change in the input signal, and not on its absolute level. It is therefore of interest to find molecular mechanisms of gene regulation that can provide such fold-change detection. Here, we demonstrate theoretically that fold-change detection can be generated by one of the most common network motifs in transcription networks, the incoherent feed-forward loop (I1-FFL), in which an activator regulates both a gene and a repressor of the gene. The fold-change detection feature of the I1-FFL applies to the entire shape of the response, including its amplitude and duration, and is valid for a wide range of biochemical parameters.

INTRODUCTION

Gene regulation networks are composed of a small set of recurring interaction patterns called network motifs (Milo et al., 2002; Shen-Orr et al., 2002). Each motif has been experimentally found to perform specific dynamical functions (reviewed in Alon, 2007). In cases studied so far, these motifs seem to preserve their autonomous functions even in their natural contexts, wired into the regulatory networks of the cell.

One of the most common network motifs is the incoherent type-1 feedforward loop (I1-FFL), which appears hundreds of times in bacteria (Eichenberger et al., 2004; Mangan et al., 2006; Milo et al., 2002) and in yeast (Lee et al., 2002; Milo et al., 2002). In animal cells, the I1-FFL has been discovered in the transcriptional networks of human embryonic stem cell (Boyer et al., 2005) and hematopoietic stem cell (Swiers et al., 2006) and downstream of the Notch signaling pathway (Krejci et al., 2009).

An I1-FFL is a regulatory pattern in which an activator X controls a target gene Z and also activates a repressor of that target gene, Y. The repressor Y may be a transcription factor, or microRNA, such as found in c-Myc/E2F1 regulation

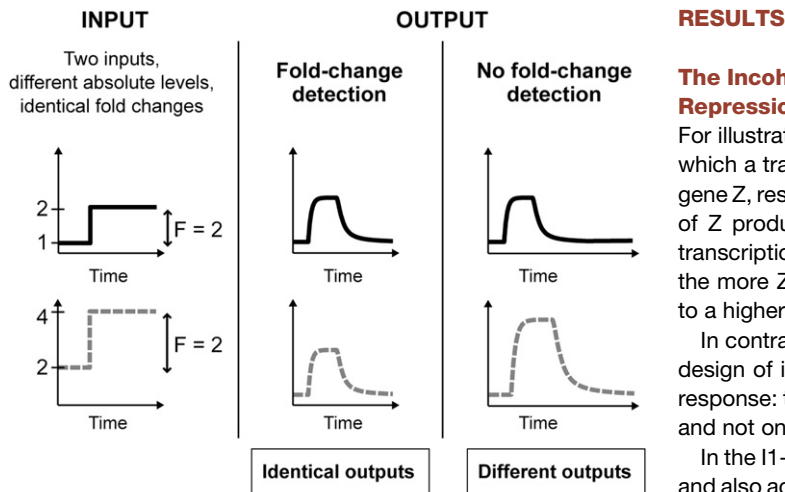
(O'Donnell et al., 2005) and in eye patterning in *Drosophila* (Li et al., 2009). Previous studies have demonstrated that the I1-FFL can generate a temporal pulse of Z response (Basu et al., 2004; Mangan and Alon, 2003; Mangan et al., 2006), accelerate the response time of Z (Mangan and Alon, 2003; Mangan et al., 2006), and act as a band-pass amplitude filter that provides maximal Z response for intermediate levels of X activity (Entus et al., 2007; Kaplan et al., 2008; Kim et al., 2008).

Here, we demonstrate an additional function for the I1-FFL: the I1-FFL can generate a response to fold-changes in the input signal, rather than absolute levels. This fold-change detection property means that the dynamics of the output (amplitude and duration of the transcription of gene Z) depend only on the relative change in input signal, not on its absolute levels. Figure 1 provides an example: a signal that changes from, say, level 1 to 2 provides exactly the same output as a signal that goes from 2 to 4 because both represent a 2-fold increase in input. In contrast, a nonfold detection system results in different outputs for these two step stimuli.

Evidence for such fold-change responsiveness was recently demonstrated in mammalian signaling systems. In the Wnt signaling pathway, Goentoro and Kirschner (2009 [this issue of *Molecular Cell*]) present evidence that gene expression and the embryonic phenotype appear to correlate with fold-changes, rather than absolute levels, of the activator β -catenin. In the ERK signaling system, Cohen-Saidon and colleagues (2009 [this issue of *Molecular Cell*]) present evidence that fold-changes in nuclear ERK (the activator X in our notation), as opposed to its absolute levels, are the more precise outcome of ligand stimulation.

Reading fold-changes intuitively requires that cells remember the past activity level of the transcription factor and compare it to the present level after stimulation. This comparison has to extend the entire duration of the dynamics (both transient and steady state) if the target gene's dynamics are to be entirely dependent only on fold-changes in the transcription factor, and not on absolute levels. Current models of gene regulation do not show this property. This study demonstrates that such a perfect temporal comparison is theoretically feasible and that the almost minimal circuit to accomplish this temporal comparison happens to be one of the recurrent motifs in transcriptional networks, the type-1 incoherent feed-forward loop.

The fold-change detection property occurs for a wide range of biochemical parameters for the I1-FFL interactions, provided that the activator is in its linear regime, and the repressor

**Figure 1. Fold-Change Detection**

Fold-change detection means that the dynamics of the output (amplitude and duration of the transcription of gene Z) depend only on the fold-changes in the level of the input signal, and not on the absolute levels of the input signal.

saturates the promoter of the target gene (Z). The fold-change detection property of the I1-FFL can provide gene regulation with an analog of Weber's Law, a feature of many sensory systems (e.g., vision, smell, hearing, taste, and touch), in which signal discrimination is relative to the background signal (Laming, 1986; Ross and Murray, 1996; Weber, 1905). Fold-change detection may help cells maintain sensitivity to noisy signals across a wide dynamic range and perhaps cope with variation in the regulatory protein concentrations.

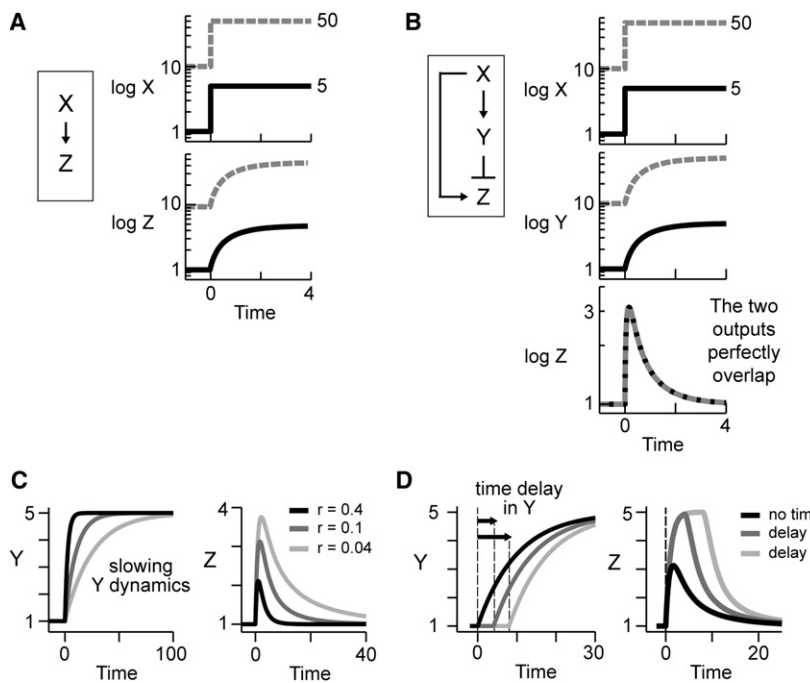
The Incoherent Feedforward Loop with Strong Repression Responds to Fold-Changes in Signal

For illustration, Figure 2A shows how simple gene regulation, in which a transcription factor X activates transcription of a target gene Z, responds to input steps. In simple regulation, the amount of Z produced depends directly on the absolute level of the transcription factor X. The more transcription factor is around, the more Z is produced. A higher basal level of X corresponds to a higher basal transcription of Z (dashed lines).

In contrast, we now demonstrate that the I1-FFL, with proper design of its regulatory elements, can show a different type of response: the output Z depends on the fold-change in the input, and not on its absolute levels.

In the I1-FFL, a transcription factor X activates a target gene Z and also activates Y, which represses Z strongly (Y nearly saturates the Z promoter) and X acts in a linear fashion (X is far from saturating the Y and Z promoters; equations 1 and 2 in Figure 3). In this case, we find that the response of Z depends only on the fold-change in the level of the activator X, and not on its absolute levels.

To demonstrate fold-change detection, we provide two input steps that have an identical fold-change but different absolute levels (Figure 2B, X, solid and dashed lines). We find that the response of Z is a pulse that shows exact adaptation to its basal level. The shape of the pulse is identical for both input steps (Figure 2B, Z, the solid and dashed lines overlap). The height and duration of the response thus depend on fold-changes in input, and not on its absolute levels. Variation in the basal activity level of the transcription factor X can be completely compensated, such that gene transcription depends only on the fold-changes.

**Figure 2. The Incoherent Feedforward Loop Can Provide Fold-Change Detection**

(A) In simple gene regulation, two inputs with different absolute levels but identical fold-changes give two different profiles of Z transcription.

(B) In a properly designed I1-FFL (see text), two inputs with different absolute levels but identical fold-changes give two identical profiles of Z transcription (dashed and full lines overlap).

(C and D) The amplitude and duration of the response Z can be increased by slowing the dynamics of Y (C) or by introducing a delay in the response of Y to X (D).

In all of the plots, time is in arbitrary units. Using typical biochemical rate constants, the response time is in the range of minutes to hours (see text). The plots were generated using equations 7 and 8 in Figure 3 with $r = 0.1$, except in (C), in which r varies.

Fold-change detection in I1-FFL

Dynamic equations for the I1-FFL

In the I1-FFL, both X and Y regulate the Z promoter, generally described by an input function (Bintu et al., 2005):

$$G(X, Y) = \beta_0 \frac{X/K_1}{1 + X/K_1 + Y/K_2 + XY/K_3} \quad (1)$$

When repression by Y is strong, so that $Y/K_2 \gg (1 + X/K_1 + XY/K_3)$

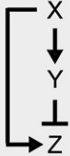
we can write to a first approximation:

$$G(X, Y) = \frac{\beta_2 X}{Y} \quad (2)$$

where $\beta_2 = \beta_0 K_2 / K_1$. The resulting dynamic equations for Y and Z are (Alon, 2007):

$$\frac{dY}{dt} = \beta_1 X - \alpha_1 Y \quad (3)$$

$$\frac{dZ}{dt} = \frac{\beta_2 X}{Y} - \alpha_2 Z \quad (4)$$



Dimensional analysis shows that I1-FFL provides fold-change detection

Let us define the following dimensionless variables,

$$y = \frac{Y}{\beta_1 X_0 / \alpha_1} \quad z = \frac{Z}{\beta_2 \alpha_1 / \beta_1 \alpha_2} \quad (5)$$

$$F = \frac{X}{X_0} \quad \tau = \alpha_1 t \quad (6)$$

and rescale equations 3–4,

$$\frac{dy}{d\tau} = F - y \quad (7)$$

$$r \frac{dz}{d\tau} = \frac{F}{y} - z \quad (8)$$

This scaling shows that the dynamics of the I1-FFL depends only on one parameter:

$$r = \frac{1/\alpha_2}{1/\alpha_1} \frac{\text{half-life of } Z}{\text{half-life of } Y} \quad (9)$$

Thus, the dynamics of Z (eqn. 8) depends on fold-changes in X (F), and not on the absolute level of X: a feature called fold-change detection.

The I1-FFL circuit with fold-change detection can maintain equal responses to a series of stimuli with identical steps (Figure S1 available online). Such a property can be useful in case the old signal is not cleared before the cells need to respond to a new stimulus. Our examples so far included sharp steps in X, but fold response is also seen for gradually changing signal profiles (Figure S1). For illustration, Figure S2 shows how all other network motifs, including positive and negative autoregulation, coherent FFLs, and single-input modules, respond to the absolute levels of the input.

Fold-Change Detection in I1-FFL Arises Because the Repressor Y Acts as a Memory of the Activator X

The intuitive reason for the fold-change detection property of the I1-FFL is that the repressor Y acts as a memory of the activator X (Friedland et al., 2009; Gardner et al., 2000). The I1-FFL with strong repression allows Y to act as a reference memory of previous levels of X and to normalize the activation of Z accordingly. In this manner, Y mediates a continual temporal comparison between the present and past levels of X. At long time-scales, the memory is adjusted to the new level of the activator X, and the response Z returns to its basal level (Figure 2C).

Mathematically, fold-change detection can be seen via dimensional analysis. The dynamic equations for Y and Z can be rescaled so that the stimulus X drops out, and only the fold-change in input level, $F(t) = X(t) / X_0$, drives the dynamics of Z (equations 7–9 in Figure 3). In a special case, an analytical solution can be obtained that explicitly shows the strict dependence on fold-changes in the input (see Supplemental Data).

Tuning the Duration and Amplitude of Fold-Change Detection

The timescales for the dynamics of Z can be tuned to range from minutes to hours to days by changing the degradation rates of Y and Z (α_1 and α_2 in equations 3 and 4 in Figure 3). The time to

Figure 3. Mathematical Description of the Incoherent Feedforward Loop as a Fold-Change Detector

reach the peak of the response is on the order of the half-life of the repressor Y, and the time for Z to adapt back to basal levels is on the order of the half-life of Z.

The amplitude of the Z response can be tuned in two ways. First, the slower the dynamics of the repressor Y compared to the dynamics of the target Z, the higher the amplitude of the response (Figure 4C). This may occur, for example, when the repressor is a relatively stable protein or inhibitory RNA, and Z is an unstable protein or mRNA.

Second, the amplitude and duration of the response is increased when a time delay is incorporated so that Y is activated by X at a delay relative to Z

(Figure 4D). Such a delay in expression of a target gene is seen in diverse systems (e.g., Mdm2 expression is delayed by ~100 min relative to other genes activated by the same factor, p53) (Lahav et al., 2004). Such delays can be differentially controlled for different genes by controlling delays in transcription, translation, localization, splicing, and so on.

Fold-Change Detection Occurs for a Wide Range of Parameters in the I1-FFL

Up until now, we examined a model of the I1-FFL that is in the limit within which Y saturates the Z promoter and X is linear for the X and Z promoters (equation 2 in Figure 3). To go beyond this limiting case, we tested the behavior of a more complete model of the I1-FFL. In this model, standard Michaelis-Menten-like terms describe the action of X and Y on the promoters (equation 1 in Figure 3) (Alon, 2007; Bintu et al., 2005).

We tested the model by varying its biochemical parameters (binding affinities, degradation rates, and production rates). We considered three possible types of mechanisms for the way that the two regulators X and Y bind the Z promoter: (1) binding of X and Y is mutually exclusive; (2) binding of X and Y is independent; and (3) binding of X and Y is cooperative. For each set of biochemical parameters, we computed the response to two step stimuli with different absolute levels but identical fold-changes (Figure 5A).

In all three cases, there is a range of parameters that provides good fold-change detection (Figures 5B–5D). The light-colored region in Figures 5B–5D indicates the range of parameters in which the response to the two step stimuli is identical to within 10%. The lower panel of Figure 5 shows examples of Z dynamics across the parameter range. This suggests that the I1-FFL can be designed to show fold-change detection in a way that does not require fine-tuning of parameter values and only requires that certain parameter ratios are large.

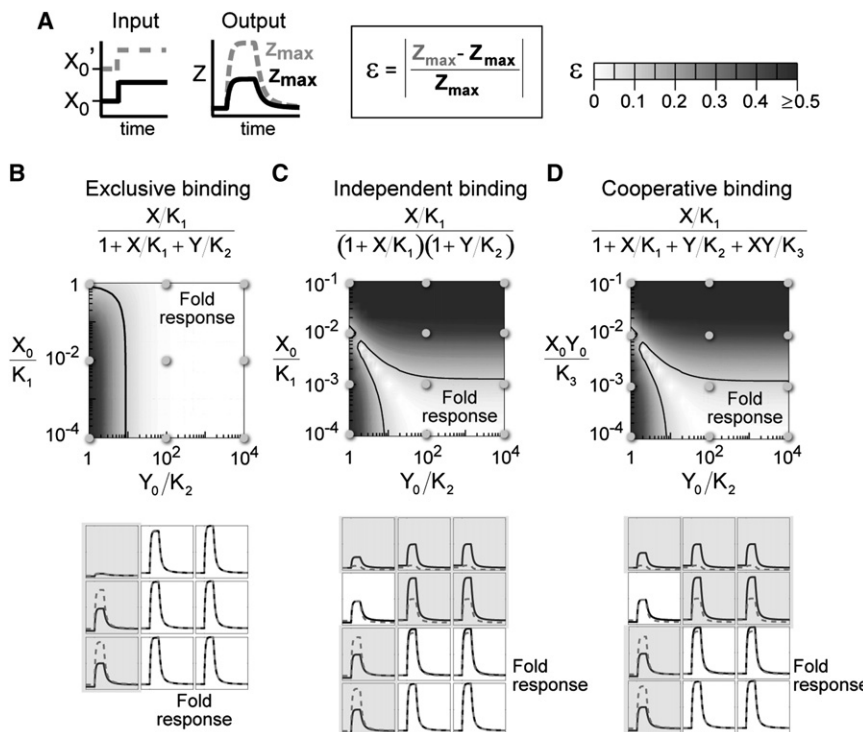


Figure 4. I1-FFL Shows Fold-Change Detection over a Wide Range of Parameters

(A) Model parameters were varied. For each choice of parameters, we provided two step inputs with the same fold-change, $F = 10$, and different absolute levels, $X_0' = 10 X_0$. As a measure of the fold-change detection property, we computed the relative difference (ϵ) in the amplitude of the Z response (Z_{\max}) for the two step inputs.

(B–D) Three detailed designs of the Z promoter input function were considered, in which binding of X and Y is exclusive (B), independent (C), or cooperative (D). In all cases, the light region indicates the parameter range in which fold-change detection occurs, in the sense that the two step inputs produce identical outputs within 10% (contour line delineates $\epsilon = 0.1$).

Parameters: K_i are binding constants, X_0 is the basal input level, and $Y_0 = \beta_1 X_0 / \alpha_1$, with β_1 and α_1 defined in equation 3 in Figure 3.

The parameter range for fold-change detection is greatest for the case in which X and Y binding is mutually exclusive. In this case, fold-change detection requires only that Y saturates the Z promoter ($Y_0/K_2 \gg 1$, Figure 5B). If both X and Y can bind the promoter such that their binding is independent of each other, fold-change detection requires also that X activation of the Z promoter is linear ($X_0/K_1 \ll 1$, Figure 5C). If X and Y bind cooperatively, fold-change detection requires further that the simultaneous binding of both activators be relatively rare compared to the binding of Y alone ($X_0 Y_0 / K_3 \ll 1$, Figure 5D).

In short, fold-change detection requires that the ratio of Y concentration to its effective binding constant to the Z promoter is large, $Y_0/K \sim 10$. This can be achieved either by having high levels of Y , say $Y = 100$ nM and affinity $K = 10$ nM, or lower levels of Y and higher affinity, $Y = 10$ nM and $K = 1$ nM. (For reference, note that 10 nM represents ~ 10 molecules in a bacterium and ~ 1000 molecules in a fibroblast nucleus). In the cases considered here, fold-change detection also requires that X be in the linear regime in regulating the Y promoter.

Because Y strongly represses the promoter, fold-change detection operates at a small fraction of the promoter's maximal strength. An appropriate combination of a strong promoter and strong repression can be used to provide the needed expression level of the output gene Z .

The present simulations indicate that the I1-FFL can also be designed in such a way that it does not show fold-change detection properties. This is expected if X is not in its linear regime or if cooperative binding of X and Y to the Z promoter is near saturation. In these cases, the I1-FFL shows either a response that depends on the absolute level of the input or a weak response.

We also tested a different way of implementing an I1-FFL. Here, instead of acting as a transcriptional repressor, Y promotes degradation of the target gene Z (Levchenko and Iglesias, 2002; Tyson et al., 2003). This is also similar to the “proportioner” node in the adapting circuits discussed in Ma et al. (2009). With appropriate choice of parameters, we find that this version of the I1-FFL can also show fold-change detection (Figure S3).

It is likely that additional circuits can provide fold-change detection. One possible direction is integral feedback circuits that provide precise adaptation (Barkai and Leibler, 1997; Ma et al., 2009; Yi et al., 2000). Not all circuits with precise adaptation, however, are expected to show fold-change detection. Figure 4 (lower-left curves in lower panels) shows parameters in which I1-FFL displays almost precise adaptation but poor fold-change detection.

DISCUSSION

This study suggests that the I1-FFL, a common network motif, can provide fold-change detection. Fold-change detection means that the amplitude and duration and indeed the entire shape of the response depend on the fold changes in the input, and not on its absolute levels. Fold-change detection occurs for a wide range of biochemical parameters of the I1-FFL, in which the repressor saturates its promoter and the activator works in the linear regime.

Are there advantages to fold-change detection, rather than absolute detection, in gene regulation circuitry? One can suggest at least two advantages related to cellular variation in the concentration of transcription factors and to rapidly varying noise in their activity level (Figure 5).

The first potentially useful property of fold-change detection regards the observation that the nuclear level of transcription factors can vary by several-fold between individual cells

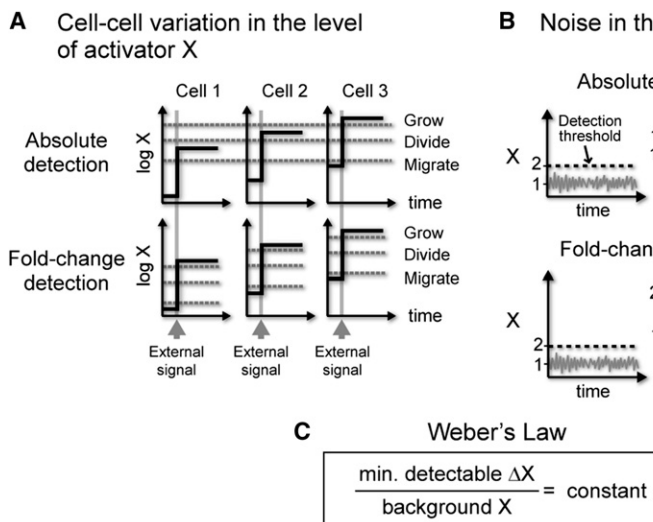


Figure 5. Fold-Change Detection May Provide Signaling Advantages in Noisy Environment

(A) Fold-change detection ensures that each cell responds reliably to an external signal despite variation in the basal level of X. In fold-change detection, cells sense relative changes from the basal level, and not absolute levels or absolute changes.

(B) Fold-change detection rescales the meaningful change in signal according to the background noise. In fold-change detection, $\Delta X = 1$ when background $X = 1$ gives the same information as $\Delta X = 10$ when background $X = 10$.

(C) Fold-change detection in the I1-FFL can provide a transcriptional analog of Weber's Law in sensory system, which states that the minimal detectable change in signal scales linearly with the background signal.

(Cohen-Saidon et al., 2009; Sigal et al., 2006). For example, in the ERK system, the nuclear level of ERK2 (which corresponds to X in the present notation) varies by up to 4-fold across individual cells (Cohen-Saidon et al., 2009). When an external signal arrives (the growth factor EGF), the nuclear level of ERK2 in each cell transiently rises by approximately the same fold-change over the basal level (Figure 5A; Cohen-Saidon et al., 2009). Thus, more ERK2 enters the nucleus in cells with a high basal ERK2 level than in cells with a low level. An absolute detection mechanism would generate different downstream responses in different cells due to the different absolute level of nuclear ERK2 (Figure 5A). In contrast, a fold-change detection mechanism, such as that provided by the I1-FFL, can allow all cells to have an identical response to the external signal, despite cell-cell variation in the basal level of the activator X (Figure 5A).

A second potentially useful property of fold-change detection is the ability to maintain sensitivity despite noise in the X activity (Figure 5B). Such noise can result from rapid fluctuations in the external signal level (e.g., external fluctuations in EGF concentration as it varies in space and time). Noise strength, defined as the standard deviation of a signal around its mean, is known to increase with signal strength. In many systems, the standard deviation of a signal increases proportionally to \sqrt{X} . Thus, a background signal of 1 might have noise of ± 0.1 , whereas a background signal of 10 might have a higher noise of ± 0.3 . This increasing noise leads to a fundamental problem with absolute detection mechanisms. If we had an absolute detection mechanism and would like it to detect changes of 0.3 above a background signal of 1, we would run into trouble when the background signal rises to 10 because noise in the signal would trigger false-positive responses (Figure 5B). A fold-change detection mechanism can address this problem: it allows detection of a signal that changes by 0.3 above a background of 1 but obtains a similar response only to changes of 3 above a background of 10.

Fold-change detection, therefore, assigns meaning to a signal in reference to the background signal level, allowing responses only to a signal that rises sufficiently above the noise. In other

words, signal discrimination is proportional to the background level. This is analogous to Weber's Law in sensory systems, which states that the minimal detectable change in stimulus is linear in the background stimulus (Figure 5C) (Ross and Murray, 1996) or, more generally, that the response amplitude to a change in signal is inversely proportional to the background signal level. It would be fascinating to test whether naturally occurring incoherent FFLs, found in numerous systems, act as fold-change detection elements that provide gene regulation with the ability to reliably detect signals above a variable and noisy background.

SUPPLEMENTAL DATA

Supplemental Data include five figures and can be found with this article online at [http://www.cell.com/molecular-cell/supplemental/S1097-2765\(09\)00859-4](http://www.cell.com/molecular-cell/supplemental/S1097-2765(09)00859-4).

ACKNOWLEDGMENTS

For suggestions and critical reading of the manuscript, the authors thank Cellina Cohen-Saidon, Michael Springer, Eduardo Sontag, Jessica Gray, and Adam Palmer. O.S. is grateful to the Azrieli Foundation for the award of an Azrieli Fellowship. L.G. is a Robert Black Fellow of the Damon Runyon Foundation (DRG-1958-07). This work was supported by the Kahn Family Foundation (U.A.), R01 HD037277 (M.W.K.), the Novartis-Harvard-Hebrew University program (M.W.K.), and the Israel Science Foundation (U.A.).

Received: August 20, 2009

Revised: November 13, 2009

Accepted: November 18, 2009

Published: December 10, 2009

REFERENCES

- Alon, U. (2007). *An Introduction to Systems Biology* (Boca Raton, FL: Chapman & Hall/CRC).
- Barkai, N., and Leibler, S. (1997). Robustness in simple biochemical networks. *Nature* 387, 913–917.
- Basu, S., Mehreja, R., Thiberge, S., Chen, M.T., and Weiss, R. (2004). Spatiotemporal control of gene expression with pulse-generating networks. *Proc. Natl. Acad. Sci. USA* 101, 6355–6360.

- Bintu, L., Buchler, N.E., Garcia, H.G., Gerland, U., Hwa, T., Kondev, J., and Phillips, R. (2005). Transcriptional regulation by the numbers: models. *Curr. Opin. Genet. Dev.* 15, 116–124.
- Boyer, L.A., Lee, T.I., Cole, M.F., Johnstone, S.E., Levine, S.S., Zucker, J.P., Guenther, M.G., Kumar, R.M., Murray, H.L., Jenner, R.G., et al. (2005). Core transcriptional regulatory circuitry in human embryonic stem cells. *Cell* 122, 947–956.
- Cohen-Saidon, C., Cohen, A.A., Sigal, A., Liron, Y., and Alon, U. (2009). Dynamics and variability in ERK2 response to EGF in individual living cells. *Mol. Cell* 36, this issue, 885–893.
- Eichenberger, P., Fujita, M., Jensen, S.T., Conlon, E.M., Rudner, D.Z., Wang, S.T., Ferguson, C., Haga, K., Sato, T., Liu, J.S., and Losick, R. (2004). The program of gene transcription for a single differentiating cell type during sporulation in *Bacillus subtilis*. *PLoS Biol.* 2, e328.
- Entus, R., Aufderheide, B., and Sauro, H.M. (2007). Design and implementation of three incoherent feed-forward motif based biological concentration sensors. *Syst. Synth. Biol.* 1, 119–128.
- Friedland, A.E., Lu, T.K., Wang, X., Shi, D., Church, G., and Collins, J.J. (2009). Synthetic gene networks that count. *Science* 324, 1199–1202.
- Gardner, T.S., Cantor, C.R., and Collins, J.J. (2000). Construction of a genetic toggle switch in *Escherichia coli*. *Nature* 403, 339–342.
- Goentoro, L., and Kirschner, M.W. (2009). Evidence that fold-change, and not absolute level, of β -catenin dictates Wnt signaling. *Mol. Cell* 36, this issue, 872–884.
- Kaplan, S., Bren, A., Dekel, E., and Alon, U. (2008). The incoherent feed-forward loop can generate non-monotonic input functions for genes. *Mol. Syst. Biol.* 4, 203.
- Kim, D., Kwon, Y.K., and Cho, K.H. (2008). The biphasic behavior of incoherent feed-forward loops in biomolecular regulatory networks. *Bioessays* 30, 1204–1211.
- Krejci, A., Bernard, F., Housden, B.E., Collins, S., and Bray, S.J. (2009). Direct response to Notch activation: signaling crosstalk and incoherent logic. *Sci. Signal* 2, ra1.
- Lahav, G., Rosenfeld, N., Sigal, A., Geva-Zatorsky, N., Levine, A.J., Elowitz, M.B., and Alon, U. (2004). Dynamics of the p53-Mdm2 feedback loop in individual cells. *Nat. Genet.* 36, 147–150.
- Laming, D. (1986). *Sensory Analysis* (London: Academic Press).
- Lee, T.I., Rinaldi, N.J., Robert, F., Odom, D.T., Bar-Joseph, Z., Gerber, G.K., Hannett, N.M., Harbison, C.T., Thompson, C.M., Simon, I., et al. (2002). Transcriptional regulatory networks in *Saccharomyces cerevisiae*. *Science* 298, 799–804.
- Levchenko, A., and Iglesias, P.A. (2002). Models of eukaryotic gradient sensing: application to chemotaxis of amoebae and neutrophils. *Biophys. J.* 82, 50–63.
- Li, X., Cassidy, J.J., Reinke, C.A., Fischboeck, S., and Carthew, R.W. (2009). A microRNA imparts robustness against environmental fluctuation during development. *Cell* 137, 273–282.
- Ma, W., Trusina, A., El-Samad, H., Lim, W.A., and Tang, C. (2009). Defining network topologies that can achieve biochemical adaptation. *Cell* 138, 760–773.
- Mangan, S., and Alon, U. (2003). Structure and function of the feed-forward loop network motif. *Proc. Natl. Acad. Sci. USA* 100, 11980–11985.
- Mangan, S., Itzkovitz, S., Zaslaver, A., and Alon, U. (2006). The incoherent feed-forward loop accelerates the response-time of the gal system of *Escherichia coli*. *J. Mol. Biol.* 356, 1073–1081.
- Milo, R., Shen-Orr, S., Itzkovitz, S., Kashtan, N., Chklovskii, D., and Alon, U. (2002). Network motifs: simple building blocks of complex networks. *Science* 298, 824–827.
- O'Donnell, K.A., Wentzel, E.A., Zeller, K.I., Dang, C.V., and Mendell, J.T. (2005). c-Myc-regulated microRNAs modulate E2F1 expression. *Nature* 435, 839–843.
- Ross, H.E., and Murray, D.J. (1996). *E.H. Weber on the Tactile Senses* (East Sussex, UK: Erlbaum Taylor & Francis).
- Shen-Orr, S.S., Milo, R., Mangan, S., and Alon, U. (2002). Network motifs in the transcriptional regulation network of *Escherichia coli*. *Nat. Genet.* 1, 64–68.
- Sigal, A., Milo, R., Cohen, A., Geva-Zatorsky, N., Klein, Y., Alaluf, I., Swerdlin, N., Perzov, N., Danon, T., Liron, Y., et al. (2006). Dynamic proteomics in individual human cells uncovers widespread cell-cycle dependence of nuclear proteins. *Nat. Methods* 3, 525–531.
- Swiers, G., Patient, R., and Loose, M. (2006). Genetic regulatory networks programming hematopoietic stem cells and erythroid lineage specification. *Dev. Biol.* 294, 525–540.
- Tyson, J.J., Chen, K.C., and Novak, B. (2003). Sniffers, buzzers, toggles and blinkers: dynamics of regulatory and signaling pathways in the cell. *Curr. Opin. Cell Biol.* 15, 221–231.
- Weber, E.H. (1905). *Tatsinn und Gemeingefühl* (Leipzig, Germany: Verlag von Wilhelm Englemann).
- Yi, T.M., Huang, Y., Simon, M.I., and Doyle, J. (2000). Robust perfect adaptation in bacterial chemotaxis through integral feedback control. *Proc. Natl. Acad. Sci. USA* 97, 4649–4653.

ST-NOTES (4 November)

► Universal features of sensory system :-

exact

(i) Adaptation - example: pupil dilation

(ii) sensing of relative changes rather than absolute changes

Example : 1 candle added in a room

with one candle vs

1 candle added in a room
with chandeliers of 50 candles

Weber's Law :- ($\Delta x_{\min} = K x_0$)

x_0 : initial weight

added small weight \Rightarrow just-noticeable difference is proportional to measure the minimal detectable increase in background signal at which people felt extra weight.

Relative sensing is lost at very weak signals on the brink of detection by very strong signals that saturate the receptors.

For alls, sensing relative changes is imp. in order to be robust to noise in the input. To respond correctly, all must tell difference b/w a the input signal & noise.

(2)

Incoherent feedforward loop

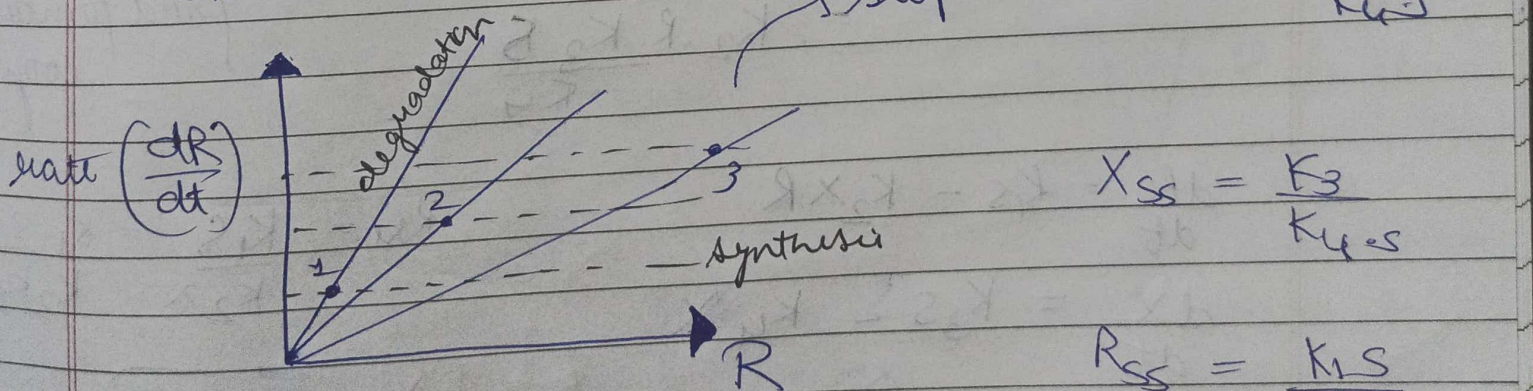
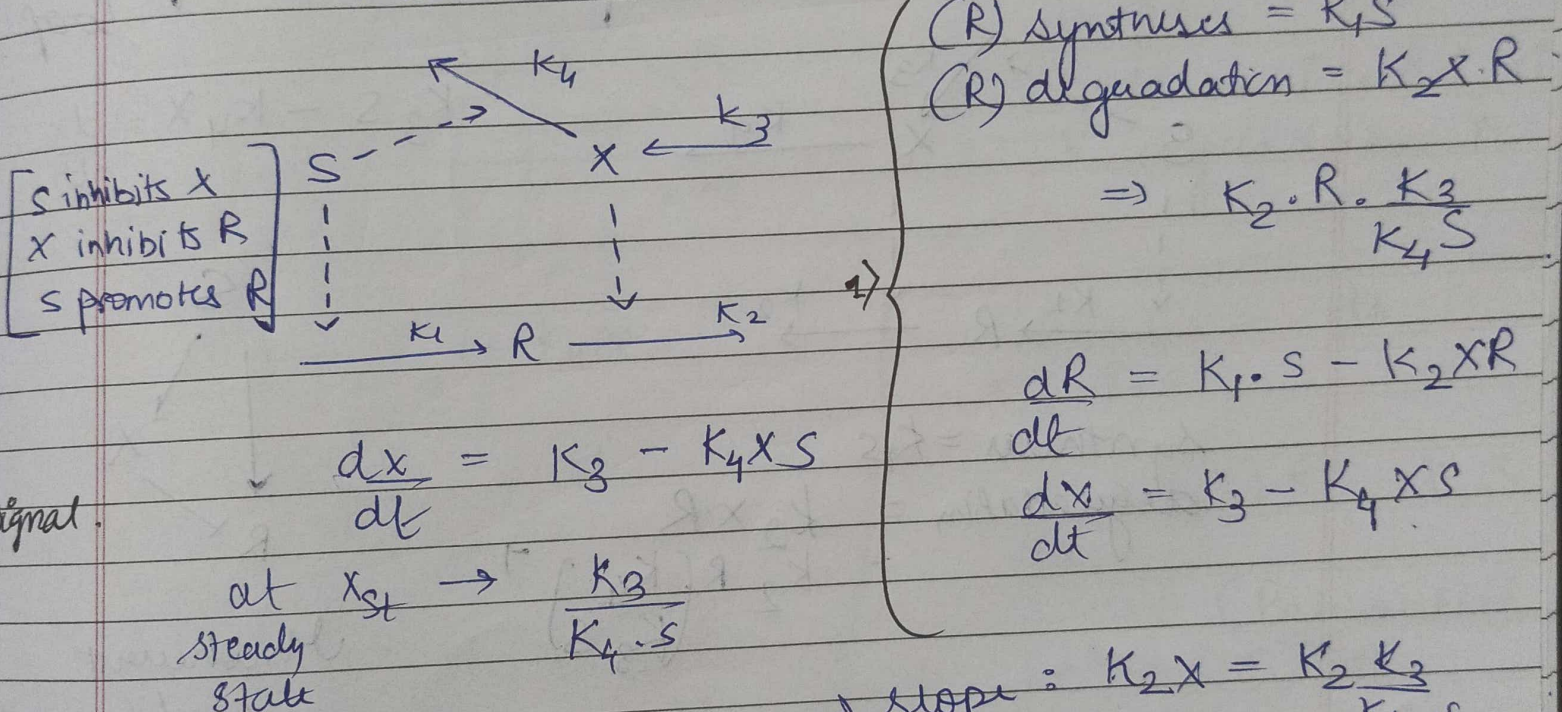
► Bacterial chemotaxis

$$\begin{array}{l}
 \begin{array}{c} x \\ \downarrow \\ y \\ \perp \\ z \end{array} \quad \frac{dy}{dt} = K_{xy}x - K_{yz}y \\
 \frac{dz}{dt} = (K_{xy}x)(K_{yz}z) - K_{zz}z \\
 \frac{dz}{dt} = p_2(K^+ > K_{xz}) \cdot \Theta(y^+ < K_{yz}) - K_z z
 \end{array}$$

Attraction

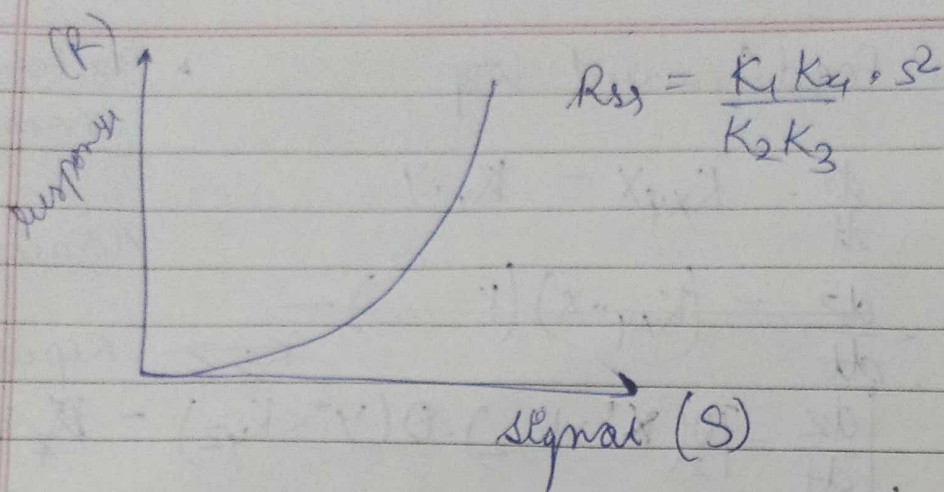
Repulsion

1 Problem on ultrasensitivity: two linear modules

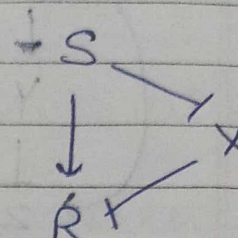


degradation depends on R
synthesis depends on S

$$\begin{aligned}
 R_{ss} &= \frac{k_1 S}{k_2 X_{ss}} \\
 &= \frac{k_1 \cdot S \cdot k_3}{k_2 \cdot k_4 \cdot S} \\
 R_{ss} &= \frac{k_1 k_4 \cdot S^2}{k_2 \cdot k_3}
 \end{aligned}$$

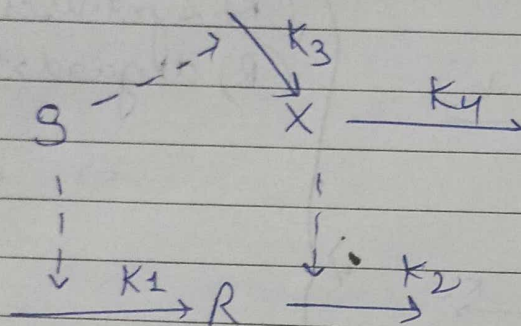


$$R_{ss} = \frac{K_1 K_4 + S^2}{K_2 K_3}$$

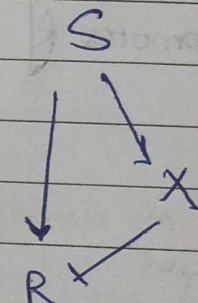


coherent
feedforward
loop

2) Two linear modules: Adaptation



$$K_3 S - K_4 X = \frac{dx}{dt}$$



Measurement
feed forward
loop

$$\text{synthesis} = K_1 S$$

$$\text{degradation} = K_2 X \cdot R$$

$$= K_2 \cdot R \left(\frac{K_4}{K_3 \cdot S} \right)^{-1}$$

$$= K_2 \cdot R \cdot \frac{K_3 \cdot S}{K_4}$$

$$\frac{dR}{dt} = K_1 S - K_2 X \cdot R$$

$$R_{ss} = \frac{K_1 S}{K_2 X} = \frac{K_1 S K_4}{K_2 K_3 S}$$

$$\frac{dX}{dt} = K_3 S - K_4 X$$

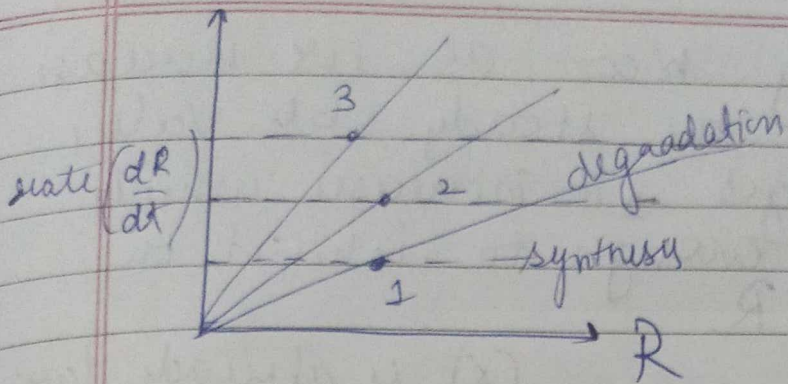
then only until x_0
 $\frac{dX}{dt} = K_3 S$

$$x_{ss} = \frac{K_3 S}{K_4}$$

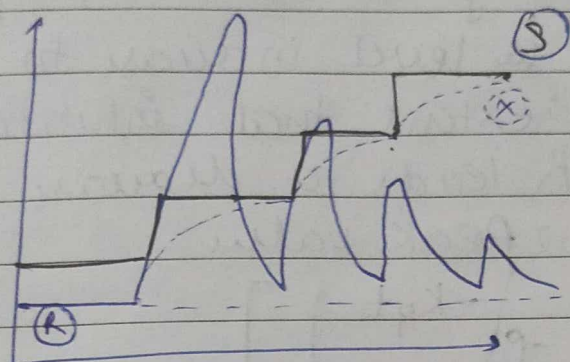
$$R_{ss} = \frac{K_1 K_4}{K_2 K_3}$$

* Final steady state [Response] is independent of S [Signal]

Date _____
Page _____



If we increase S & keep increasing the signal, the steady state doesn't change.



Perfect Adaptation

- $S \uparrow$
- synthesis \uparrow , $R \uparrow$, $X \uparrow$
- degradation \uparrow

$$\frac{dx}{dt} = k_3 S - k_4 x \quad \text{time}$$

$$\frac{dx}{dt} = k_3 S - k_4 x$$

$$\int \frac{dx}{k_3 S - k_4 x} = \int dt$$

$$\left[\frac{1}{k_4} \ln(k_3 S - k_4 x) \right]_0^{x_t} = t$$

$$\ln(k_3 S - k_4 x_t) - \ln(k_3 S) = -k_4 t$$

$$\ln\left(1 - \frac{k_4}{k_3 S} \cdot x_t\right) = -k_4 t$$

$$\frac{k_4}{k_3 S} \cdot x_t = 1 - e^{-k_4 t}$$

$$x_t = \frac{k_3}{k_4} (1 - e^{-k_4 t}) \cdot S$$

$$\frac{dR}{dt} = ds$$

$$\frac{dR}{dt} + (k_2 x) R = k_1 S$$

$$IF = \int e^{\int \frac{k_2 \cdot k_3}{k_4} S (1 - e^{-k_4 t}) dt} dt$$

(Bernoulli)

R finally reaches to the steady state which is approx same as initial state

- Peaks are decreasing b'coz as we increase the stimulus (S), the steady state value of (X) also changes \rightarrow it increases which is high enough to inhibit the production of R .

$S \uparrow \quad R \uparrow \quad - (X) \text{ is already large enough to inhibit } (R) \text{ before its}$
 $X \uparrow \quad \Rightarrow \text{the level increase to such an extent that inhibition of } R \text{ leads to decrease in the peak value}$

$$[X(t) = \frac{K_3 \cdot S}{K_4} (1 - e^{-K_4 t})]$$

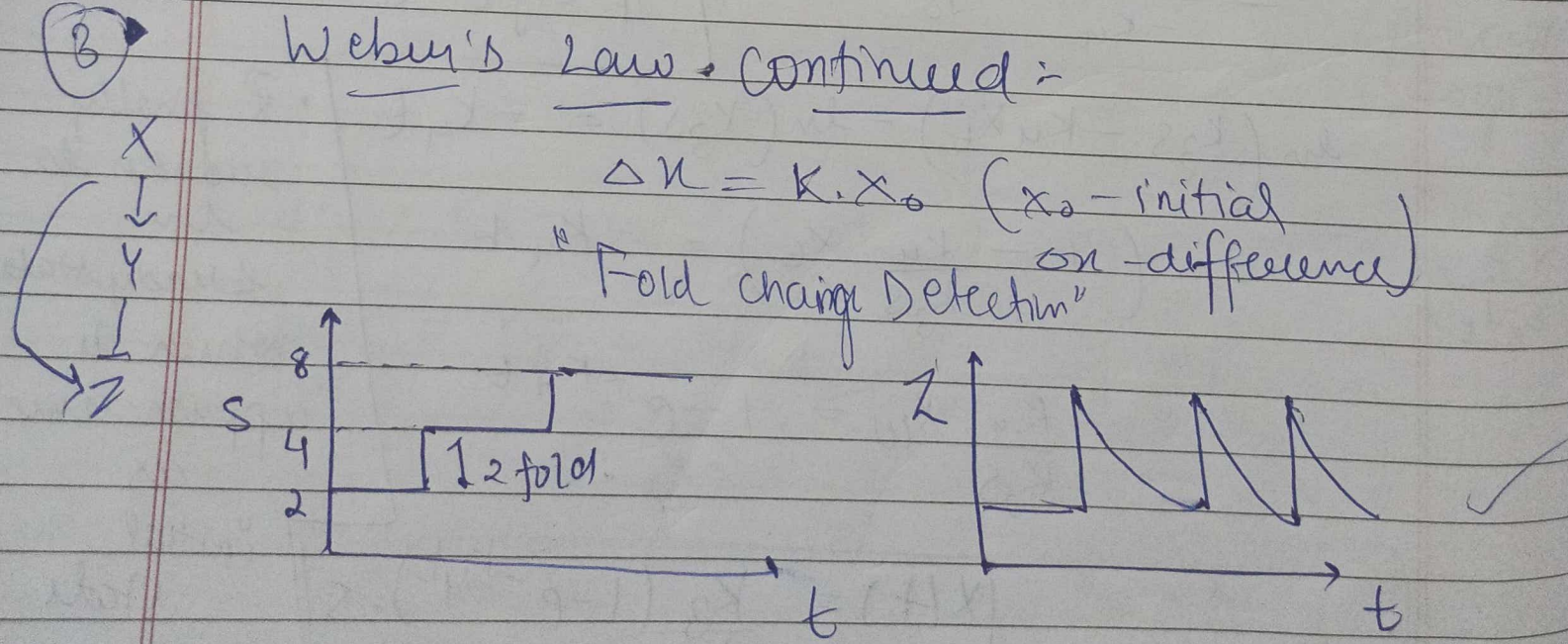
$$\frac{dR}{dt} = K_1 S - K_2 R \cdot \frac{K_3 \cdot S}{K_4} (1 - e^{-K_4 t})$$

$$[\frac{dR}{dt} = K_1 S - \frac{K_2 K_3 \cdot S \cdot R}{K_4} (1 - e^{-K_4 t})]$$

⑥ Weber's Law - Continued :-

$$\Delta x = K \cdot x_0 \quad (x_0 - \text{initial on-difference})$$

"Fold change Detection"



We sense to relative change.

* "Fold change detection" is different from ADAPTATION.

→ Any system that does fold detection also performs adaptation

due to "It comes back to the same steady state"

S.

→ Adaptation is requirement of fold detection.

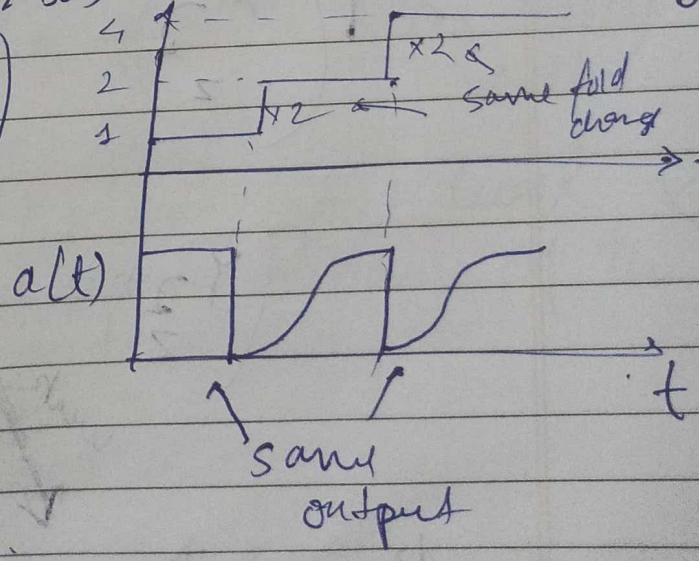
Book

→ Fold change of the signal → entire shape of the curve depends only on the signal output normalised by its background

Considering a system with output $a(t)$

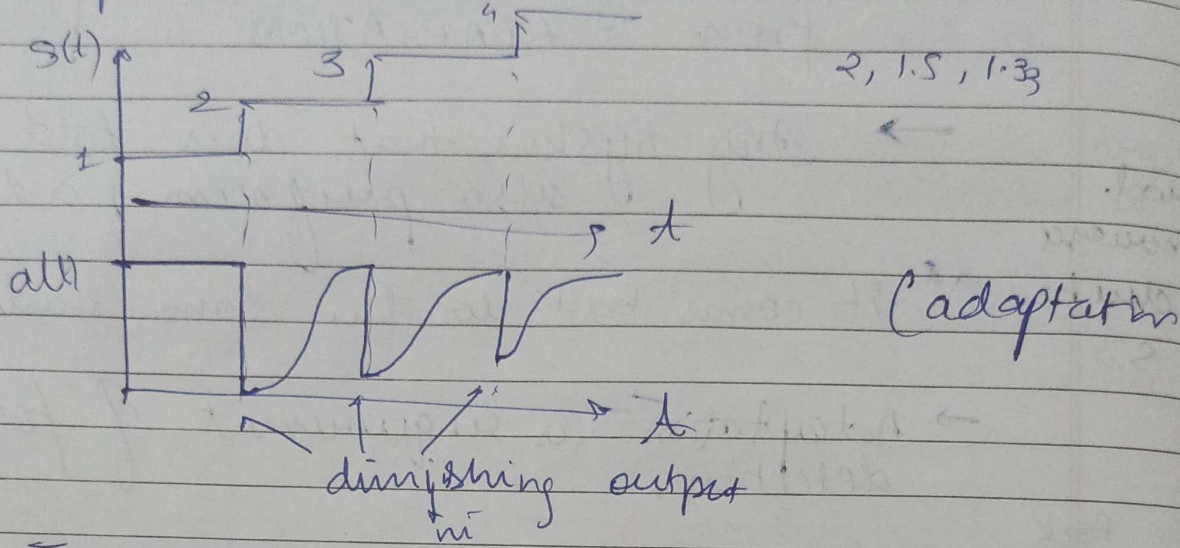
\rightarrow response curve whose entire shape including peak amplitude & response time depends only on relative and not on background change in input $\left(\frac{S(t)}{S_0} \right)$ $S(t)$ absolute change signal S_0

If $\left[\frac{S(t)}{S_0} \right] = K$ [remain constant]
then output also remains constant



Peak remain same until the fold changes.

Now if $\frac{S(t)}{S_0} = k \left[\frac{x}{K_x} - \text{diminisher} \right]$ then the output will also diminish



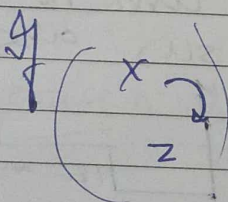
→ Type II-FFL can provide FCD when

(i) Binding of x to its target promoter is weak

$$\frac{x}{x + K_x} \approx \frac{x}{K_x}$$

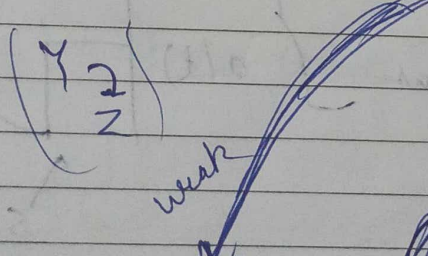
(ii) Binding of y (repressor) is strong

$$\frac{y}{y + K_y} \approx \frac{1}{1 + y/K_y} \approx \frac{1}{y}$$



$$\text{thus } \frac{dz}{dt} = \beta_z[x] - \alpha_z[z]$$

$$\frac{dz}{dt} = \beta_z x^n - \alpha_z z \quad x^n + K_x^n$$



$$\frac{dz}{dt} = \beta_y \frac{y^n}{K_y^n + y^n} - \alpha_{zy} z$$

$$\frac{dx}{dt} = \beta_x \left(\frac{x}{K_x} \right)^n - \alpha_{xz} z$$

$$\frac{dy}{dt} = \beta_y \left(\frac{y}{K_y} \right)^n - \alpha_{zy} z$$

weak

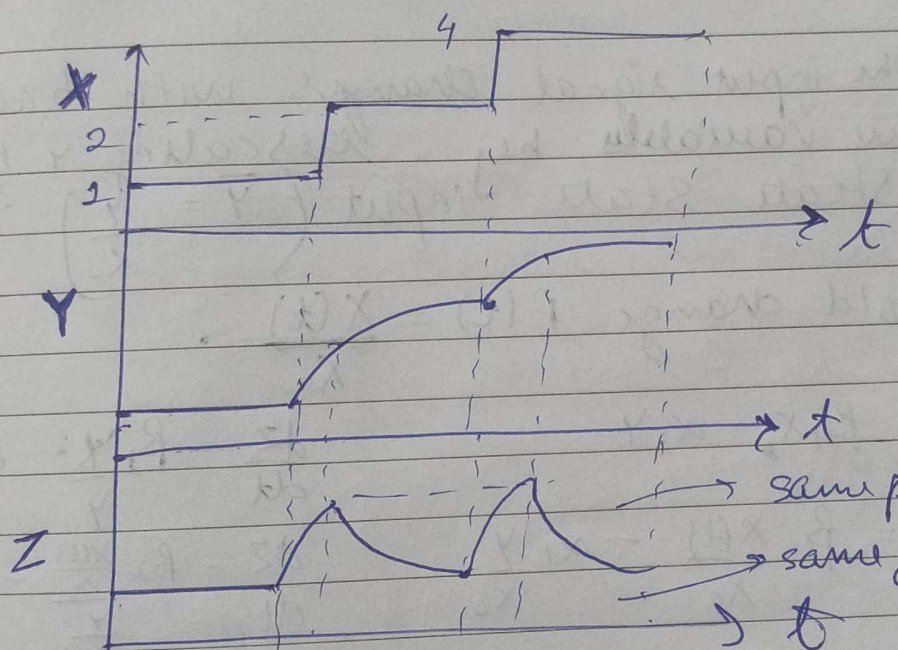
strong

(i) means concⁿ of X should be low to activate
 (ii) production

(ii) means concⁿ of Y should be high to activate (Z) production.

then we can write

$$\left[\begin{array}{l} \frac{dy}{dt} = \beta_1 X - \alpha_1 Y \\ \frac{dz}{dt} = \beta_2 \frac{X}{Y} - \alpha_2 Z \end{array} \right] \quad \begin{array}{l} (a) \\ (b) \end{array}$$



for that
particular
 x ,
 y changes

But z is
remain
same
as initial
state.

• supervisor Y does not adapt
 Instead, it tracks the input level X ,
 like an internal representation of the
 input

Eq(a), Eq(b) have Pcs :-

Show :- Exact adaptation should be
 thru

For exact adaptation;

we solve the steady-state condition

$$\frac{dy}{dt} = 0 \quad \frac{dz}{dt} = 0 \quad \text{for a constant input } X_0$$

$$Y_{st} = \frac{B_1 X_0}{\alpha_1}$$

$$Z_{st} = \frac{B_2 X_0}{\alpha_2 Y_{st}} = \frac{B_2 X_0 \alpha_1}{\alpha_2 B_1 X_0}$$

$$Z_{st} = \frac{\beta_2 \cdot \alpha_1}{\alpha_2 \cdot B_1}$$

Independent of X_0 (Exact Adaptation)

Now,

let the input signal changes with time $X(t)$.
Define new variables by rescaling Y &
the steady state input ($\bar{Y} = \frac{Y}{X_0}$)

define fold change $F(t) = \frac{X(t)}{X_0}$.

$$\frac{dy}{dt} = B_1 X - \alpha_1 Y$$

$$\frac{dz}{dt} = B_2 \frac{X}{Y} - \alpha_2 Z$$

$$\frac{dy}{X_0 dt} = \frac{B_1 X(t)}{X_0} - \frac{\alpha_1 Y}{X_0}$$

$$\frac{dz}{dt} = B_2 \frac{X(t)}{X_0} - \alpha_2 Z$$

$$\left[\frac{dY}{dt} = B_1 F(t) - \alpha Y \right]$$

$$\frac{dz}{dt} = B_2 F(t) - \alpha Z$$

Initial conditions are independent of X_0

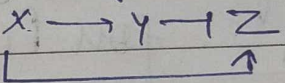
Dynamic equations & their initial conditions depends on FOLD CHANGE ($F(t)$)

and thus the output dynamics $Z(t)$ are completely determined by the fold change in input & hence displaying FCD.

FCD: breaks down in TI-PPL when γ is too small to ignore the binding coeff k_y

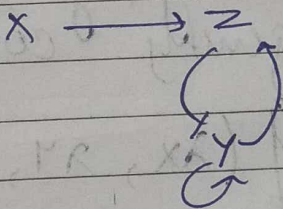
↳ less amt of γ is needed to express/inhibit FCD: occurs for $\gamma \rightarrow 0$

any value of production & removal $\alpha_{1,2}$ & $\beta_{1,2}$ → they affect the shape of dynamics by setting the amplitude & response time of the output puls.



► only FCDs: TI-PPL

NLIFBL: nonlinear integral feedback loop



HOMOGENITY

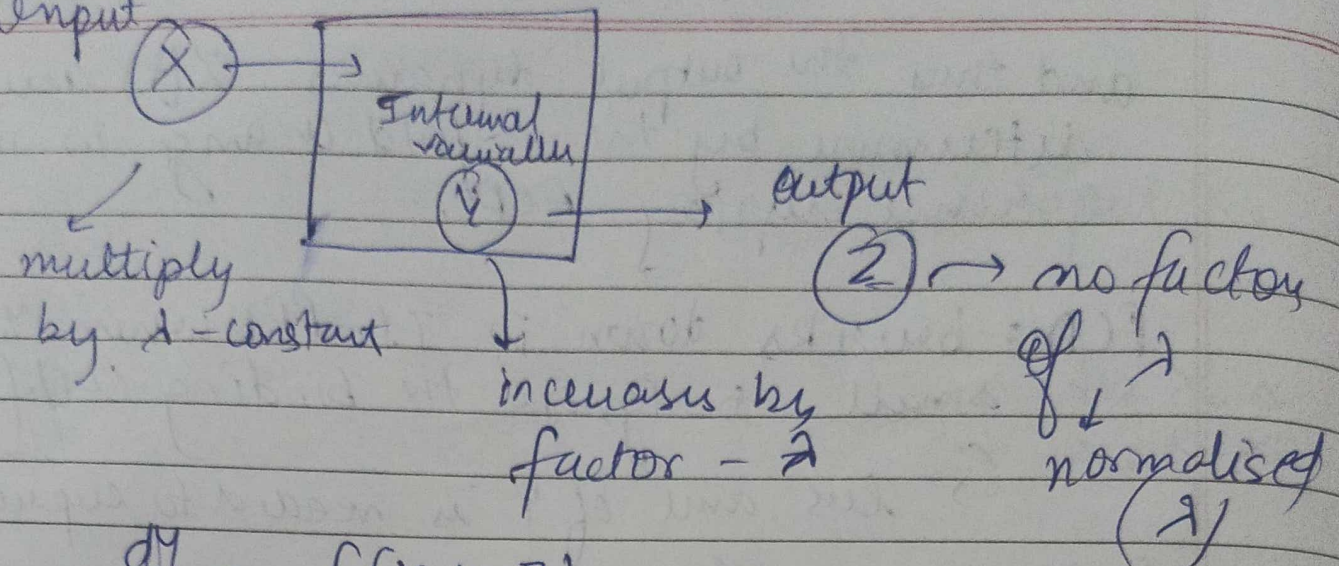
CONDITION FOR FCD TO CHECK FCD PROPERTY

This condition generalises the dimensionless variable approach used in eq (a), eq (b) proof

It requires that if the input is multiplied by a constant (λ), the system has an internal variable (y) that also (λ) by a factor of (λ).

used as a memory normalising out (λ). ← that divides the output Z

Input



$$\frac{dy}{dt} = f(x, y, z)$$

$$\frac{dz}{dt} = g(x, y, z)$$

Sufficient condⁿ
for PCB

System has a stable
steady-state solution
that the output z shows
exact adaptation &
that g, f satisfy the following
homogeneity condition for any $\lambda > 0$.

$$\begin{cases} f(\lambda x, \lambda y, z) = \lambda f(x, y, z) \\ g(\lambda x, \lambda y, z) = g(x, y, z) \end{cases}$$

If f is linear, the condⁿ is also
necessary.

$$f(x, y, z) = \beta_1 x - \alpha_1 y$$

$$f(\lambda x, \lambda y, z) = \lambda \beta_1 x - \alpha_1 \lambda y$$

$$\lambda f(x, y, z) = \lambda (\beta_1 x - \alpha_1 y)$$

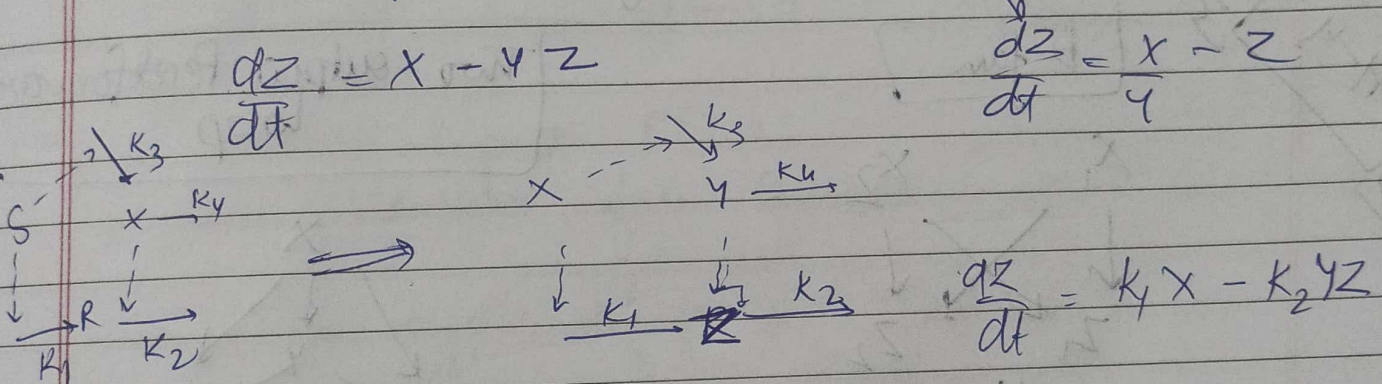
Similarly ; $g(x, y, z) = \beta_2\left(\frac{x}{y}\right) - \alpha_2(z)$

$$g(x, \lambda y, z) = \beta_2\left(\frac{x}{y}\right) - \alpha_2(z)$$

$$g(\lambda x, \lambda y, z) = g(x, y, z)$$

In case of Shiffrer (Book used in class)

↳ degradation is linear faster than transcription



does not show FCD

★ TRANSCRIPTION shows FCD ($\frac{dy}{dt} = g$)
DEGRADATION doesn't ($\frac{dz}{dt} = g$)

↳ response time depends on absolute input change

Read Paper

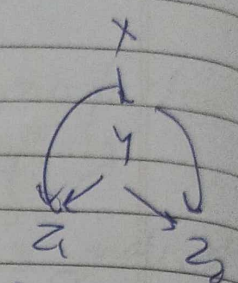
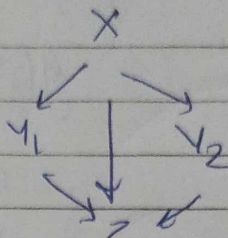
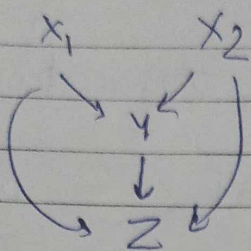
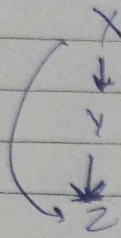
classmate

Date _____

Page _____

Video

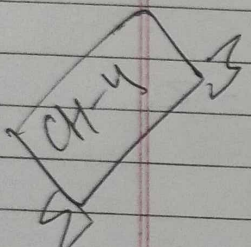
3 component system



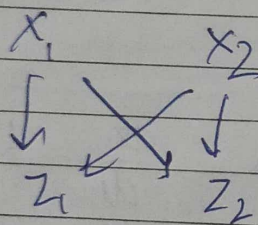
(multi-input)

(multi-output)

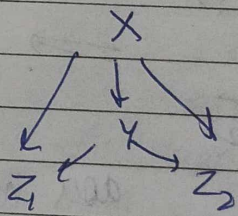
199 - Four modes subgraphs



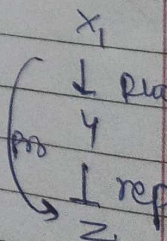
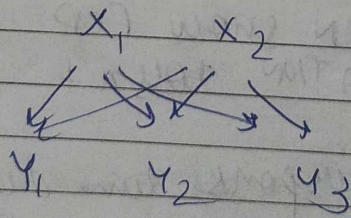
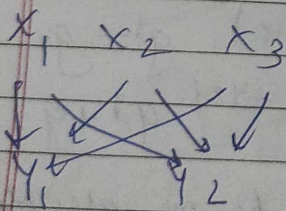
[bi-fan]

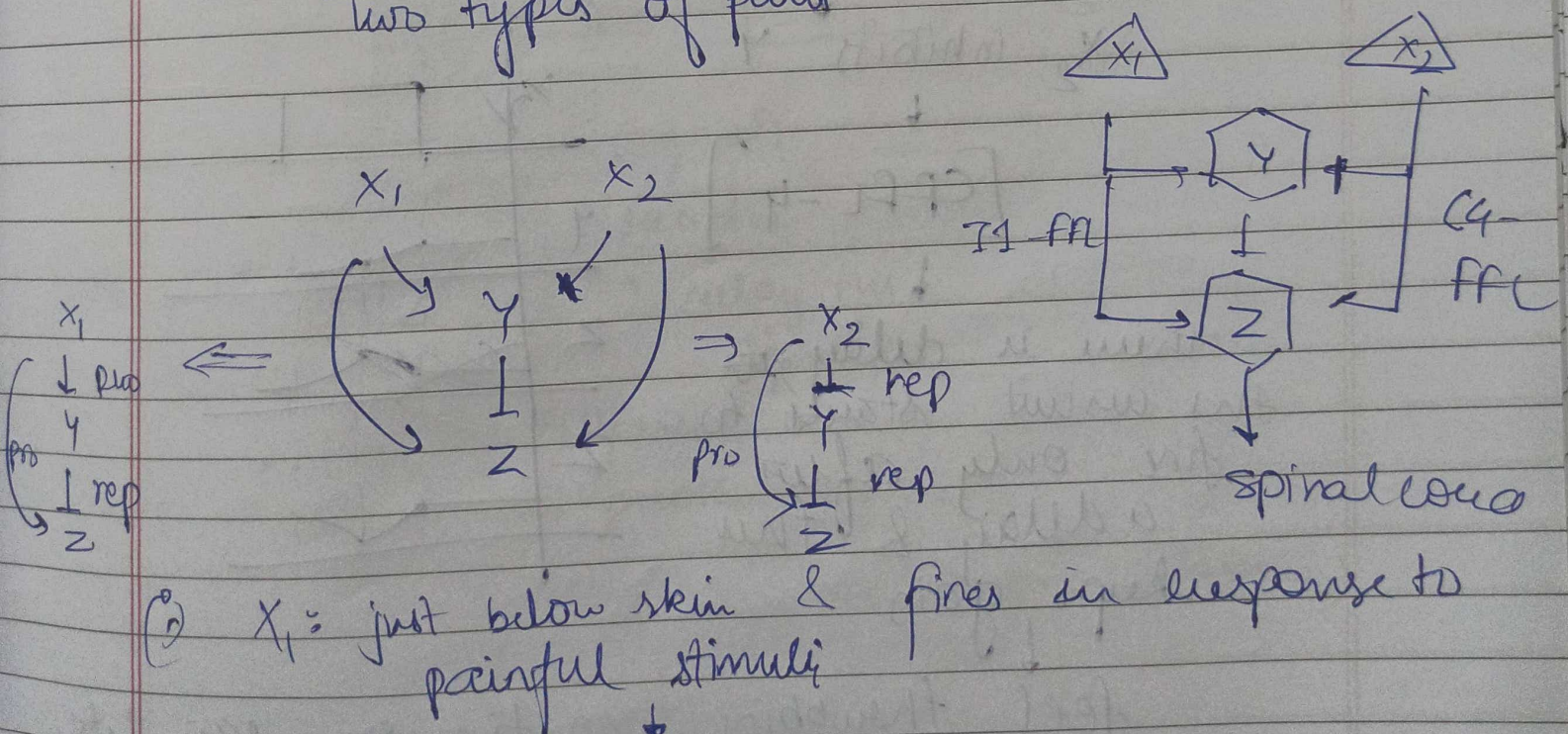
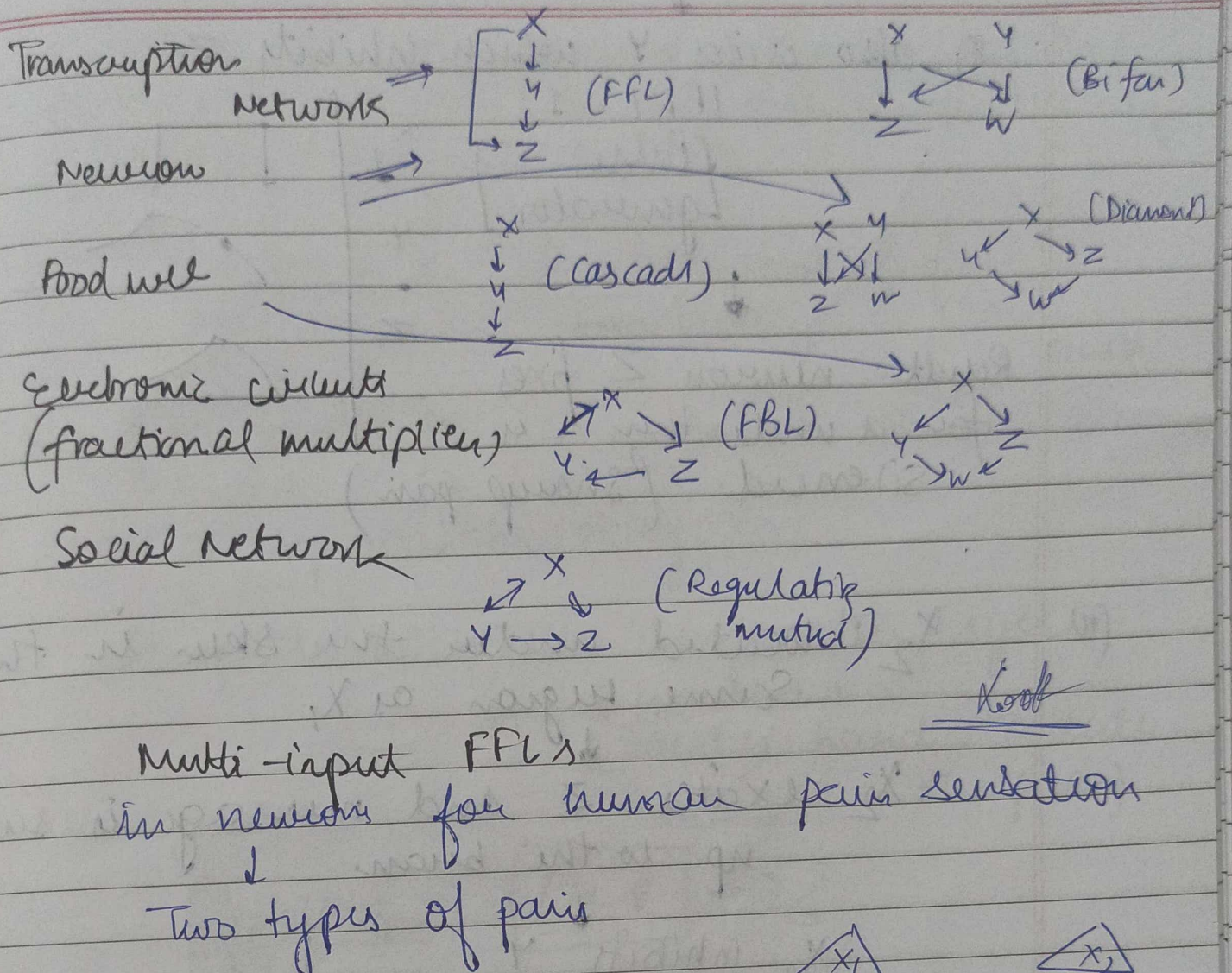


[two-output feedforward loop]



signal integration



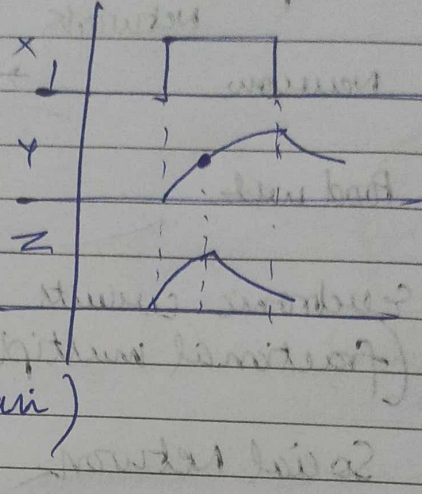


x_1 excites z (neuron) which projects up the message to spinal cord, sending pain beam

x_1 also excites y which inhibits z

[IFPL-1]

[Pulse generator]



Result: neuron Z fires
for a while then is
silenced. (sharp pain)

(ii)

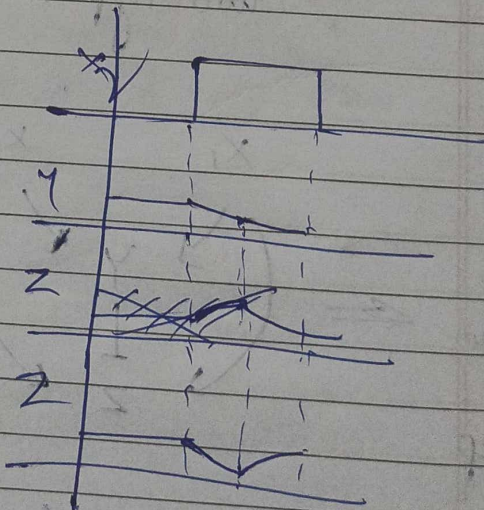
x_2 : located under the skin in the
same region as x_1 ,

x_2 excites z and message is sent
up to the brain

x_2 inhibits y

[CPFL-4]

there is delay in
the circuit starts to
fire only after
a delay & fire
keeps going



feel a fanning, continuous pain like
a burn on abrasion

- The delay is strengthened by the fact that the action potentials travel down the axon of x_2 much slower than x_1 .

pain from x_1 : short transient & fast

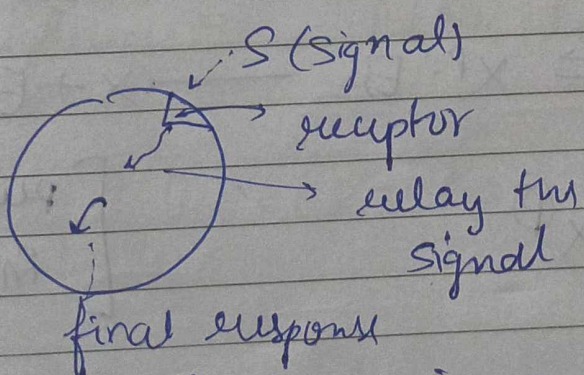
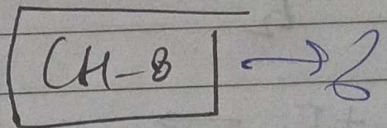
pain from x_2 : long-lasting & slow onset.

We intentionally force the circuits to interact.

How to stop the throbbing?

Stimulate $x_1 \rightarrow$ which shuts the system for a while
 (Scratch hard to dull the pain)

Signalling



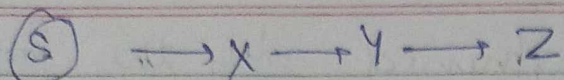
\hookrightarrow protein which

is synthesised (slow)

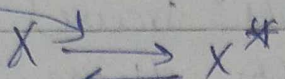
(S)

\hookrightarrow protein localisation

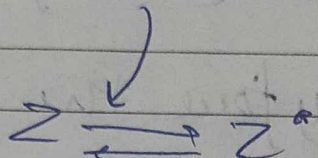
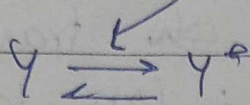
\hookrightarrow protein becoming active/inactive (Fast)



signal

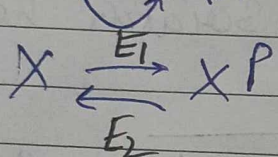
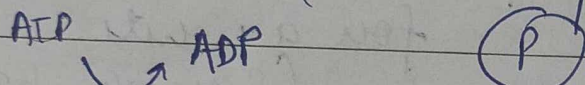
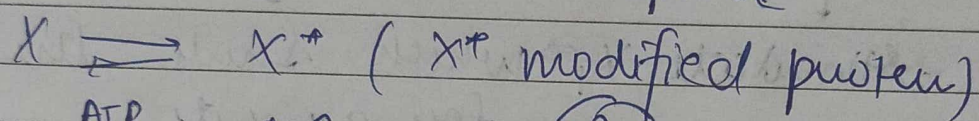


X^*, Y^*, Z^* are
active proteins



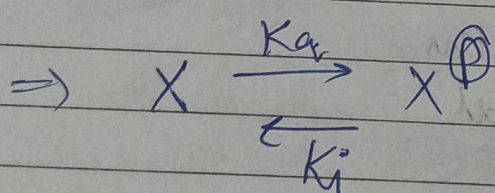
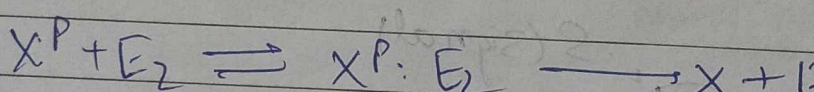
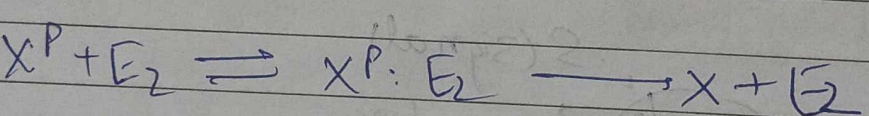
(looks like
array)

response



phosphate is
coming

E_1^P : enzymes from ATP



protein - protein
interaction

↓
protein - DNA
interaction

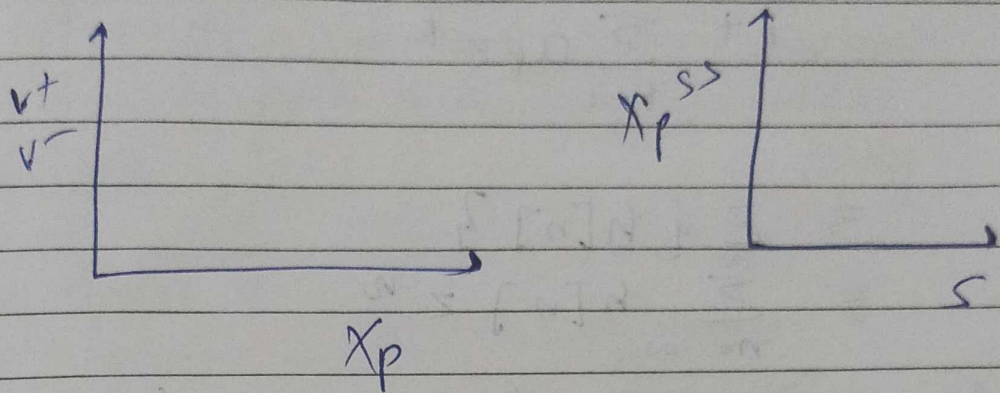
$$\frac{dX^P}{dt} = R_g \cdot X - R_i \cdot X^P$$

no new protein synthesis

$$[\text{Total conc}] X_T = X + X^P$$

MASS BALANCE]

$$\frac{dx^P}{dt} = \underbrace{k_q \cdot (x_T - x^P)}_{V+} \cdot s - \underbrace{k_i x^P}_{V-}$$



$$\frac{dx^P}{dt} = -k_q x^P s - k_i x^P + k_q x_T s$$

$$\int \frac{dx_P}{(k_q s + k_i) x_P} = \int k_q x_T s dt$$

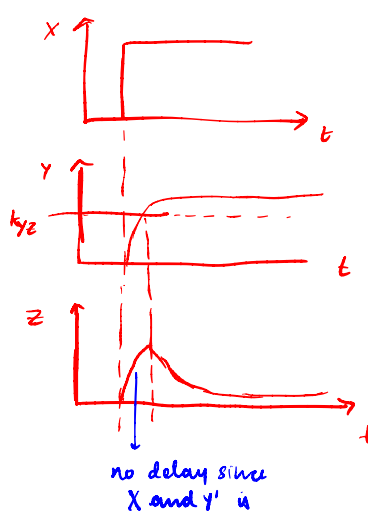
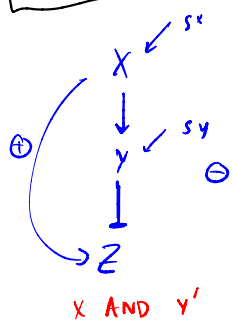
$$\int \frac{dx_P}{x_P} = - \int (k_q s + k_i) k_q x_T s dt$$

$$\ln x_P]_{x_{Pi}}^{x_{Pf}} = - (k_q s + k_i) k_q x_T s dt$$

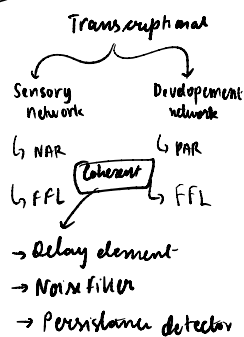
$$x_{Pf} = x_{Pi} e^{- k_q x_T s (k_q s + k_i) t}$$

$^{14}\text{N} \rightarrow ?$

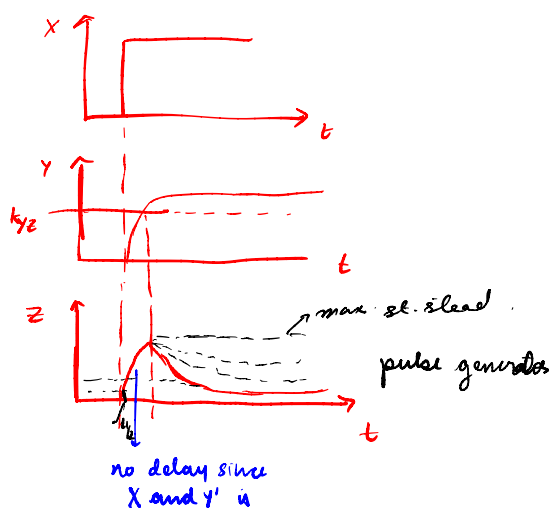
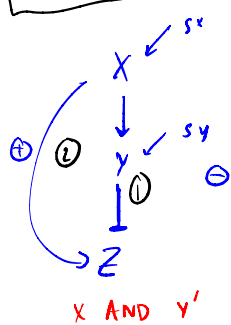
I FFL



Oct 27th



I FFL



If you don't have the first arm
z reaches the maximum it can possibly go.

Loop ① acts as a "break" in an F1 car.

$$\frac{dx}{dt} = \frac{\beta x^n}{x^n + k^n} - \alpha_2 x \quad [NAR]$$

$$z = z_m (1 - e^{\alpha_2 t})$$

$$z_{st} = z_m (1 - e^{-\alpha_2 t + \frac{1}{2}})$$

$$z_m = \frac{\beta z}{\alpha_2} \quad (\text{without } y)$$

$$z_{st} = \frac{\beta z}{\alpha_2} \quad (\text{with } y)$$

$$\frac{dx}{dt} = \frac{\beta z^n k^n}{k^n + y^n} - \alpha_2 z \quad (x=1)$$

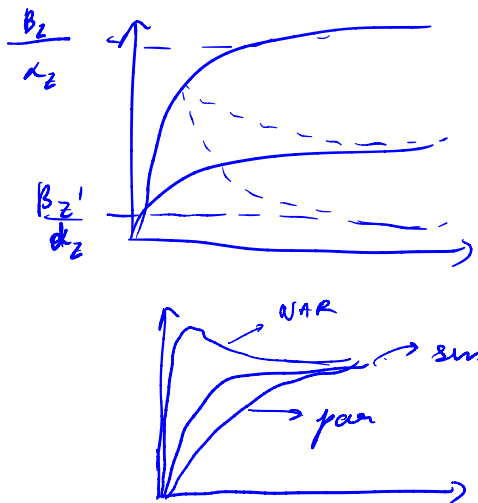
$$F = \frac{z_m}{z_{st}} = \frac{1}{2} \beta (1 - e^{-\alpha_2 t y_m})$$

$$t_{1/2} = \frac{1}{\alpha_2} \ln \left(\frac{2F}{2F-1} \right)$$

As you

if $F=1$
 $\frac{1}{\alpha_2}$

increase P , the system goes towards zero.



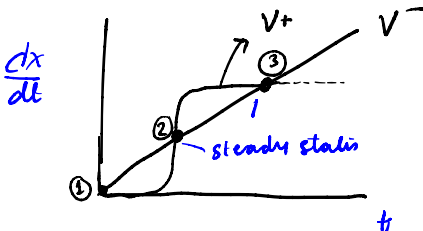
If I have high β .

To achieve fast response time i cannot change α since that will give completely different steady state. So you will have to change b .

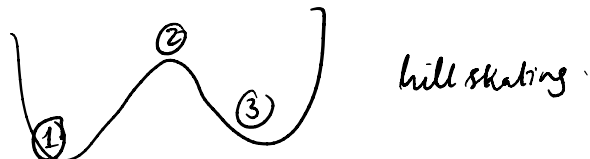
"Assignment"

$$\text{PAR } \left\{ \frac{dx}{dt} = \rho_0' + \beta x - \alpha x \right.$$

$$\left. \frac{dx}{dt} = \rho_0' + \frac{\beta x^n}{K^n + x^n} - \alpha x \right. \begin{matrix} \sim \\ \sim \\ V^+ \end{matrix} \quad \begin{matrix} \sim \\ \sim \\ V^- \end{matrix}$$

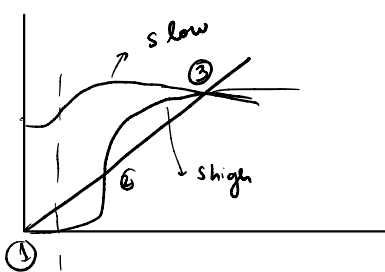


① and ③ are stable
② unstable



It has a major role in creating multistability sets.

$$\frac{dx}{dt} = \left(\rho_0' + \frac{\beta x^n}{K^n + x^n} \right) s - \alpha x \quad \begin{matrix} \downarrow \\ \text{input} \end{matrix}$$

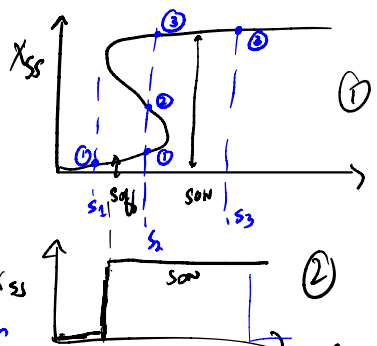


Based on value of s , we can see no of steady states

toggle switch (like our light or fan)
Not exactly but rough idea.

Buzzer

This is like a push button switch



So S_{off} and S_{on} are like thresholds for activation / deactivation.

there is a difference here.
They both work like a switch.

PAR



$$\frac{dx}{dt} = \beta' + \beta x - \alpha x$$



one value
1st steady state

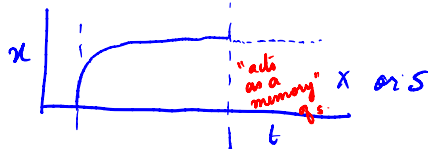
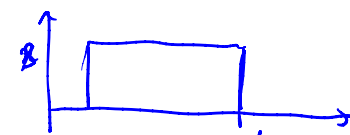
second value
third steady state

or v... depending
on which is higher.



X or S

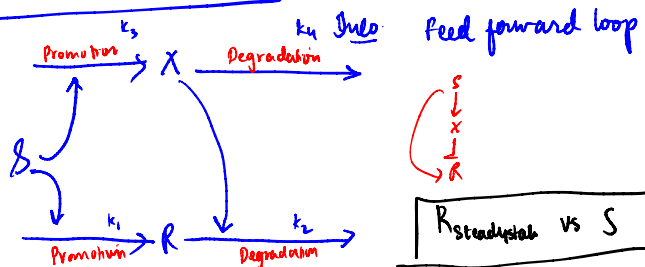
X and S



Development networks
need memory to be able
to remember its own
cell structure.

And that the cell structure
cannot change just because
it remembers itself.

How does your nose work?



$$\frac{dx}{dt} = k_3 s - k_4 x \quad X_{ss} = \frac{k_3 s}{k_4}$$

$$\frac{dr}{dt} = k_1 s - k_2 r \quad R_{ss} = \frac{k_1 s}{k_2} = \frac{k_3 s}{k_4 k_2}$$



This is how your nose
works. If you
smell perfume
initially you have
a response, but with time it
"adapts" to stimuli.

Gene X reaches
a constant
value.
Res doesn't
depend on
signal →
so steady-state
is the same
state as before
stimuli

fold
detection
can only
detect fold
change, w/
change in
spine membrane's

